MARCOS EDUARDO VIANA DE ARAUJO

DRYING KINETICS AND MODELING OF THE PHYSICAL PROPERTIES OF BEAN GRAINS

Thesis submitted to the Agricultural Engineering Graduate Program of the Universidade Federal de Viçosa in partial fulfillment of the requirements for the degree of *Doctor Scientiae*.

Adviser: Paulo Cesar Corrêa

VIÇOSA - MINAS GERAIS
2023

Ficha catalográfica elaborada pela Biblioteca Central da Universidade Federal de Viçosa - Campus Viçosa

T
A663d
2023

Araujo, Marcos Eduardo Viana de, 1995-
Drying kinetics and modeling of the physical properties of bean grains / Marcos Eduardo Viana de Araujo. – Viçosa, MG, 2023.
1 tese eletrônica (117 f.): il. (algumas color.).

Texto em inglês.
Orientador: Paulo César Corrêa.
Tese (doutorado) - Universidade Federal de Viçosa, Departamento de Engenharia Agrícola, 2023.
Referências bibliográficas: f. 65-85.
DOI: https://doi.org/10.47328/ufvbbt.2023.230
Modo de acesso: World Wide Web.

1. Feijão - Medição. 2. Grãos - Medição. 3. Grãos - Tamanho. 4. Análise numérica. 5. Análise volumétrica. I. Corrêa, Paulo César, 1951-. II. Universidade Federal de Viçosa. Departamento de Engenharia Agrícola. Programa de Pós-Graduação em Engenharia Agrícola. III. Título.

CDD 22. ed. 633.372

Bibliotecário(a) responsável: Alice Regina Pinto Pires CRB-6/2523

MARCOS EDUARDO VIANA DE ARAUJO

DRYING KINETICS AND MODELING OF THE PHYSICAL PROPERTIES OF BEAN GRAINS

Thesis submitted to the Agricultural Engineering Graduate Program of the Universidade Federal de Viçosa in partial fulfillment of the requirements for the degree of *Doctor Scientiae*.

APPROVED: April 24, 2023.

Assent:

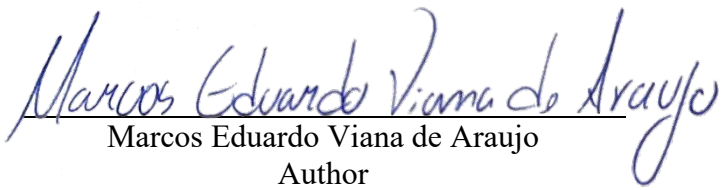

Marcos Eduardo Viana de Araujo
Author

Paulo Cesar Corrêa
Adviser

ACKNOWLEDGEMENTS

To God, who guided me throughout my journey with infinite love and patience. Your breath of life in me sustained me and gave me the courage to question realities and always propose a new world of possibilities.

To my parents, who, with their unconditional love, supported and guided me during this journey. At all times, they spared no effort to make all this possible. My sincere and eternal thanks to those who renounce their dreams to give life to their children's dreams.

To Eloiny Guimarães Barbosa, for her trust, friendship, and patience, for the nights required to complete all the experiments, for her invaluable criticisms and suggestions in writing this thesis, and for always being by my side. Your love and affection made this journey much easier, and I will forever be grateful.

To Professor Paulo Cesar Corrêa, supervisor not only of the thesis but also of life, for his trust, encouragement, and guidance, which allowed the conclusion of this work.

To Professor Marcio Arêdes Martins, for the teachings that extend far beyond the academy and for all the help he has given me to achieve the highest goals.

To Professor Yuanhui Zhang for having me in his E2 research group at the University of Illinois at Urbana-Champaing. His valuable teachings were and will significantly help throughout my academic and professional life.

To Professor Tetuo Hara, for his advice and valuable academic, professional, and personal teachings.

To the friends of the National Storage Training Center (CENTREINAR) for the constant exchange of knowledge and support.

To everyone who somehow made this moment come true, whether with advice, suggestions, incentives, support, or trust.

To the Federal University of Viçosa for the opportunity to complete the postgraduate course.

To the Conselho Nacional de Desenvolvimento Científico e Tecnológico (CNPq), for granting the scholarship.

To the Coordenação de Aperfeiçoamento de Pessoal de Nível Superior (CAPES), to granting the scholarship.

This study was financed in part by the Coordenação de Aperfeiçoamento de Pessoal de Nível Superior – Brasil (CAPES) – Finance Code 001.

"Madness is wanting different results doing everything exactly the same"
(Albert Einstein)

GENERAL ABSTRACT

ARAUJO, Marcos Eduardo Viana de, D.Sc., Universidade Federal de Viçosa, April, 2023. **Drying kinetics and modeling of the physical properties of bean grains**. Adviser: Paulo Cesar Corrêa.

Common bean is one of the most produced and consumed legumes worldwide. The nutritional quality of this food has made it a fundamental constituent in the diet of thousands of people every day. However, the losses observed during the productive chain of this culture show that the equipment and operations are dimensioned/conducted inefficiently. Over the years, technological advances in the food industry have required up-to-date data on the engineering properties of agricultural products, aiming to optimize processes and reduce losses at all stages of the agricultural production chain. Although the determination of the properties of several products is available in the literature, the genetic improvement and advancement of cultivars have made the industry optimize its processes based on obsolete data, which no longer represent the characteristics of the material. Given the above, this study aimed to determine and model the geometric properties (circularity, sphericity, geometric diameter, projected area, surface area, volume, and surface-to-volume ratio), physical (real and apparent specific gravity, porosity, and 1000-grain mass), aerodynamics (terminal velocity and drag coefficient), and thermal (specific heat, thermal conductivity, and thermal diffusivity) of common bean grain as a function of water content. Furthermore, the drying kinetics and thermodynamic properties (enthalpy, entropy, and Gibbs free energy) of drying were obtained for different temperatures. This comprehensive determination of the properties and behavior of bean grains during drying will be of great use not only for industry but for all areas that require specific knowledge of the evaluated properties. To determine the aforementioned properties, except for drying kinetics and thermodynamic properties, bean grains with an initial water content of 0.41 (decimal, d.b.) were dried at 45 ± 2 °C to different levels of water content. The properties were obtained experimentally, and regression models were adjusted to represent the variation of properties as a function of water content. To obtain the geometric properties, an algorithm in the Phyton language was developed to obtain the characteristic dimensions of the grains from digital images. The results were compared to the traditional method, where measurements are obtained by a digital caliper. To determine the drying kinetics and thermodynamic properties of the drying of bean grains, the grains were subjected to drying at different temperatures (40, 50, 60, 70, and 80 ± 2 °C). The experimental data

were adjusted to literature models commonly used to describe the drying process of agricultural products. In addition, a CFD (Computational Fluid Dynamics) analysis was carried out to demonstrate the feasibility of computational modeling in predicting the drying process. The results obtained in this study showed that the use of digital images to obtain the characteristic dimensions of grains was highly effective. Among the geometric properties, projected area and volume showed the greatest variations during drying. The Araujo-Copace model satisfactorily described the volumetric contraction of the grains. Among the physical, aerodynamic, and thermal properties, the 1000-grain weight, the drag coefficient, and the thermal conductivity showed the greatest variations during the drying process. The modified Henderson and Pabis model satisfactorily represented the drying kinetics of bean grains at all evaluated drying temperatures. CFD analysis proved to be a powerful tool for predicting the drying process, with low errors compared to experimental data. The effective diffusion coefficient and the thermodynamic properties of drying showed values consistent with those found for other agricultural products.

Keywords: Moisture diffusivity. Numerical modeling. *Phaseolus vulgaris*. Size and shape. Volumetric contraction.

RESUMO GERAL

ARAUJO, Marcos Eduardo Viana de, D.Sc., Universidade Federal de Viçosa, abril de 2023. **Cinética de secagem e modelagem das propriedades físicas de grãos de feijão**. Orientador: Paulo Cessar Corrêa.

O feijão é uma das leguminosas mais produzidas e consumidas em todo mundo. A qualidade nutricional desse alimento, o tornou constituinte fundamental na dieta de milhares de pessoas todos os dias. No entanto, as perdas observadas durante a cadeia produtiva dessa cultura, mostram que os equipamentos e operações são dimensionados/conduzidas de forma ineficiente. Ao longo dos anos, o avanço tecnológico da indústria de alimentos tem exigido dados atualizados sobre as propriedades de engenharia dos produtos agrícolas, com o objetivo de otimizar os processos e reduzir perdas em todos os passos da cadeia produtiva agrícola. Embora a determinação das propriedades de vários produtos esteja disponível na literatura, o melhoramento genético e avanço de cultivares tem feito com que a indústria otimize seus processos baseando-se em dados obsoletos, que não mais representam as características do material. Diante do exposto, este estudo objetivou determinar e modelar as propriedades geométricas (circularidade, esfericidade, diâmetro geométrico, área projetada, área superficial, volume e relação superfície-volume), físicas (massa especifica real e aparente, porosidade e massa de 1000-grãos), aerodinâmicas (velocidade terminal e coeficiente de arrasto), e térmicas (calor específico, condutividade térmica e difusividade térmica) de grão de feijão comum em função do teor de água. Além disso, a cinética de secagem e as propriedades termodinâmicas (entalpia, entropia e energia livre de Gibbs) da secagem foram obtidas para diferentes temperaturas. Essa determinação abrangente das propriedades e comportamento dos grãos de feijão durante a secagem será de grande utilidade não apenas para indústria, mas para todas as áreas que exijam o conhecimento específico das propriedades avaliadas. Para determinação das propriedades supracitadas, com exceção da cinética de secagem e propriedades termodinâmicas, grãos de feijão com teor de água inicial de 0,41 (decimal, d.b.) foram secos à 45 ± 2 °C até diferentes níveis de teor de água. As propriedades foram obtidas experimentalmente e modelos de regressão foram ajustados para representar a variação das propriedades em função do teor de água. Para obtenção das propriedades geométricas, um algoritmo em linguagem Phyton foi desenvolvido para obter as dimensões características dos grãos a partir de imagens digitais. Os resultados foram comparados ao método tradicional, onde as medições são obtidas por um paquímetro digital. Para determinação da cinética de secagem e das propriedades termodinâmicas da secagem dos grãos de feijão, os grãos foram

submetidos à secagem em diferentes temperaturas (40, 50, 60, 70 e 80 ± 2 °C). Os dados experimentais foram ajustados à modelos da literatura comumente utilizados para descrever o processo de secagem de produtos agrícolas. Além disso, uma análise em CFD (Computational Fluid Dynamics) foi realizada para demonstrar a viabilidade da modelagem computacional na previsão do processo de secagem. Os resultados obtidos neste estudo mostraram que o uso de imagens digitais para obtenção das dimensões características dos grãos foi altamente eficaz. Dentre as propriedades geométricas, área projetada e volume apresentaram as maiores variações durante a secagem. O modelo Araujo-Copace descreveu satisfatoriamente a contração volumétrica dos grãos. Dentre as propriedades físicas, aerodinâmicas e térmicas, o peso de 1000-grãos, o coeficiente de arrasto e a condutividade térmica apresentaram as maiores variações durante o processo de secagem. O modelo de Henderson e Pabis modificado representou satisfatoriamente a cinética de secagem dos grãos de feijão em todas as temperaturas de secagem avaliadas. A análise em CFD se mostrou uma poderosa ferramenta para predição do processo de secagem, com erros baixos se comparado aos dados experimentais. O coeficiente de difusão efetivo e as propriedades termodinâmicas da secagem apresentaram valores consistentes com os encontrados para demais produtos agrícolas.

Palavras-chave: Difusividade de umidade. Modelagem numérica. *Phaseolus vulgaris*. Tamanho e forma. Contração volumétrica.

SUMMARY

GENERAL INTRODUCTION

Common bean (*Phaseolus vulgaris*) is one of the most produced and consumed legumes worldwide. This legume is widely consumed in underdeveloped countries mainly due to its high protein content (higher than 20%) at a lower cost than proteins of animal origin (Ribeiro et al., 2023). In addition to being an excellent source of protein, other compounds such as vitamins, minerals, carbohydrates, fiber, and phenolic compounds have made this food an essential constituent in the diet of millions of people daily (Valencia-Mejía et al., 2019). Most of the beans harvested are dried and stored to ensure that the product can be offered throughout the year. Drying grains and seeds reduce their water activity, increasing the product's shelf life. In addition, reducing the water content reduces the weight and volume of the product, facilitating and reducing storage and transportation costs (Pravallika et al., 2023).

So that beans can be offered continuously throughout the year, the harvested beans must be cleaned, dried, separated, transported, and finally stored. Therefore, knowledge of grain properties is crucial in reducing costs and optimizing each process (Onwe et al., 2020). The removal of water during the drying process causes structural and physical-chemical changes in the material. Over the years, several studies have demonstrated the importance of obtaining the engineering properties of grains as a function of water content (Jan et al., 2018; Bajpai et al., 2019; Mohite et al., 2019). The management and development of highly productive cultivars, good quality, resistant to diseases, and environmentally adaptable, can influence the structure and properties of grains, making determining these properties essential and significant for each product.

Data referring to the size and shape of grains and seeds are widely used to design and optimize sieves, separators, and seeder discs, better understand heat and mass transfer, and for various operations that use air movement and flow in post-harvest operations (Araujo et al., 2018). The characteristic dimensions of the grains (length, width, and thickness) are essentially obtained using manual measurement with calipers. This method has some limitations regarding the number of data collected, the quality of the measures, and obtaining reliable data for grains and seeds of small size. Therefore, some authors have developed algorithms to get these dimensions based on digital images in recent years. Cervantes et al. (2016) highlighted that using digital images allows obtaining data more quickly for a wide range of shape parameters and grains and seeds of all sizes.

Physical, aerodynamic, and thermal properties are essential throughout the grain and seed production chain. Knowing the behavior of these properties during drying allows the elaboration of effective strategies to optimize different processes and equipment. While the geometric properties allow the grains to be separated and classified by sieves, the physical and aerodynamic properties allow them to be separated, classified, and transported by densimetric or pneumatic methods. It is known that each particle or product presents different reactions in relation to the aerodynamic forces that act on them when subjected to airflow. Therefore, obtaining data about these properties becomes a fundamental requirement for the correct operation and development of machines.

Drying is a complex process that simultaneously involves heat and mass transfer, which are affected by the internal and external resistances of the product (Adnouni et al., 2023). The grain's thermal properties largely govern the heat transfer during desorption. Several authors have already demonstrated that these properties are highly dependent on the water content of the product, and the data are necessary for the optimization and correct operation of thermal processes (Matouk et al., 2018; Oriola et al., 2020; Ikegwu, 2021; Adeyanju et al. al., 2022). In addition to drying, data referring to thermal properties can be helpful in any operation involving heat transfer, such as bleaching, cooking, heating, and cooling (Mohsenin, 1986).

In addition to thermal properties, a detailed understanding of the drying process also requires knowledge of the drying kinetics of the product and its thermodynamic properties. Knowledge of the kinetic behavior of drying is a fundamental factor for the design, optimization, and control of drying (Bissaro et al., 2022). This technique helps to understand how the water removal progress occurs and is essential to determine the most suitable conditions for drying (Najib et al., 2022). At the same time, obtaining thermodynamic properties play a fundamental role in describing reactions and phenomena that occur at the intramolecular level in biological materials (Karataş and Arslan, 2022). The study of these properties allows for calculating the energy required for drying, evaluating the properties of water and its relationship with the microstructure of food, and studying the physical phenomena that occur on the surface of the product (Öztekin et al., 2022).

The traditional approach to obtaining drying curves is based on experiments, where the product is weighed periodically during the drying process at different temperatures. However, the continuous advancement of computers has made researchers worldwide turn their attention to the numerical modeling of this process. Azmir et al. (2020) highlighted that numerical approaches had become powerful tools, allowing new procedures to be developed

and optimized with relatively low costs. Among the various numerical techniques, computational fluid dynamics (CFD) has gained prominence in the scientific community (Prommuak et al., 2020). This tool allows several drying conditions to be evaluated without restarting experiments. Computer simulation allows of assessing parameters such as water content, drying air velocity, grain, and drying air temperature in experimentally inaccessible locations. Furthermore, the simulations are sensitive to small changes, and obtaining local data is possible after building the numerical model (Malekjani and Jafari, 2018).

Although drying is an essential operation in post-harvest processing, and updated data on grain properties during this process are necessary for designing and optimizing equipment and techniques, the literature on obtaining the dimensional, physical, aerodynamic, and thermal properties and the drying kinetics and determination of thermodynamic properties of bean grains are scarce. Besides, most of the data needs to be updated and completed. Therefore, this study aimed to comprehensively evaluate and model the dimensional (by the standard method and digital images), physical, aerodynamic, and thermal properties of bean grains during drying. In addition, experimentally and numerically (CFD) determine the drying kinetics for different temperatures.

REFERENCES

Adeyanju, J.A., Abioye, A.O., Adekunle, A.A., Ajala, A.S., Oloyede, A.A., Afolayan, E.T. Assessment of Physical and Thermal Properties of Velvet Bean (Mucuna pruriens) as Potentials for Development of Processing Machines. **Journal of Engineering and Technology**, v.7, p.122-125, 2022

Adnouni, M., Jiang, L., Zhang, X.L., Zhang, L.Z., Pathare, P.B., Roskilly, A.P. Computational modelling for decarbonised drying of agricultural products: Sustainable processes, energy efficiency, and quality improvement. **Journal of Food Engineering**, v.338, 111247, 2023.

Araujo, M.E.V., Barbosa, E.G., Gomes, F.A., Teixeira, I.R., Lisboa, C.F., Araujo, R.S.L, Corrêa, P.C. Physical properties of sesame seeds harvested at different maturation stages and thirds of the plant. **Chilean Journal of Agricultural Research**, v.79, p.495-502, 2018.

Azmir, J., Hou, Q., Yu, A. CFD-DEM study of the effects of food grain properties on drying and shrinkage in a fluidised bed. **Powder Technology**, v.360, p.33-42, 2020.

Bajpai, A., Kumar, Y., Singh, H., Prabhakar, P.K., Meghwal, M. Effect of moisture content on the engineering properties of Jamun (*Syzgium cuminii*) seed. **Journal of Food Process Engineering,** v.43, e13325, 2019.

Bissaro, C.A., de Souza Matias, G., Defendi, R.O., de Matos Jorge, L.M. Modeling the drying kinetics of soybeans under intermittent operation in thin layer. **Food and Bioproducts Processing**, v.136, p.226-235, 2022.

Cervantes, E., Martín, J.J., Saadaoui, E. Updated Methods for Seed Shape Analysis. **Scientifica (Cairo)**, v.2016, 5691825, 2016.

Ikegwu, O.J. Effect of moisture and temperature on thermal conductivity of pigeon pea seeds. **Agricultural Engineering International: CIGR Journal**, v.23, p.217-224, 2021.

Jan, K.N., Panesar, P.S., Singh, S. Effect of moisture content on the physical and mechanical properties of quinoa seeds. **International Agrophysics**, v.33, p.41-48, 2018.

Karataş, M., Arslan, N. Moisture sorption isotherms and thermodynamic properties of cowpea (Vigna unguiculate L. Walp) stored in a chamber under controlled humidity and temperature. **Journal of Food Process Engineering**, v.45, p.1-14, 2022.

Malekjani, N., Jafari, S.M. Simulation of food drying processes by Computational Fluid Dynamics (CFD); recent advances and approaches. **Trends in Food Science & Technology**, v.78, p.206-223, 2018.

Matouk, A.M., El-Kholy, M.M., Tharwat, A., Shamala, S.F. Thermal properties of some legume seeds. **Journal of Soil Sciences and Agricultural Engineering**, v.9, p.261-267, 2018.

Mohite, A.M., Sharma, N., Mishra, A. Influence of different moisture content on engineering properties of tamarind seeds. **Agricultural Engineering International: CIGR Journal**, v.21, p.220-224, 2019.

Mohsenin, N.N. **Physical properties of plant and animal materials**. New York: Gordon and Breach Publishers, 1986. 841p.

Najib, T., Heydari, M.M., Meda, V. Combination of germination and innovative microwave-assisted infrared drying of lentils: effect of physicochemical properties of different varieties on water uptake, germination, and drying kinetics. **Applied Food Research**, v.2, 100040, 2022.

Onwe, D.N., Umani, K.C., Olosunde, W.A., Ossom, I.S. Comparative analysis of moisture-dependent physical and mechanical properties of two varieties of African star apple (*Chrysophyllum albidum*) seeds relevant in engineering design. **Scientific African**, v.8, e00303, 2020.

Oriola, K.O., Hussein, J.B., Oke, M.O., Abimbola, A. Description and evaluation of physical and moisture-dependent thermal properties of jack bean seeds (*Canavalia ensiformis*). **Journal of Food Processing and Preservation**, v.45, e15166, 2020.

Öztekin, Y.B., Aktaş, M., Dolgún, E.C., Bilim, H.C., Sacilik, K. Drying kinetics and thermodynamic properties of Uzun pistachios dried by convective drying. **Journal of Food Processing and Preservation**, v.46, p.1-13, 2022.

Pravallika, K., Chakraborty, S., Singhal, R.S. Supercritical drying of food products: An insightful review. **Journal of Food Engineering**, v.343, 111375, 2023.

Prommuak, C., Tharangkool, N., Pavasant, P., Ponpesh, P., Jarunglumlert, T. Computational fluid dynamic design of spent coffee ground cabinet dryer using recycled heat from air compressor. **Chemical Engineering Research and Design**, v.153, p.75-84, 2020.

Ribeiro, J.V.V., Graziani, D., Carvalho, J.H.M., Mendonça, M.M., Naves, L.M., Oliveira, H.F., Campos, H.M., Fioravanti, M.C.S., Pacheco, L.F., Ferreira, P.M. Pedrino, G.R., Ghedini, P.C., Fernandes K.F., Batista, K.A., Xavier, C.H. **Current Research in Food Science**, v.6., 100410, 2023.

Valencia-Mejía, E., Batista, K.A., Fernández, J.J.A, Fernandes, K.F. Antihyperglycemic and hypoglycemic activity of naturally occurring peptides and protein hydrolysates from easy-to-cook and hard-to-cook beans (*Phaseolus vulgaris* L.). **Food Research International**, v.121, p.238-246, 2019.

CHAPTER 1

DIGITAL IMAGE ANALYSIS AS AN ALTERNATIVE TECHNIQUE TO OBTAIN THE GEOMETRIC PROPERTIES OF BEAN GRAINS (*PHASEOLUS VULGARIS* L.) DURING DRYING

Abstract: The geometric properties of grains are essential for the separation, design, and operation of equipment and process control throughout the production chain. Obtaining these properties may require time and care by the conventional method; therefore, image processing has gained space as an equally accurate alternative for obtaining grain dimensions. This study aimed to determine the geometric properties of bean grains during drying. The image processing technique was used to improve the acquisition of the dimensions of the grains, compared to the traditional method using a caliper. Common bean grains harvested with a water content of 0.41 (decimal d.b.) were dried to different water contents in a tray dryer at 45 ± 2°C and characterized by their size and shape properties. The image processing technique was satisfactory for obtaining the size and shape of the bean grains. All properties showed a significant difference ($P \leq 0.05$) during drying, except for circularity. Geometric diameter, projected area, surface area, and volume reduced during drying, with values varying between 7.54–7.35mm, 64.11–59.01 mm^2, 191.35–180.31 mm^2, and 225.0–208.1 mm^3, respectively. The sphericity and the surface-to-volume ratio increased with the reduction of the water content varying between 64.6-66% and 0.85-0.87, respectively. The bean grains showed a volumetric contraction of 7.7%, satisfactorily represented by the Araujo-Copace model.

Keywords: Mathematical modeling; Optimization. Size and shape. Volumetric contraction.

1. INTRODUCTION

The common bean (*Phaseolus vulgaris* L.) is one of the most consumed legumes in the world. Although the origin of the common bean is America, the marketing and distribution of this crop currently cover almost all geographic locations around the globe (Hernández-Guerrero et al., 2021). The common bean is an essential source of protein, vitamins, minerals, and fiber (Ennoury et al., 2022). It is considered a crop of relevant economic and social importance, especially in developing countries (Ajermoun et al., 2022).

At world levels, grain losses due to inadequate storage conditions (high product water content, inadequate temperature, and relative humidity in warehouses, among others) can reach 30% (Sandoval-Peraza et al., 2021). Due to the seasonality of common bean production, storage becomes essential so that the demand for the product can be supplied outside the production period (Bento et al., 2022). However, before storage, the beans must be transported, separated, cleaned, and dried, ensuring the quality of the product. For these processes to be carried out efficiently, it is necessary to know several properties of the grains, of which we can highlight the geometric properties (Araujo et al., 2018). Oliveira et al. (2021) reported that knowledge about the size and shape of the grain is essential for the optimization and improvement of any process that involves the movement and flow of air during the production chain of agricultural products. Furthermore, Eissa et al. (2010) reported that separating grains and seeds according to their geometric properties guarantees the best performance of post-harvest processing equipment and, consequently, better final product quality.

Reducing the product's water content during drying can directly affect its geometric properties and quality. Monitoring the geometric properties of grains and seeds during drying is essential for this process to be carried out as quickly, safely, and economically as possible (Lisboa et al., 2019). The optimal design and commercial viability of new equipment can be readily evaluated with adequate information on the behavior of dimensional grain properties with reduced water content. With the increase in demand for data on the geometric properties of grains and seeds for equipment design and process optimization, several authors sought to evaluate and model the variation of these properties for different agricultural products during drying, such as kenaf seeds (Izli, 2015), yellow lentils (Isik and Izli, 2016), sorghum grains (Gely and Pagano, 2017), African star apple seeds (Onwe et al., 2020), coffee cherries (Araujo et al., 2021a), among others and generally reported immediate changes with water content.

Technically, data for analyzing the size and shape of grains and seeds can be obtained in manual and computational ways. The traditional and standard way is to measure the grains' length, width, and thickness using a caliper or similar equipment. However, the manual method has some limitations in the number of data collected, the quality of measurements, and obtaining reliable data for tiny grains and seeds, among others. On the other hand, computational methods have gained space in recent years with the advancement in digital image processing. In previous work, Araujo et al. (2018) used digital image analysis to obtain some geometric properties of sesame seeds harvested from different thirds of the plant. They showed that the computational method is much faster and more efficient than the conventional method, even for tiny seeds. By using digital images, it is possible to automatically obtain data for various shape parameters, for grains and seeds of all sizes, and for several grains simultaneously (Cervantes et al., 2016).

Although the importance of geometric properties is known, the changes caused by the genetic improvement and adaptation of species over the years make the industries and studies be carried out with obsolete and incomplete data. Therefore, the aim of this study was to determine and model the geometric properties and volumetric shrinkage of bean grains obtained by standard methodology and by digital image analysis. Namely, this is the first study in the literature to determine and model the geometric properties of common bean grains during the drying process in a comprehensive and detailed manner using a caliper and digital image processing.

2. MATERIAL AND METHODS

2.1. Obtaining the raw material

This study was carried out at the Laboratory of Physical Properties and Quality Assessment of Agricultural Products at the National Center for Storage Training (CENTREINAR), located at the Federal University of Viçosa (UFV), Viçosa - Minas Gerais, Brazil. Common bean grains of the BRS–Estilo variety were used in this study. The samples used in this study were collected wet with an initial water content of 0.41 (decimal, d.b.), in the experimental area belonging to the Department of Agronomy of the Federal University of Viçosa (20°45'00" S, 42°56'15" W; 643 m a.s.l.). The harvested pods were subjected to the manual threshing process to reduce the mechanical damage to the wet grains. The threshed grains were submitted to an initial sorting and selected for color uniformity (eliminating green

grains that did not reach physiological maturity) and average size (eliminating sluggish and malformed grains). The threshed grains were immediately stored in the biochemical oxygen demand (BOD) chamber at 4 ± 2 °C until the beginning of the experiments.

2.2. Sample preparation

A tray dryer GrainMan 6623 was used to dry the common bean grains. The grains were dried to different water contents using a fixed temperature of 45 ± 2 °C. During drying, 4 samples of grains were taken for each reading to monitor the variation in water content. The samples were taken to an oven at 105 ± 2 °C for 24 hours, according to the standard method described in Brasil (2009), and the results were expressed on a dry basis (d.b.). A Marte® AY220 analytical balance with a precision of 0.0001g was used to measure the weights of the samples during the determination of the water content.

During drying, the bean grains were removed from the dryer and homogenized. After homogenization, the samples were taken to determine the evaluated properties. The experiments were conducted in 4 repetitions for each water content. Each repetition consisted of 10 grains. The water contents obtained were 0.407, 0.384, 0.364, 0.338, 0.274, 0.254, 0.236, 0.219, 0.200, and 0.176 (decimal, d.b.).

2.3. Geometric properties

2.3.1. Standard method

For each water content, 10 grains were selected to compose each of the four repetitions. The length (L), width (W), and thickness (T) of the grains (Figure 1) were determined using a Mitutoyo 500-174B digital caliper with a resolution of 0.01 mm, and by digital image analysis, detailed in the following subsection.

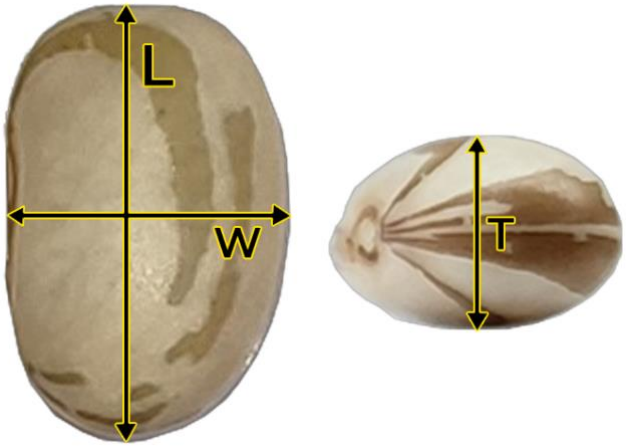

Figure 1. Orthogonal axes of common bean grains: (L) length, (W) width, and (T) thickness.

2.3.2. Image acquisition and processing

A step-shaped platform was built with cardboard to acquire the images. The 10 grains of each replicate were arranged in a row on the platform. An ISOCELL HM2 camera (Samsung) with a resolution of 108 Megapixels, Aperture Size of F1.9, and autofocus was used to capture the images, positioned approximately 0.15 m from the grain line. A 12W LED lamp next to the camera was used to reduce the formation of shadows during capturing images. A 5×5 mm square stamped on the platform was used to obtain the spatial resolution of the image automatically.

Two photos were taken for each repetition to obtain the orthogonal axes of the grains. One of the images allowed obtaining the L and W axes (top view of the grains), while the other allowed obtaining the T axis (front view of the grains). The images obtained were processed using the free software Jupyter (Anaconda®). An algorithm in Python was developed, and a summarized step-by-step of the processing is presented in Figure 2. The images initially obtained in the RGB color space were first transformed into monochromatic images. For this, the algorithm defined and used the band with the highest contrast. The images were then subjected to a noise reduction, applying a median-type smoothing filter with a 5×5 mask. After this process, the image was binarized using the OTSU method. Minimum and maximum filters were used to fill in possible flaws in the grain boundary. The negative of the binarized image was used for scanning and detecting objects (grains). With the grains identified, the algorithm performed a matrix separation of each grain, and the detection of boundaries was performed using the descriptors.

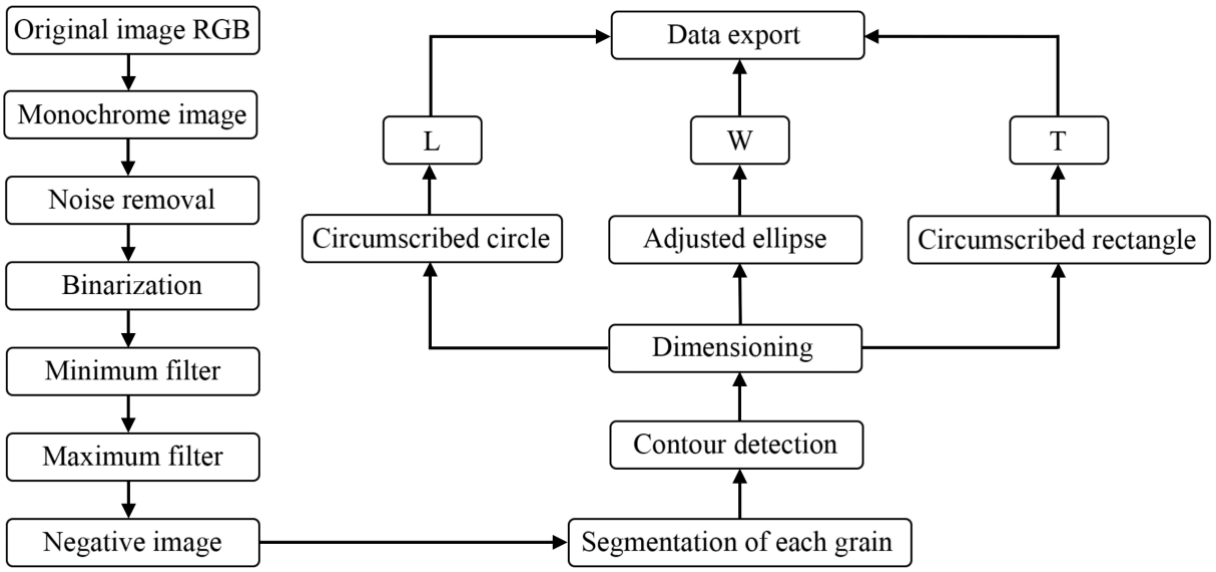

Figure 2. Algorithm for obtaining the characteristic dimensions L (length), W (width), and T (thickness) of common bean grains, using the image processing technique.

The determination of the characteristic dimensions was carried out using some shape descriptors. The most minor circumscribed circle descriptor was used to obtain the length of the grains. This descriptor allowed us to obtain the diameter of the smallest circle that involved the grain; this diameter was determined as the characteristic dimension L (length). The width of the grains was determined using the descriptor of the adjusted ellipse. This descriptor provided the diameter of the major and semi-major axis of the ellipse that best fitted the grain. The semi-major axis value was defined as the characteristic dimension W (width). The most minor circumscribed rectangle descriptor was used to obtain the grain thickness. The T axis of the grains was considered the height of this rectangle obtained by the descriptor. After obtaining all the data, the algorithm exported the data to a spreadsheet for each repetition evaluated. Figure 3 presents an example of the initial steps performed by the algorithm.

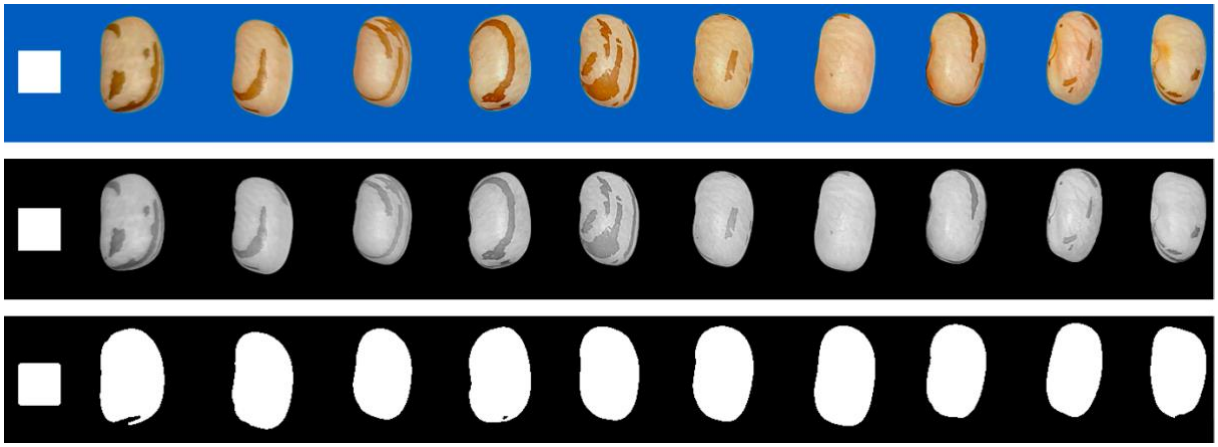

Figure 3. Example of the initial steps performed by the algorithm to obtain the characteristic dimensions of bean grains.

2.3.3. Validation of data obtained by image processing

After obtaining the grains' dimensional data by image and caliper, an analysis of the Bland-Altman plot was performed (Bland and Altman, 1995). This method can be used to compare an alternative method when the data from the reference method are available (Bahar et al., 2017). The data obtained by digital image were plotted on the Y axis for each value of the reference method (caliper) plotted on the X axis. The plotted data were submitted to linear regression to obtain the coefficients β_1 and β_0. For perfect agreement between the methods evaluated, β_1 must be equal to 1, while β_0 must be zero. The hypotheses were tested using the t-test.

2.3.4. Evaluated properties

After determining the orthogonal axes of the grains by digital image and caliper, the circularity, sphericity, geometric diameter, projected area, volume, surface area, and the surface-volume ratio were obtained according to Equations 1 to 7, respectively, as proposed by Mohsenin (1986).

$$C = \left[\frac{W}{L}\right] \times 100 \quad (1)$$

$$S = \left[\frac{(LWT)^{1/3}}{L}\right] \times 100 \quad (2)$$

$$D_g = (LWT)^{1/3} \quad (3)$$

$$A_p = \frac{\pi LW}{4} \quad (4)$$

$$V = \frac{\pi\, W\, T\, L}{6} \quad (5)$$

$$A_s = \frac{\pi WT}{2} + \left[\left(\frac{\pi L (WT)^{1/2}}{2\left[1 - \left(\frac{WT}{L^2}\right)\right]^{1/2}} \right) \sin^{-1}\left[1 - \left(\frac{WT}{L^2}\right)\right]^{1/2} \right] \quad (6)$$

$$SVR = \frac{A_s}{V} \quad (7)$$

Where,

L – Length (mm)
W – Width (mm)
T – Thickness (mm)
V – Unit volume (mm^3)
A_s – Surface area (mm^2)
S – Sphericity (%)
C – Circularity (%)
A_p – Projected area (mm^2)
D_g – Geometric diameter (mm)
SVR – Surface-to-volume ratio (decimal)

The volume ratio for each water content (V) and the initial volume (V_0) was determined during drying to evaluate the variation in bean grain size. Thus, the unitary volumetric contraction of the common beans (Ψ) was obtained according to Equation 8.

$$\Psi = \frac{V}{V_0} \quad (8)$$

The experimental data of the unit volumetric contraction index were fitted to the mathematical models commonly used to predict the volumetric contraction of agricultural products, presented in Table 1.

Table 1 – Volumetric contraction models used for agricultural products.

Reference	**Model**	**Equation**
Bala and Woods (1984) adapted	$\Psi = 1 - \beta_0 \{1 - exp[-\beta_1(U_0 - U]\}$	(9)
Corrêa et al. (2004)	$\Psi = [\beta_0 + \beta_1 exp(U)]^{-1}$	(10)
Rahman (1995)	$\Psi = 1 + \beta_0(U - U_0)$	(11)
Linear	$\Psi = \beta_0 + \beta_1 U$	(12)
Exponential	$\Psi = \beta_0 exp(\beta_1 U)$	(13)
second-degree polynomial	$\Psi = \beta_0 + \beta_1 U + \beta_2 U^2$	(14)
Araujo-Copace (Araujo et al., 2021a)	$\Psi = (\beta_0 + \beta_1 U)^{-1/\beta_2}$	(15)

Where,

U – Water content (decimal d.b.)

U_0 – Initial water content (decimal d.b.)

β_0, β_1, β_2 – Coefficients that depend on the product.

After mathematical modeling and fitting the data to the previously mentioned models, a nonlinear regression analysis was performed. The STATISTICA 8.0® software was used to apply the Gauss-Newton method to determine the parameters of the models. The choice of the model that best represented the phenomenon was based on several statistical parameters. The t-test at 5% probability was adopted to verify the significance of the regression coefficients. The high value of the coefficient of determination (R^2) and low values of the mean relative error (P) and standard deviation of the estimate (SE) were considered indicators for the best model. Furthermore, the distribution of residuals was determined to guarantee the randomness of the regression coefficients estimation. The mean relative error and the standard deviation of the estimate were obtained according to Equations 16 and 17, respectively.

$$P = \frac{100}{n} \sum_{i=1}^{n} \frac{\left|Y_i - \hat{Y}_i\right|}{Yi} \tag{16}$$

$$SE = \sqrt{\frac{\sum_{i=1}^{n}\left(Y_i - \hat{Y}_i\right)^2}{DFR}} \quad (17)$$

Where,

Y_i – Observed value;

$\hat{Y}_i$ – Estimated value;

n – Number of observed data; and

DFR – Degrees of freedom of the residue.

The Akaike Information Criterion (AIC) and Schwarz's Bayesian Information Criterion (BIC) were also used as statistical evaluators of the best model to predict the volumetric contraction of the bean grains during the drying process. AIC (Equation 18) is an evaluator that uses more complex selection, as verisimilitude is a qualitative character. BIC (Equation 19) is similar to AIC in terms of verisimilitude, but it presents different penalties regarding the number of estimated parameters (Burnham & Anderson, 2004). Lower values of both parameters indicate a better fit of the model (Akaike, 1974; Schwarz, 1978). The values of AIC and BIC were obtained using the software R 4.1.0.

$$AIC = -2\log L + 2p \quad (18)$$

$$BIC = -2\log L + p\ln(N) \quad (19)$$

Where,

p – Number of parameters in the model;

L – Maximum Likelihood; and

N – Total number of observations.

2.4. Data analysis

Analysis of variance (ANOVA) and regression were applied to the data obtained for each of the properties evaluated. The analyzes were performed using the statistical analysis software STATISTICA 8.0® and SISVAR. Regression models for each property were chosen

according to the model's fit to the experimental data and the magnitude and significance of the determination and regression coefficients.

3. RESULTS AND DISCUSSION

3.1. Comparison of methods for obtaining characteristic dimensions

Table 2 presents the coefficients of the linear regression models for the characteristic dimensions of bean grains during drying for the two methods evaluated in this study. For all characteristic dimensions, the regression adjustments showed high values for the coefficient of determination, demonstrating a high degree of correlation between the data obtained by the two methods. The regression coefficient β_1 presented values close to 1, indicating an excellent correspondence between the methods evaluated (Bland and Altman, 1995). The t-test did not show the significance for the parameter β_0; therefore, we can accept the null hypothesis and say that β_0 equals 0. This result shows that the regression line fitted to the data does not show displacement with the origin. From these results, we can assume that the method proposed (digital image) in this study to obtain the geometric properties of bean grains is satisfactory compared to the standard method (caliper).

Table 2 – Coefficients of linear regression models for the dimensions of common bean grains obtained by image and caliper during drying.

Characteristic dimension	β_0	β_1	R^2
Length (L)	0.1194	0.9892^{++}	0.9637^{**}
Width (W)	0.2365	0.9756^{++}	0.9492^{**}
Thickness (T)	0.0862	0.9817^{++}	0.9582^{**}

$^{++}$ Significant at 1% probability by the t-test, ** Significant at 1% probability by the F test.

The correspondences of the averages of the characteristic dimensions obtained by caliper and digital image are presented in Figures 4A, 3B, and 3C for length, width, and thickness, respectively. The slight difference observed between the data is associated with errors in obtaining the images and handling the caliper. The random distribution of the data around the regression line shows that the image analysis method to obtain the bean grain dimensions does not underestimate or overestimate the values compared to the reference method. There was no significant difference between the methods evaluated in this study, and

it is concluded that the methods are equivalent. This result is significant since using images to obtain geometric properties of grains reduces the time of the experiments and eliminates the errors related to the manual measurement of the grains. In addition, image acquisition and processing can be automated, eliminating the need for manual image acquisition and algorithm initialization.

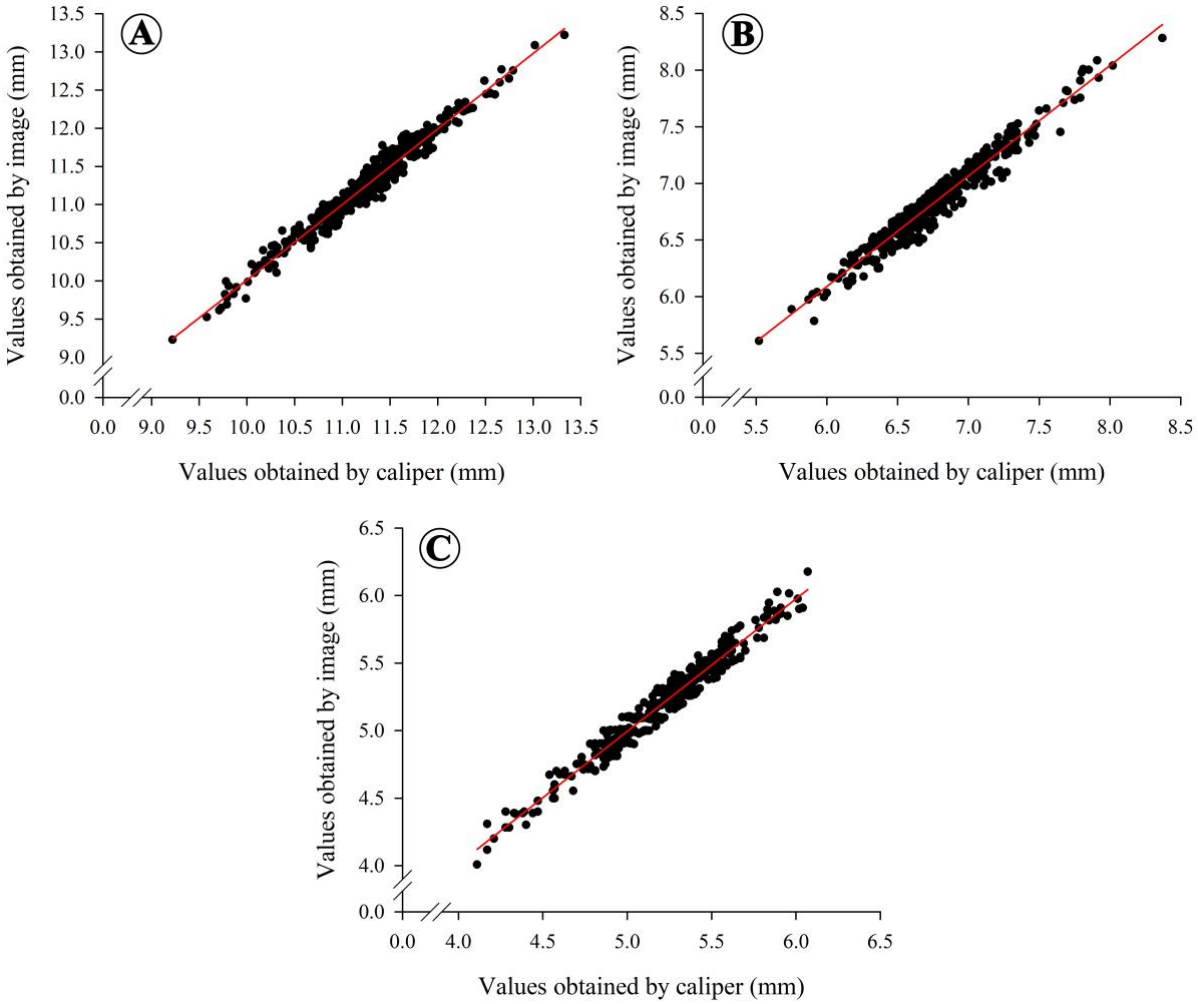

Figure 4. Correspondence of means of characteristic dimensions: length (L), width (W), and thickness (T) of bean grains obtained by caliper and image.

3.2. Geometric properties

According to the results presented by ANOVA, except for circularity, all other geometric properties of bean grains are significantly different ($P \leq 0.05$) at different water content during drying. This section presents the data for both methods evaluated in this study.

The mean circularity of the bean grains for the different water contents and their respective deviations are presented in Table 3.

Table 3 – Mean values and respective standard deviations of common bean grain circularity (C) as a function of water content.

Water content (Dry basis)	Circularity (%)	
	Caliper	Image
0.41	59.93 ± 0.240	59.97 ± 0.109
0.38	60.02 ± 0.136	60.03 ± 0.098
0.36	60.14 ± 0.106	60.16 ± 0.083
0.34	60.14 ± 0.152	60.17 ± 0.080
0.27	60.41 ± 0.137	60.39 ± 0.089
0.25	60.48 ± 0.149	60.50 ± 0.080
0.24	60.49 ± 0.172	60.53 ± 0.077
0.22	60.61 ± 0.163	60.63 ± 0.106
0.20	60.58 ± 0.138	60.61 ± 0.067
0.18	60.64 ± 0.116	60.65 ± 0.079

The circularity of the bean grains increased during drying, varying between 59.9 and 60.6% for the water contents between 0.41 and 0.18 d.b., respectively. The slight variation in this property indicates that during the drying of bean grains, a reduction of the orthogonal axes W (width) and L (length) occurs almost proportionally. Paixão et al. (2020) reported a linear increase of approximately 4% in the circularity of beans of the BRSMG Majestoso variety during the drying process. Similar behavior was also reported for passion fruit seeds (Araujo et al., 2020).

The behavior of the sphericity of the beans during drying is shown in Figure 5. The sphericity of the beans increased linearly with the reduction of the water content, varying between 66.0 and 64.6%. Standardization of the values as a function of the highest observed value was performed for the standard method (caliper) and displayed on the right Y axis. This standardization allows you to evaluate property variance without looking at absolute values. A variation of approximately 2.1% was observed during drying. These results agree with those reported for other products, such as green wheat grains (Al-Mahasneh and Rababah, 2007) and melon seeds (Bande et al., 2012) during drying. Although the variation in this property is slight during drying, these data are handy for classifying and separating common bean grains

and other varieties and species. For example, cowpea beans can have sphericity greater than 80% (Altuntas and Demirtola, 2007).

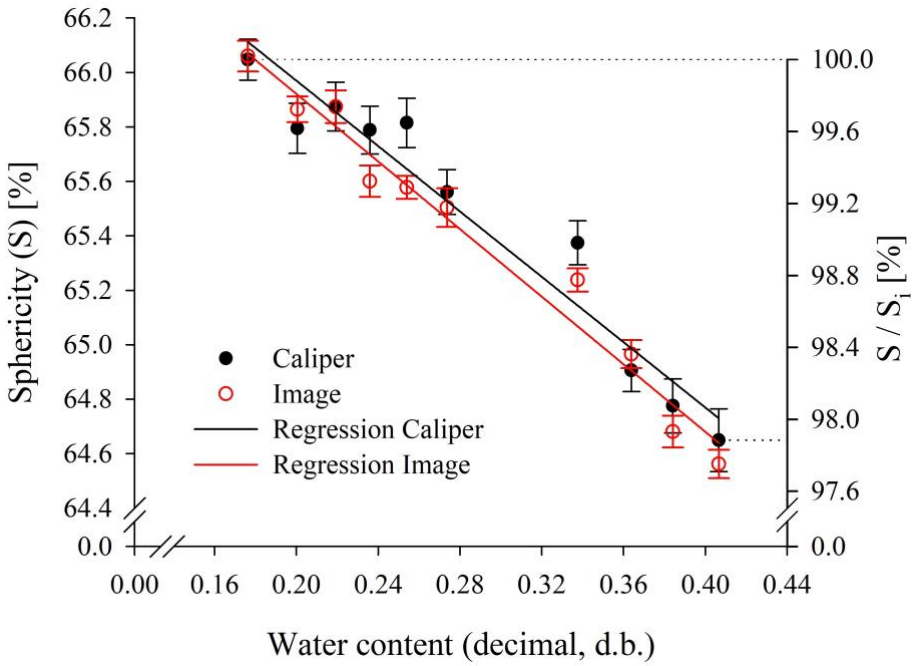

Figure 5. Observed and estimated values of the sphericity of bean grains from the digital caliper and image data. The subscript "i" represents the highest value of the property. Error bars represent the standard deviation.

Figure 6A shows the geometric diameter variation of the common beans during the drying process. The values of the geometric diameter varied between 7.54 and 7.31 mm for the water contents between 0.41 and 0.18 d.b. A nonlinear reduction of approximately 3% was observed throughout the drying process. This reduction is expected since this property is obtained by the cubed root of the three dimensions of the grains, which changes the drying process. Similar results have been reported for several agricultural products such as fenugreek (Meghwal and Goswami (2012), barley (Sologubik et al., 2013), melon grains and seeds (Obi and Offorha, 2015), sorghum grains (Gely and Pagano, 2017), ajwain seeds (Singh and Megwal, 2019), among others.

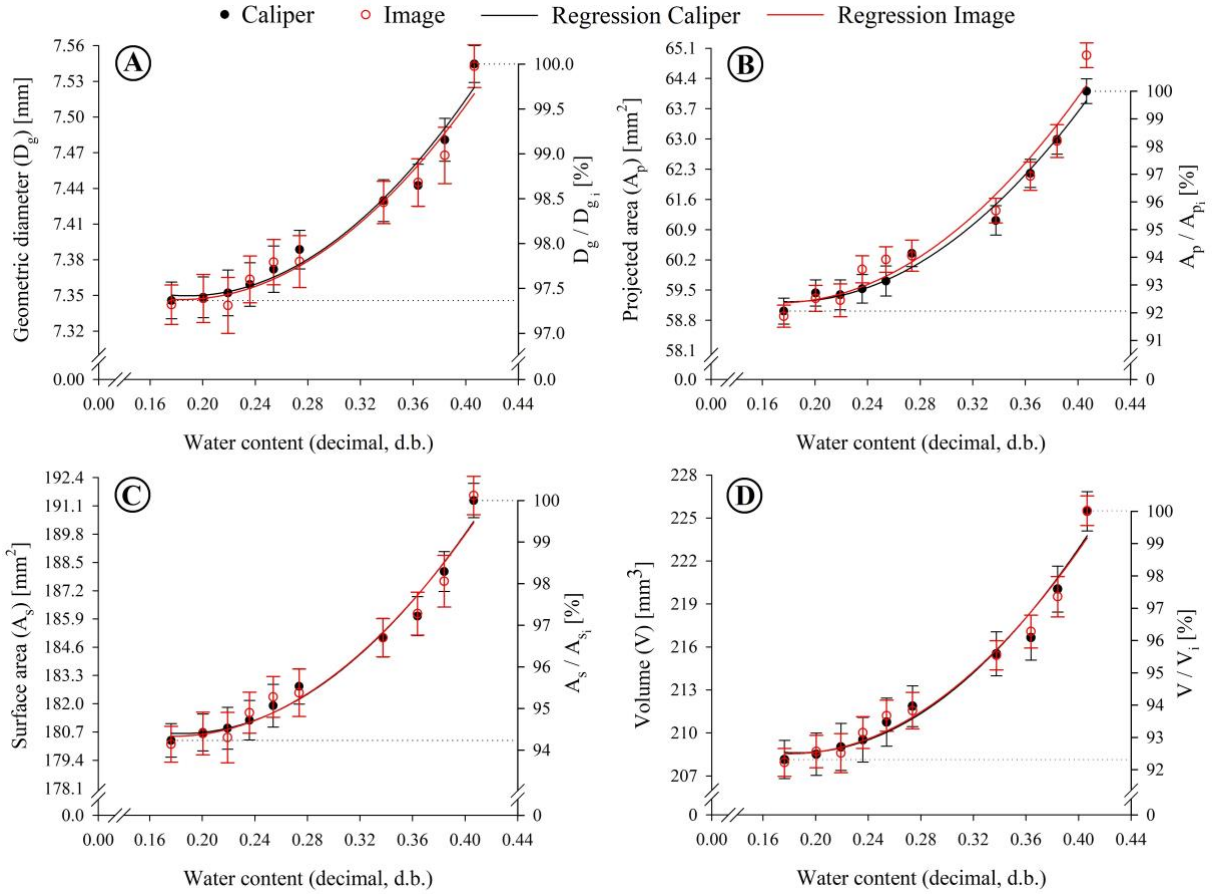

Figure 6. Observed and estimated values of the (A) geometric diameter, (B) projected area, (C) surface area, and (D) volume of bean grains from digital caliper and image data. The subscript "i" represents the highest value of the property. Error bars represent the standard deviation.

The projected area variation as a function of the water content of the common beans is shown in Figure 6B. A nonlinear reduction of this property was observed during the drying process. The projected area of the grains suffered a variation of 8%, with values varying between 59.01 and 64.11 mm^2 for the final and initial water contents, respectively. This reduction during drying is expected since the drying process results in the grains' orthogonal axes contraction. Similar results have been reported over the years for different products such as white-speckled red kidney bean grains (Isik and Unal, 2007), rice grains (Kibar et al., 2010), peanut grains (Araujo et al., 2014), safflower grains (Martins et al. 2017a), sesame and black caraway seeds (Shallangwa et al., 2021), coffee beans (Araujo et al., 2021b), among others. Among the geometric properties, the projected area can be considered one of the most important for fluid dynamics studies, as it directly affects the terminal velocity and drag coefficient of the grains (Araujo et al., 2021a).

The values of the surface area of bean grains at different water contents are shown in Figure 6C. A nonlinear reduction from 191.35 to 180.31 mm^2 was observed for the water contents between 0.41 and 0.18 d.b. The surface area underwent a total variation of about 5.7% during drying. The surface area is one of the most critical geometric parameters of a product (Li et al., 2017). These data are essential for the grain processing industries, as this property is crucial for heat and mass transfer processes. The results agree with those presented for coriander seeds (Coskuner and Karababa, 2007) and arugula seeds (Mirzabe et al., 2021).

Figure 6D shows the change in the volume of bean grains during drying. A nonlinear reduction of 7.7% with the product's water content reduction can be observed. The grain volume ranged from 225.5 to 208.1 mm^3 for the evaluated water content range. The reduction in the volume of common bean grains is more significant at the beginning of the drying process and tends to decrease when reaching low water content values. This result is directly related to the loss of water during this process. During drying, the place previously occupied by water tends to be occupied by the viscoelastic matrix of the product. These structural changes occur due to the reduction of tension inside the cells, generating the phenomenon known as shrinkage. At the beginning of drying, water migration from the product's interior to the surface happens more quickly, so water removal is more straightforward. During drying, the contraction reduces the grains' internal pores, causing water migration and, consequently, the contraction of the orthogonal axes to occur more slowly.

To clearly show the geometric change of the bean grains during drying, the percentage of variation observed for the properties of volume, surface area, projected area, and geometric diameter was plotted as a function of the water content and is shown in Figure 7. It is observed that the projected area and the volume of the grains presented the most considerable variations along the drying process. It is also observed that all properties stabilize after reaching a water content of 0.20 d.b., giving minimal variations, making it impossible to use its variation as a process control tool after reaching this water content. Although monitoring the product's water content based on its geometric properties is not yet a reality, the more significant variation in volume and projected area indicate that these properties can be used for process control in the future.

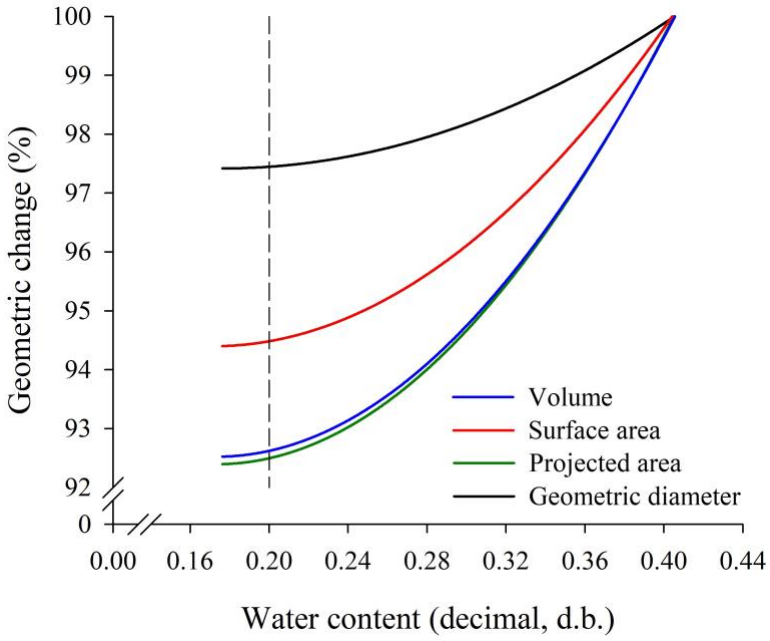

Figure 7. Geometric change of common bean grains during drying.

Under the drying conditions evaluated in this study, the reduction in water content provided a nonlinear increase (about 2.2%) in the surface-to-volume ratio of bean grains (Figure 8). The grain surface volume ratio varied between 0.85 and 0.87 for water contents ranging between 0.41 and 0.18, respectively. From de results of Figures 5C and 5D, it can be seen that the values of the surface volume ratio should increase during drying since the surface area undergoes a reduction of 5.8% during the drying process. In comparison, the volume suffers a reduction of 7.7%. These results are essential to understand how drying dynamics occur due to product shape. The higher the surface-to-volume ratio for the same product water content, the higher the heat and mass transfer rates. Similar behavior of the variation of the surface volume ratio as a function of water content was previously reported for several agricultural products such as jatropha fruits (Siqueira et al., 2012), grains (Araujo et al., 2014), and peanut fruits (Araujo et al., 2015), coffee fruits (Botelho et al., 2016), among others.

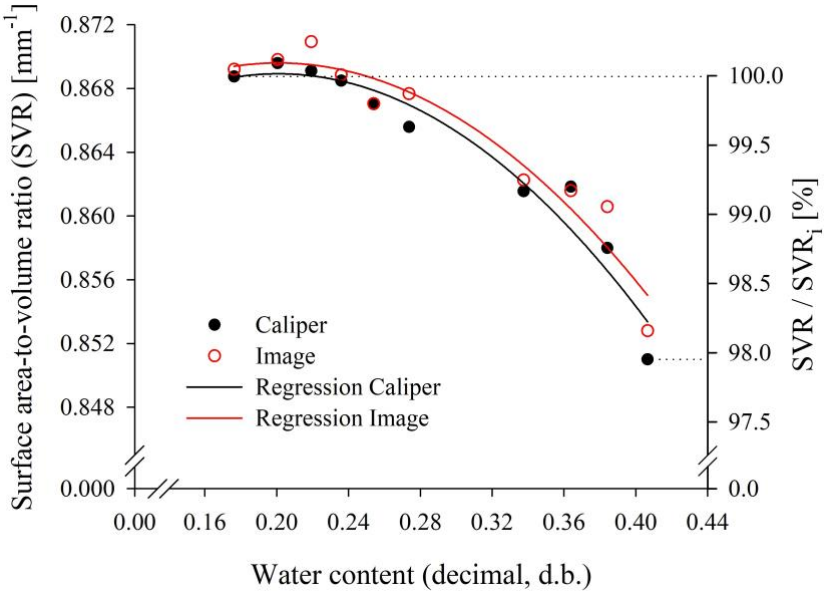

Figure 8. Observed and estimated values of the surface-to-volume ratio of bean grains from digital caliper and image data. Error bars represent the standard deviation.

Table 4 shows the values of regression coefficients for the geometric properties of common bean grains as a function of water content. High values of the coefficient of determination show that the models adequately represent the variation of the evaluated properties. Except for sphericity, which showed a linear behavior (Equation 12), all other properties better fit the second-order polynomial model (Equation 14).

Table 4 – Coefficients of regression models fitted for the geometric properties of bean grains as a function of water content.

Properties	β_0	β_1	β_2	R^2
		Caliper		
Volume	219.427	-116.149^{+}	311.925^{++}	0.972**
Sphericity	67.170	-6.001^{++}	-	0.940**
Geometric diameter	7.481	-1.393^{++}	3.692^{++}	0.972**
Projected area	62.166	-32.643^{+}	90.744^{++}	0.987**
Surface area	187.338	-72.794^{+}	197.494^{++}	0.978**
Surface-to-volume ratio	0.854	0.148^{+}	-0.368^{+}	0.944**
		Image		
Volume	218.164	-106.474^{+}	294.830^{++}	0.968**
Sphericity	67.162	-6.205^{++}	-	0.972**
Geometric diameter	7.464	-1.278^{+}	3.481^{+}	0.962**
Projected area	61.904	-31.423^{+}	91.466^{+}	0.958**
Surface area	186.455	-66.895^{+}	187.993^{+}	0.967**
Surface-to-volume ratio	0.856	0.139^{+}	-0.345^{+}	0.936**

$^{++}$ Significant at 1% probability by the t-test, $^{+}$ Significant at 5% probability by the t-test, ** Significant at 1% probability by the F test.

Table 5 shows the statistical parameters' values and the models' distribution of residues for the volumetric contraction of common bean grains during drying. The values of the regression coefficients β_0, β_1, and β_2 for each model when applied are also presented.

Table 5 – Parameters of the volumetric contraction models of common bean grains adjusted to the values obtained by caliper and image and their respective mean relative error (P), coefficients of determination (R^2), standard error of the estimate (SE), Akaike Information Criterion (AIC) and Schwarz's Bayesian Information Criterion (BIC).

Model	Model Coefficients			Statistical Parameters					Residue
	β_0	β_1	β_2	R^2	SE	P	BIC	AIC	
Caliper									
Bala and Woods (1984) adapted	0.0781	13.5155	-	0.985	0.003	0.265	-80.972	-81.879	Random
Corrêa et al. (2004)	1.3888	-0.2491	-	0.930	0.007	0.007	-80.972	-81.879	Random
Rahman (1995)	-0.3956	-	-	0.771	0.012	0.968	-56.145	-56.750	Biased
Linear	0.8622	0.2979	-	0.909	0.008	0.585	-63.060	-63.967	Biased
Exponential	0.8655	0.3152	-	0.913	0.008	0.570	-63.060	-63.967	Biased
Second-degree polynomial	0.9732	-0.5151	1.3834	0.972	0.005	0.323	-72.477	-73.687	Random
Araujo-Copace (Araujo et al., 2021a)	22.2326	-52.2062	31.9585	0.995	0.002	0.142	-90.407	-91.618	Random
Image									
Bala and Woods (1984) adapted	0.0779	13.6437	-	0.981	0.004	0.310	-78.644	-79.551	Random
Corrêa et al. (2004)	1.3869	-0.2476	-	0.931	0.007	0.007	-78.644	-79.551	Biased
Rahman (1995)	-0.3959	-	-	0.766	0.012	0.951	-56.032	-56.637	Biased
Linear	0.8625	0.2962	-	0.911	0.008	0.584	-63.417	-64.324	Biased
Exponential	0.8658	0.3134	-	0.915	0.008	0.570	-63.417	-64.324	Biased
Second-degree polynomial	0.9674	-0.4721	1.3074	0.968	0.005	0.373	-71.342	-72.552	Random
Araujo-Copace (Araujo et al., 2021a)	23.1905	-54.5338	32.5203	0.994	0.002	0.157	-88.745	-89.955	Random

Except for the Rahman model (1995), all other models used to describe the contraction of common bean grains showed high coefficient of determination values (above 90%). According to Cano-Higuita et al. (2015), this statistical parameter is critical when evaluating models with different estimated parameters. However, Kashaninejad et al. (2007) stated that the coefficient of determination while comparing regression models should not be used in isolation. Avhad and Marchetti (2016) reported that other statistical parameters, such as the mean relative error and the standard error of the estimate, ensure the correct choice of models. Values of the mean relative error of less than 10% and low values of the standard error of the estimate signify an excellent fit of the model to the data (Costa et al., 2015). In addition, a residual dispersion analysis should be performed to ensure the randomness of the coefficient estimation. Residual values close to zero without the formation of geometric shapes indicate the randomness of the model. If the waste distribution does not have these characteristics, the model is considered biased and should not be used.

The Bala and Woods, second-degree polynomial and Araujo-Copace models showed low values of the mean relative error and standard error of the estimate, and the highest values of the coefficient of determination, both for the data obtained by caliper and by image. Only the models mentioned showed random dispersion of residues, adequately representing the volumetric contraction of common bean grains during drying for both the evaluated cases. The Araujo-Copace model was selected to represent the volumetric contraction of bean grains during drying. This model presented the best values for all statistical assessed parameters. In addition, the Araujo-Copace model presented the lowest values for the parameters AIC and BIC. This result indicates that the model can be more accurate in representing the phenomenon studied, as these parameters consider factors such as the analysis of the degree of parameterization of the models (Ferreira Junior et al., 2018). Gomes et al. (2018) also stated that the lower the AIC and BIC values, the more suitable the models.

The correspondence of the values observed and estimated by the Araujo-Copace model is shown in Figure 9A. The high degree of correlation between the data shows that the model satisfactorily represented the volumetric contraction of the common bean grains. The values estimated by the model and observed can be seen in Figure 9B. The bean grains showed a volumetric contraction of 7.7% during the drying process, for water contents varying between 0.41 and 0.18 (decimal, d.b.). The volumetric contraction of agricultural products is highly dependent on the characteristics of the solid and viscoelastic matrices of the product; therefore, different products present different percentages of reduction of their volume during the drying process. In previous work, Araujo et al. (2020) reported a

volumetric contraction of passion fruit seeds of only 4% during drying. Martins et al. (2017b) observed a 13% reduction in safflower grains.

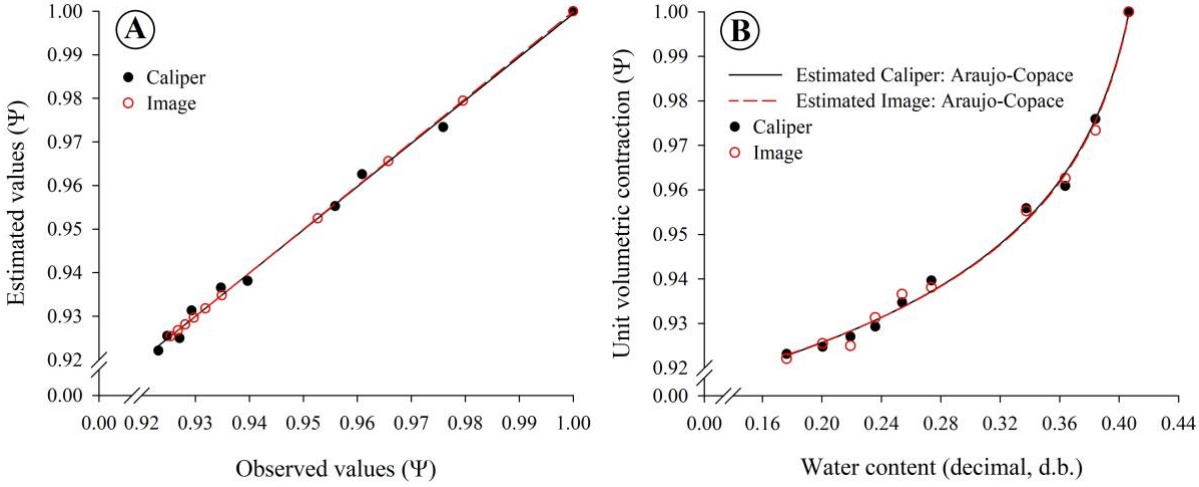

Figure 9. (A) Correspondence of observed and estimated values and (B) observed and estimated values by Araujo-Copace for volumetric contraction of bean grains during drying.

4. CONCLUSION

Based on the results obtained in this study, the following conclusions were made for the range of water content evaluated.

- Digital image processing was satisfactory for obtaining the dimensions of bean grains, providing reliable data in a faster and more practical way.
- Among the geometric properties evaluated, only the circularity showed no significant difference ($P \leq 0.05$) during the drying process.
- The sphericity and the surface volume ratio of the bean grains increased with the reduction of the water content varying between 64.6-66% (+2.1%) and 0.85-0.87 (+2.2%), respectively. On the other hand, the geometric diameter, projected area, surface area, and volume reduced during drying, with values varying between 7.54–7.31mm (-3.0%), 64.11–59.01 mm^2 (-8.0%), 191.35–180.31 mm^2 (-5.7%), 225.0–208.1 mm^3 (-7.7%), respectively.
- Among the empirical models used, the Araujo-Copace model was selected to describe the volumetric contraction of bean grains during drying. The bean grains presented a volumetric contraction of 7.7%, indicating that the grains suffered a slight variation of the orthogonal axes during drying.

5. REFERENCES

Ajermoun, N., Aghris, S., Ettadili, F., Alaoui, O.T., Laghrib, F., Farahi, A., Lahrich, S., Bakasse, M., Saqrane, S., El Mhammedi, M.A. Phytotoxic effect of the insecticide imidacloprid in *Phaseolus vulgaris* L. plant and evaluation of its bioaccumulation and translocation by electrochemical methods. **Environmental Research**, v.214, 113794, 2022.

Akaike, H. A new look at the statistical model identification. **IEEE Transactions Automatic Control**, v.19, p.716–723, 1974.

Al-Mahasneh, M.A., Rababah, T.M. Effect of moisture content on some physical properties of green wheat. **Journal of Food Engineering**, v.79, p.1467-1473, 2007.

Altuntas, E., Demirtola, H. Effect of moisture content on physical properties of some grain legume seeds. **New Zealand Journal of Crop and Horticultural Science**, v.35, p.423-433, 2007.

Araujo, M.E.V., Barbosa, E.G., Oliveira, A.C.L., Milagres, R.S., Pinto, F.A.C., Corrêa, P.C. Physical properties of yellow passion fruit seeds (*Passiflora edulis*) during the drying process. **Scientia Horticuturae**, v.261, 109032, 2020.

Araujo, M.E.V., Barbosa, E.G., Gomes, F.A., Teixeira, I.R., Lisboa, C.F., Araujo, R.S.L, Corrêa, P.C. Physical properties of sesame seeds harvested at different maturation stages and thirds of the plant. **Chilean Journal of Agricultural Research**, v.79, p.495-502, 2018.

Araujo, M.E.V., Corrêa, P.C., Barbosa, E.G., Martins, M.A. Variation of the physical and aerodynamic properties of coffee cherries during drying: Determination and modeling. *Journal of* **Food Process Engineering**, v.44, e13801, 2021a.

Araujo, M.E.V., Corrêa, P.C., Barbosa, E.G., Martins, M.A. Determination and modeling of physical and aerodynamic properties of coffee beans (*Coffea arabica*) during the drying process. **Journal of Food Processing and Preservation**, v.45, e15698, 2021b.

Araujo, W.D., Goneli, A.L.D., Orlando, R.C., Martins, E.A.S., Hartman Filho, C.P. Propriedades físicas dos frutos de amendoim durante a secagem. **Revista Caatinga**, v.28, p.170-180, 2015.

Araujo, W.D., Goneli, A.L.D., Souza, C.M.A., Gonçalves, A.A., Vilhasanti, H.C.B. Propriedades físicas dos grãos de amendoim durante a secagem. **Revista Brasileira de Engenharia Agrícola e Ambiental**, v.18, p.279-286, 2014.

Avhad, M.R., Marchetti, J.M. Mathematical modeling of the drying kinetics of Hass avocado seeds. **Industrial Crops and Products**, v.91, p.76-87, 2016.

Bahar, B., Tuncel, A.F., Holmes, E.W., Homles, D.T. An interactive website for analytical method comparison and bias estimation. **Clinical Biochemistry**, v.50, p.1025-1029, 2017.

Bala, B.K., Woods, J.L. Simulation of deep bed malt drying. **Journal of Agricultural Engineering Research**, v.30, p.235-244, 1984.

Bande, Y.M., Adam, N.M., Azmi, Y., Jamarei, O. Moisture-dependent physical and compression properties of bitter melon (*Citrullus colocynthis lanatus*) seeds. **International Journal of Agricultural Research**, v.7, p.243-254, 2012.

Bento, J.A.C., Morais, D.K., Berse, R.S., Bassinello, P.Z., Caliari, M., Soares Júnior, M.S. Functional, thermal, and pasting properties of cooked carioca bean (*Phaseolus vulgaris* L.) flours. **Applied Food Research**, v.2, 100027, 2022.

Bland, J.M., Altman, D.G. Comparing methods of measurement: why plotting difference against standard method is misleading. **The Lancet**, v.346, p.1085-1087, 1995.

Botelho, F.M., Correa, P.C., Botelho, S.C.C., Vargas-Elías, G.A., Almeida, M.D.S.D., Oliveira, G.H.H. Propriedades físicas de frutos de café robusta durante a secagem: determinação e modelagem. **Coffee Science**, v.11, p.65-75, 2016.

BRASIL. Ministério da Agricultura, Pecuária e Abastecimento. **Regras para análise de sementes**. Secretaria de Defesa Agropecuária. Brasília: MAPA/ACS, 399p. 2009.

Burnham, K.P., Anderson, D.R. Multi model inference: Under-standing AIC and BIC in model selection. **Sociological Methods Research**, v.33, p.261–304, 2004.

Cano-Higuita, D.M., Villa-Vélez, H.A., Telis-Romero, J., Váquiro, H.A., Telis, V.R.N. Influence of alternative drying aids on water sorption of spray dried mango mix powders: a thermodynamic approach. **Food and Bioproducts Processing**, v.93, p.19-28, 2015.

Cervantes, E., Martín, J.J., Saadaoui, E. Updated Methods for Seed Shape Analysis. **Scientifica (Cairo)**, v.2016, 5691825, 2016.

Corrêa, P.C., Botelho, F.M., Botelho, S.C.C., Goneli, A.L.D. Isotermas de sorção de água de frutos de *Coffea canefora*. **Revista Brasileira de Engenharia Agrícola e Ambiental**, v.18, p.1047-1052, 2014.

Corrêa, P.C., Ribeiro, D.M., Resende, O., Afonso Júnior, P.C., Goneli, A.L.D. Mathematical modeling for representation of coffee berry volumetric shrinkage. In: International Drying Symposium, **14**, São Paulo. *Anais*... São Paulo (CD ROM). 2004.

Coskuner, Y., Karababa, E. Physical properties of coriander seeds (*Coriandrum sativum* L.). **Journal of Food Engineering**, v.80, p.408-416, 2007.

Costa, J.M.G., Silva, E.K., Hijo, A.A.C.T, Azevedo, V.M., Borges, S.V. Physical and Thermal Stability of Spray-Dried Swiss Cheese Bioaroma Powder. **Drying Technology**, v.33, p.346-354, 2015.

Eissa, A.H.A., Mohamed, M.A., Moustafa, H., Abdul, R.O.A. Moisture dependent physical and mechanical properties of chickpea seeds. **International Journal of Agricultural and Biological Engineering**, v.3, p.80-93, 2010.

Ennoury, A., BenMrid, R., Nhhala, N., Roussi, Z., Latique, S., Zouaoui, Z., Nhiri, M. River's Ulva intestinalis extract protects common bean plants (*Phaseolus vulgaris* L.) against salt stress. **South African Journal of Botany**, v.150, p.334-341, 2022.

Ferreira Junior, W. N., Resende, O., Oliveira, D. E. C., Costa, L. M. Isotherms and isosteric heat desorption of *hymenaea stigonocarpa* mart. seeds. **Journal of Agricultural Science**, v.10, p.504–512, 2018.

Gely, M.C., Pagano, A.M. Effect of moisture content on engineering properties of sorghum grains. **Agricultural Engineering International: CIGR Journal**, v.19, p.200-209, 2017.

Gomes, F. P., Resende, O., Sousa, E. P., Oliveira, D. E. C., Araújo Neto, F. R. Drying kinetics of crushed mass of 'jambu': Effective diffusivity and activation energy. **Revista Brasileira de Engenharia Agrícola e Ambiental**, v.22, p.499–505, 2018.

Hernández-Guerrero, C.J., Villa-Ruano, N., Zepeda-Vallejo, L.G., Hernandéz-Fuentes, A.D., Ramirez-Estrada, K., Zamudio-Lucero, S., Hidalgo-Martínez, D., Becerra-Martínez, E. Bean cultivars (*Phaseolus vulgaris* L.) under the spotlight of NMR metabolomics. **Food Research International**, v.150, 110805, 2021.

Isik, E., Izli, N. Effects of Moisture Content on Some Physical Properties of the Yellow Lentil. **Journal of Agricultural Sciences**, v.22, p.307-316, 2016.

Isik, E., Unal, H. Moisture-dependent physical properties of white speckled red kidney bean grains. **Journal of Food Engineering**, v.82, p.209-216, 2007.

Izli, N. Effect of moisture on the physical properties of three varieties of kenaf seeds. **Journal of Food Science and Technology**, v.52, p.3254-3263, 2015.

Kashaninejad, M., Mortazavi, A., Safekordi, A., Tabil, L.G. Thin-layer drying characteristics and modeling of pistachio nuts. **Journal of Food Engineering**, v.78, p.98-108, 2007.

Kibar, H.; Öztürk, T.; Esen, B. The effect of moisture content on physical and mechanical properties of rice (*Oryza sativa* L.). **Spanish Journal of Agricultural Research**, v.8, p.741-749, 2010.

Li, H., Qian, Y., Cao, Peng, Yin, W., Dai, F., Hu, F., Yan, Z. Calculation method of surface shape feature of rice seed based on point cloud. **Computers and Electronics in Agriculture**, v.142, p.416-423, 2017.

Lisboa, H.M., Araujo, H., Paiva, G., Oriente, S., Pasquali, M., Duarte, M.E., Mata, M.E.R.M.C. Determination of characteristic properties of mulatto beans (*Phaseolus vulgaris* L.) during convective drying. **Journal of Agriculture and Food Research**, v.1, 100003, 2019.

Martins, E.A.D., Goneli, A.L.D., Hartmann Filho, C.P., Mauad, M., Siqueira, V.C., Gonçalves, A.A. Physical properties of safflower grains. Part I: Geometric and gravimetric characteristics. **Revista Brasileira de Engenharia Agrícola e Ambiental**, v.21, p.344-349, 2017a.

Martins, E.A.D., Goneli, A.L.D., Gonçalvez A.A., Hartmann Filho, C.P., Rech, J., Oba, G.V. Physical properties of safflower grains. Part II: Volumetric shrinkage. **Revista Brasileira de Engenharia Agrícola e Ambiental**, v.21, p.350-355, 2017b.

Meghwal, M., Goswami, T.K. Effect of moisture content on physical and textural properties of fenugreek seeds. Food In: **Global Science Books**, v.6, p.14–21, 2012.

Mirzabe, A.H., Hajiahmad, A., Asadollahzadeh, A.H. Moisture-dependent engineering properties of arugula seed relevant in mechanical processing and bulk handling. **Journal of Food Process Engineering,** v.44, e13704, 2021.

Mohsenin, N.N. **Physical properties of plant and animal materials**. New York: Gordon and Breach Publishers, 1986. 841p.

Obi, O.F., Offorha, L.C. Moisture-dependent physical properties of melon (*Citrullus colocynthis lanatus*) seed and kernel relevant in bulk handling. **Cogent Food Agriculture**, v.1, 1020743, 2015.

Oliveira, J.A.V., Coradi, P.C., Alvez, C.Z., Teodoro, P.E., Alvarez, R.C.F. Correlation of physical properties for establishments of standardized groups of soybean seed technologies in post-harvest. **Journal of Stored Products Research**, v.93, 101854, 2021.

Onwe, D.N., Umani, K.C., Olosunde, W.A., Ossom, I.S. Comparative analysis of moisture-dependent physical and mechanical properties of two varieties of African star apple (*Chrysophyllum albidum*) seeds relevant in engineering design. **Scientific African**, v.8, e00303, 2020.

Paixão, A.A., Corrêa, P.C., Baptestini, F.M., Zeymer, J.S., Bustos-Vanegas, J.D. Physical properties of beans of the BRSMG majestoso cultivar during drying. **Bioscience Journal**, v.36, p.1911-1918, 2020.

Rahman, S. **Food properties handbook**. Boca Ratón: CRC Press LLC. 1995. 500p.

Sandoval-Pereza, M., Chel-Guerrero, L., Betancur-Ancona, D. Some physicochemical and functional properties of the rich fibrous fraction of hardened beans (*Phaseolus vulgaris* L.) and its addition in the formulation of beverages. **International Journal of Gastronomy and Food Science**, v.26, 100440, 2021.

Schwarz, G. Estimating the dimension of a model. **The Annals of Statistics**, v.6, p.461–464, 1978.

Shallangwa, Y.Y., Alkali, A.H., Aviara, N.A. Evaluation of moisture-dependent geometric and gravimetric properties of small-sized sesame and black caraway seeds using image analysis. **International Journal of Food Properties**, v.24, p.415-432, 2021.

Singh, H., Meghwal, M. Physical and thermal properties of various ajwain (*Trachyspermum ammi* L.) seed varieties as a function of moisture content. **Journal of Food Process Engineering**, v.43, e13310, p.1-14, 2019.

Siqueira, V.C., Resende, O., Chaves, T.H., Soares, F.A.L. Forma e tamanho dos frutos de pinhão-manso durante a secagem em cinco condições de ar. **Revista Brasileira de Engenharia Agrícola e Ambiental**, v.16, p.864-870, 2012.

Sologubik, C.A., Campanone, L.A., Pagano, A.M., Gely, M.C. Effect of moisture content on some physical properties of barley. **Industrial Crops and Products**, v.43, p.762–767, 2013.

CHAPTER 2

PHYSICAL, AERODYNAMIC, AND THERMAL PROPERTIES OF COMMON BEAN GRAINS (*PHASEOLUS VULGARIS* L.) DURING DRYING

Abstract: Understanding the behavior of bean grains' physical, aerodynamic, and thermal properties during drying is crucial for designing and optimizing equipment and processes during post-harvest. The lack of updated and complete data leads the industry to develop and handle equipment inappropriately, resulting in considerable losses. Given the above, this study aimed to evaluate and model the variation of common bean grain's physical, thermal and aerodynamic properties as a function of water content. Common bean grains were harvested wet and dried in a tray dryer to different water contents. The grains were submitted for evaluation of their physical (real and apparent specific mass, porosity, and mass of 1000 grains), aerodynamic (terminal velocity and drag coefficient), and thermal (specific heat, thermal conductivity, and thermal diffusivity) properties for each water content obtained. Among the physical properties, the 1000-grain weight showed the most significant variation during drying (16.2%), followed by porosity (14.7%), bulk density (7.0%), and true density (2.1%). The drag coefficient showed the most significant variation (43.1%) among the evaluated aerodynamic properties, followed by terminal velocity (22.3%). For thermal properties, thermal conductivity showed the greatest variation (47.2%), followed by thermal diffusivity (43.1%) and specific heat (13.3%). The results will be beneficial for developing and optimizing processes in the bean production chain.

Keywords: Bean drying. Grain density. Heat transfer. Terminal velocity.

1. INTRODUCTION

Common bean (*Phaseolus vulgaris* L.) is the most produced and consumed legume worldwide (Rawal and Navarro, 2019). The nutritional quality of common beans extends far beyond the valuable source of protein and fiber, being also rich in vitamins, mineral nutrients such as iron and zinc (Huertas et al., 2022), and polyphenolic compounds with antioxidant properties (Wei et al., 2022). In addition to playing an essential socio-economic role, bean production in developing countries is crucial to alleviating poverty and ensuring food security for smallholder farmers (Ajermoun et al., 2022; Momanyi et al., 2022). Although common bean grains can be eaten fresh after maturity, most beans are dried and stored for future consumption (Momanyi et al., 2022). The drying operation has been widely used to preserve agricultural products, as reducing water content to certain levels inhibits microbial growth and enzymatic modifications (Corrêa et al., 2019). In addition, it provides less volume and mass for transport, therefore requiring less space for storage.

During the drying process, the reduction in the water content of the bean grains leads to several changes in their physical, aerodynamic, and thermal properties and their quality. Evaluating and obtaining relevant data on these properties of agricultural products is inherently a critical factor in reducing costs, defining storage strategies, and sizing and operating equipment in the main post-harvest operations of the product (Onwe et al., 2020). Munder et al. (2017) highlighted the practical importance of these properties for structural design, machine design, process, and control engineering, among others.

Growing awareness of the quality of food products has led to an increased demand for data on their physical properties. Assessing and obtaining relevant data on these properties is critical in reducing costs, defining storage strategies, and sizing and operating equipment in critical post-harvest product operations. In this context, several authors have sought to evaluate changes in physical properties dependent on water content for various products and, in general, report direct changes with moisture, such as lentil seeds (Gharibzahedi et al., 2011), guar seeds (Vishwakarma et al., 2012), kola nuts (Kareem et al., 2013), moringa seeds (Aviara et al., 2013), barley grains (Sologubik et al., 2013), coriander seeds (Sharanagat and Goswami, 2014), kenaf seeds (Izli, 2015), sorghum grains (Gely and Pagano, 2017), akuamma seeds (Ndukwu et al., 2019), passion fruit seeds (Araujo et al., 2020), among others. Managing and developing highly productive cultivars with good quality, resistance to diseases, and environmentally adaptable can influence the structure and properties of grains, making determining these properties essential and particularly important for each product.

Knowledge of aerodynamic properties is essential for airflow processes in post-harvest operations. Data referring to terminal velocity and drag coefficient are vital parameters to optimize processes such as pneumatic transport, separating grains and undesirable products (impurities, inferior materials), and selection. In addition, these data allow the separation of the grains at different water contents due to the variation in actual density and geometric properties during drying (Araujo et al., 2021a). It is known that each product or particle presents different reactions to the aerodynamic forces that act on them when they are subjected to airflow. Therefore, determining these properties is fundamental for correctly operating airflow machines and equipment. From these data, it is possible to define the ideal airspeed ranges for separating, cleaning, transporting, or effectively classifying grains (Shahbazi, 2015).

The thermal properties of the grains largely govern their heat transfer. Thermal conductivity, specific heat, and thermal diffusivity are the main properties responsible for thermal control during this process. With the reduction of water content during drying, these properties are altered, and consequently, the thermal exchange between the grains and the drying air is altered. According to Mohsenin (1986) and Pabis et al. (1998), the thermal properties are highly relevant to understand the drying processes due to the restrictions of the flow of heat and mass transfer. In this sense, knowledge of these properties is essential for modeling, designing, and optimizing processes and processing equipment in operations based on heat treatment, such as dehydration, bleaching, cooking, heating, cooling, steaming, and freezing, among others (Bitra et al., 2010).

Despite the proven importance of agricultural products' physical, thermal, and aerodynamic properties and the influence of water content on them, complete studies on these properties for common bean grains were not found in the literature. Therefore, this study aimed to mathematically determine and model the variation in bean grain's physical, aerodynamic, and thermal properties during drying.

2. MATERIAL AND METHODS

2.1. Obtaining the raw material

This study was carried out at the Laboratory of Physical Properties and Quality Assessment of Agricultural Products at the National Center for Storage Training (CENTREINAR), located at the Federal University of Viçosa (UFV), Viçosa - Minas Gerais,

Brazil. Common bean grains of the BRS–Estilo variety were used in this study. The samples used in this study were collected wet with an initial water content of 0.41 (decimal, d.b.) in the experimental area belonging to the Department of Agronomy of the Federal University of Viçosa (20°45'00" S, 42°56'15" W; 643 m a.s.l.). The harvested pods were subjected to the manual threshing process to reduce the mechanical damage to the wet grains. The threshed grains were submitted to an initial sorting and selected for color uniformity (eliminating green grains that did not reach physiological maturity) and average size (eliminating sluggish and malformed grains). The threshed grains were immediately stored in the biochemical oxygen demand (BOD) chamber at 4 ± 2 °C until the beginning of the experiments.

2.2. Sample preparation

The beans were dried in a GrainMan 6623 cylindrical tray dryer (Seedburo, Illinois, USA) at 45 ± 2 °C until different levels of water content. The water contents of the samples were determined by the standard oven method, at 105 ± 2 °C, for 24 hours, in four replications (BRASIL, 2009) and expressed on a dry basis (d.b.). The weight of the samples was obtained on a Marte® AY220 analytical balance with a precision of 0.0001g (Minas Gerais, Brazil).

During drying, the bean grains were removed from the dryer and homogenized. After homogenization, the samples were taken to determine the physical, aerodynamic, and thermal properties. The experiments were conducted in 4 repetitions for each water content. The water contents obtained were 0.407, 0.384, 0.364, 0.338, 0.274, 0.254, 0.236, 0.219, 0.200, and 0.176 (decimal, d.b.).

2.3. Physical properties

2.3.1. Bulk and true density

Common bean grain density can be defined as the ratio between mass and volume occupied by the grains. When this concept is applied to a single grain, that is, the ratio between the mass and volume of a single grain, we obtain the true density of the product (Equation 1). When this concept is applied to a mass of grains, we obtain the product's bulk density (Equation 2).

$$\rho_u = \frac{m_u}{V_u} \quad (1)$$

$$\rho_{ap} = \frac{m}{V} \quad (2)$$

Where,

ρ_u – True density, kg m^{-3};

m_u – Mass of a single grain, kg;

V_u – Volume of a single grain, m^3;

m – Product mass, kg; and

V – Volume of product mass, m^3.

The volume complementation methodology proposed by Moreira et al. (1985) and described in ASTM D 792 (1991) was used to obtain the true density of the bean grains during drying. Sunflower oil was used as filling fluid in 25 mL glass pycnometers. A cylindrical container (Ohaus one pint dry) with a fixed and known volume was used to determine the bulk density. A funnel with a discharge valve attached to a rod allowed the cylinder container to be filled under the same conditions. A leveler placed on the main shaft of the equipment allowed the grains to be leveled at the maximum limit of the container volume. To obtain the mass of the empty container and, subsequently, the mass of the container filled with grains, a digital balance (Marte® AS2020) with an accuracy of 0.01 g was used.

2.3.2. Porosity

The porosity of bean grains can be expressed as the ratio between the volume occupied by air in the intergranular spaces and the total volume of the grain mass (Mohsenin, 1986). From the data obtained regarding true and bulk density, it is possible to obtain the porosity (ε) of the grains according to Equation 3.

$$\varepsilon = 1 - \left(\frac{\rho_{ap}}{\rho_u}\right) \quad (3)$$

2.3.3. 1000-grain weight

The 1000-grain weight of the common bean grains during drying was determined using the counting method (eight sub-samples of 100 grains per repetition) with mass determination on an analytical balance with a precision of 0.0001 g according to the methodology prescribed in the Rules for Seed Analysis – RAS (BRASIL, 2009). The mass of one thousand seeds was determined by multiplying by ten the mean of the eight subsamples for each repetition.

2.4. Aerodynamic properties

2.4.1. Terminal velocity

The terminal velocity of the bean grains, defined as the velocity capable of keeping the product afloat, was obtained experimentally using a cylindrical tray dryer (GrainMan 6623) equipped with a centrifugal fan. This dryer has two valves that allow the control of the airflow in the trays. The grains were arranged unitarily in the flotation zone. The tests started with the airflow equal to 0, and the valves were opened until the grains started to float. The airflow velocity was measured using a digital hot-wire thermo-anemometer with an accuracy of 0.1 m s^{-1} (Instrutherm TARF-180). Four terminal velocity readings were taken at different points on the tray to obtain the mean terminal velocity.

2.4.2. Drag coefficient

When evaluating a grain in free fall, subjected to an upward airflow, the following forces are observed: the weight force ($\vec{F}_g$), the buoyant force ($\vec{E}$) and the drag force ($\vec{F}_r$). When the product starts moving at a constant velocity in this flow (terminal velocity), these vector quantities reach equilibrium so that we can write:

$$\overrightarrow{F_r} = \overrightarrow{F_g} - \vec{E}$$

That is,

$$\frac{1}{2}\, C_d\, \rho_f A_p V_t^2 = mg\, \frac{(\rho_p - \rho_f)}{\rho_p}$$

Thus, isolating the drag coefficient (C_d), Equation 4 is obtained, which is shown as a safe means of determining the drag coefficient by several authors when the terminal velocity is known (Matouk, 2008; Mohsenin, 1986; Shahbazi et al., 2014; Araujo et al., 2021). The weight of the grains was obtained on an analytical balance (Marte® AY220) with a precision of 0.0001g.

$$C_d = \frac{2mg\ (\rho_p - \rho_f)}{\rho_p\ \rho_f\ A_p\ V_t^2} \tag{4}$$

Where,

C_d – Drag coefficient, dimensionless;

m – Mass of the product, kg;

g – Acceleration of gravity, m s^{-2};

V_t – Terminal velocity, m s^{-1};

ρ_f – Fluid density, kg m^{-3};

ρ_p – Product true density, kg m^{-3}; and

A_p – Projected particle area, m^2.

The projected area of bean grains during drying was obtained by Equation 5, according to Mohsenin (1986). Furthermore, in this study, the Reynolds number was calculated for each water content, based on each sample's average terminal velocity and geometric diameter, according to Equations 6 and 7, respectively (Mohsenin, 1986). The grains used to determine the terminal velocity experimentally were measured using a Mitutoyo 500-174B digital caliper with a resolution of 0.01mm.

$$A_p = \frac{\pi LW}{4} \tag{5}$$

$$Re = \frac{D_g \rho_f V_t}{\mu} \tag{6}$$

$$D_g = (LWT)^{1/3} \tag{7}$$

Where,

Re – Reynolds number, dimensionless;

D_g – Geometric diameter, m;

ρ_f – Air density, kg m^{-3};

L – Beans length, m;

W – Beans width, m;

T – Beans thickness, m; and

μ – Fluid dynamic viscosity, kg m^{-1} s^{-1}.

2.5. Thermal properties

The direct mixture calorimeter method was used to determine the specific heat of common bean grains during drying. In this study, four calorimeters consisted of a thermos each, with glass wool insulation and PVC outer coating. The calorimeter's thermal insulation was carried out to obtain the least possible interference from the environment during the experiments. A K-type probe thermocouple was installed in the center of the rubberized cover of each calorimeter. The thermocouples were connected to an ICP CON LR-7518 data acquisition module and an ICP CON LR-7520 serial converter module connected to the computer for automatic data collection over time. In addition to the thermocouples installed on the calorimeter covers, two K-type thermocouples were also connected to the modules for monitoring the ambient and grain temperatures.

The calorimeter constants were obtained by determining the temperature variation of the water placed inside them. A known amount of distilled water at high temperature was added to the calorimeters. Subsequently, a known amount of distilled water at a low temperature was added. Assuming that the calorimeters were adiabatic, and the energy balance could determine their caloric capacity, the constant of the calorimeters was obtained according to Equation 8 (Azadbakht et al., 2013).

$$C = \frac{Cp_a\left[m_{aq}\left(T_{aq} - T_{eq}\right) - m_{af}\left(T_{eq} - T_{af}\right)\right]}{T_{eq} - T_{af}} \quad (8)$$

Where,

C – Calorimeter constant, kJ kg^{-1};

Cp_a – Specific heat of water, kJ kg^{-1} K^{-1};

m_{aq} – Hot water mass, kg;

T_{aq} – Hot water temperature, K;

T_{eq} – Equilibrium temperature, K;

m_{af} – Cold water mass, kg; and

T_{af} – Cold water temperature, K.

To determine the specific heat of the bean grains, 100g of product with known temperature was transferred into each calorimeter. Subsequently, heated distilled water with known temperature and mass was added to the calorimeters. The product sample and the water were stirred, and temperature readings were taken until equilibrium. The data collection system automatically recorded the mixture temperature value every 15 seconds. Equilibrium was considered when the temperature variation after 5 readings was less than 0.1°C. With the equilibrium temperature data, the specific heat of the grains was obtained according to Equation 9.

$$Cp_p = \frac{Cp_a m_{aq}(T_{aq} - T_{eq}) + C\,(T_{aq} - T_{eq})}{m_p(T_{eq} - T_p)} \quad (9)$$

Where,

Cp_p – Specific heat of the product, kJ kg^{-1} K^{-1};

m_p – Product mass, kg; and

T_p – Product temperature, K.

The thermal conductivity of the grains was determined using the theoretically infinite cylinder method. A metallic cylinder was used, and the hypothesis of one-dimensional heat conduction in the radial direction was considered (Bitra et al., 2010). A power source set to 2.2 V and 1.1 A was used to power a nickel-chromium conductor wire positioned axially in the center of the cylinder (Ramaswamy et al., 2003). Seven K-type thermocouples, evenly spaced, were positioned radially in the center of the cylinder to acquire grain mass temperature data. The thermocouples were connected to an ICP CON LR-7518 data acquisition module and an ICP CON LR-7520 serial converter module connected to the

computer. Data were automatically collected at 5-minute intervals. Mass grain temperature increased after a period of constant temperature, and at this point, time was measured against temperature. The thermal conductivity was calculated from the data obtained according to Equation 10.

$$k = \frac{q}{4\pi(T_1 - T_2)} \ln\left(\frac{t_2}{t_1}\right) \quad (10)$$

Where,

k – Thermal conductivity, W m^{-1} K^{-1};

q – Power dissipated by the source per unit length, W m^{-1};

T_1 – Initial temperature, K;

T_2 – Final temperature, K;

t_1 – Initial time, s; and

t_2 – Final time, s.

From the results of specific heat and thermal conductivity of the product, the thermal diffusivity was calculated according to Equation 11 (Mohsenin, 1980).

$$\alpha = \frac{k}{\rho_{ap}\, Cp_p} \quad (11)$$

Where,

α – Thermal diffusivity, m^2 s^{-1};

2.6. Data analysis

Analyzes of variance (ANOVA) and regression were applied to the data obtained for each of the properties evaluated. The analyzes were performed using the statistical analysis software STATISTICA 8.0® and SISVAR. Regression models for each property were chosen according to the model's fit to the experimental data and the magnitude and significance of the determination and regression coefficients.

3. RESULTS AND DISCUSSION

Analysis of variance showed a significant effect ($P \leq 0.05$) of water content on all properties evaluated in this study. The results presented in the following subsections will be significant for the industry, optimizing processes and developing new and more efficient equipment. The pooled results of the bean grains' physical, aerodynamic, and thermal properties during drying will allow us to understand how each property is affected by the water content and how this data matrix can be used for modeling, optimization, and process control.

3.1. Physical properties

Variations in the physical properties of common bean grains as a function of water content are shown in Figure 1. The bean grains showed a linear reduction in true density during drying (Figure 1A). The true density varied between 1167.4 and 1193.1 kg m^{-3} for water contents of 0.176 and 0.407 (decimal, d.b.), respectively. This result indicates that, proportionally, there is a more significant reduction in mass compared to the volume of bean grains during drying. Altuntas and Yildiz (2007) reported a similar result for faba bean grains, with values varying between 1206.2 and 1151.3 kg m^{-3} during drying. Isik and Unal (2011) found a reduction of approximately 12.6% in the true density of white kidney beans with a reduction in the product's water content. Data on the variation in the true density of the grains during drying are crucial for the correct design and operation of equipment. If, on the one hand, size and shape properties allow the separation of grains based on sieves, true density data are used to optimize separation by ventilation or other densimetric methods (Khodabakhshian et al., 2018).

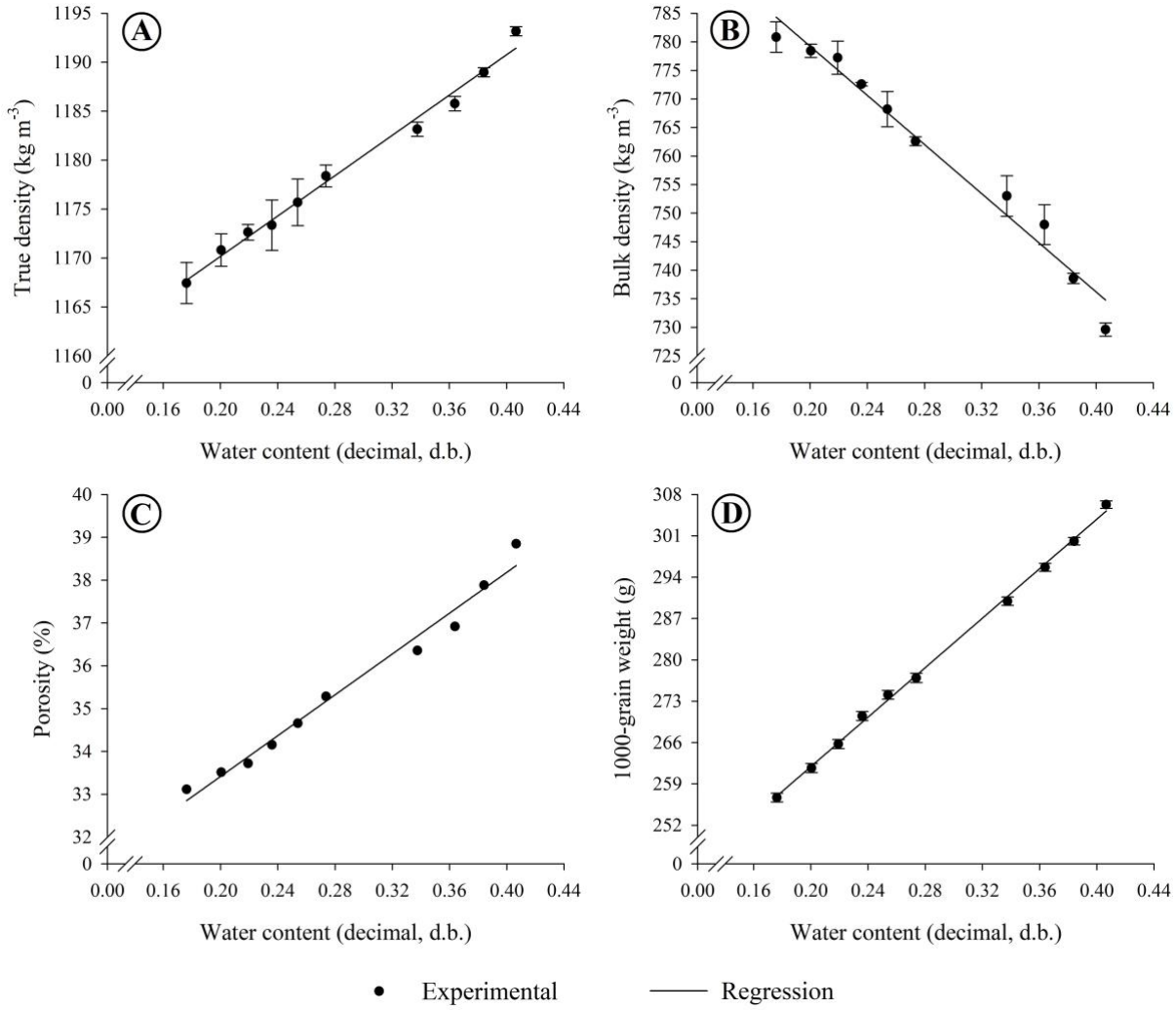

Figure 1. Physical properties of common bean grains during drying, (A) true density, (B) bulk density, (C) porosity, and (D) 1000-grain weight. Error bars represent the standard deviation.

Unlike the behavior observed for true density, a linear increase in bulk density of common bean grains was observed during drying (Figure 1B). Within the range of water content evaluated in this study, the bulk density of the bean grains varied between 729.6 and 780.8 kg m^{-3}. This result is directly related to the porosity of the grain mass. The increase in bulk density shows that, proportionally, the volume of grain mass suffered a greater reduction compared to their mass. This result is confirmed by the linear porosity reduction from 38.9 to 33.1%, shown in Figure 1C. It is easy to associate that with the reduction of porosity, the greater the volume occupied by grains within the same dimensional delimitation. Therefore, for a fixed volume, the reduction in porosity means that more grains and, consequently, more mass can be added. Similar results were reported by Cetin (2007) during the drying of

barbunia bean seeds (*Phaseolus vulgaris* L. cv. 'Barbunia'). Knowing the association between bulk density and porosity is essential, as these properties are directly related to drying, aeration, and storage processes. They affect resistance to airflow, heat exchange, and water vapor diffusion in grain mass (Vashishth et al., 2020).

The variation of the 1000-grain weight of the common bean grains during drying is shown in Figure 1D. Bean grains showed a linear reduction of this property during drying, varying values between 306.3 and 256.7 g. The reduction of this property during drying was expected since water removal during the process makes the grain lighter. Similar results were reported for common bean grains of the BRSMG Majestoso cultivar (Paixão et al., 2020). The 1000-grain weight can be considered one of the most important components of grain yield, being directly related to the quality and final price of the product, especially for seeds (Song et al., 2018; Shi et al., 2019).

3.2. Aerodynamic properties

The behavior of the aerodynamic properties of common bean grains during drying is shown in Figure 2. The bean grains showed a linear reduction in terminal velocity (Figure 2A) from 8.4 to 6.5 m s^{-1} with a reduction in water content of 0.407 to 0.176 (decimal, d.b.), respectively. These results are in line with those reported for various agricultural products such as mung bean seeds (Shahbazi et al., 2015), chickpea seeds and dry bean seeds (Soylu et al., 2020), rice beans (Bhushan and Raigar, 2020), among others. The terminal velocity of an agricultural product is highly dependent on the unit mass per frontal unit area of the grain that is acted upon by the airflow. Therefore, the behavior of bean grains in an airflow depends on their aerodynamic properties (terminal velocity and drag coefficient) and physical properties (true density and projected area). With this, the importance of determining these properties together is highlighted so that the data can be used efficiently to optimize various post-harvest operations, such as separation, cleaning, classification, and transport.

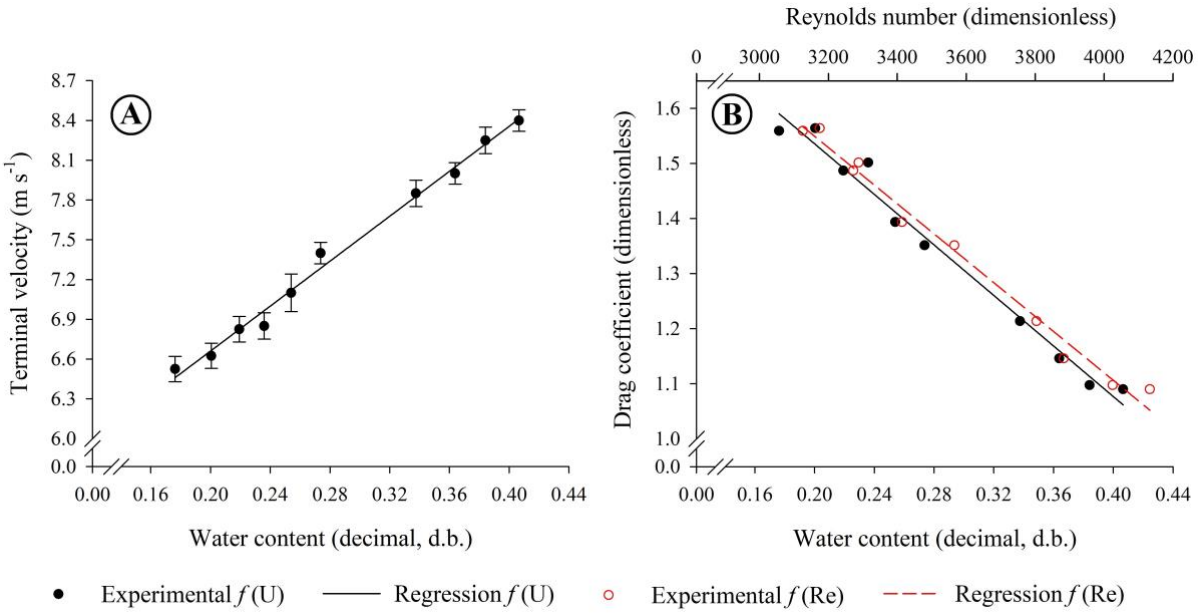

Figure 2. Aerodynamic properties of common bean grains during drying, (A) terminal velocity, and (B) drag coefficient. Error bars represent the standard deviation. *f (U): as a function of water content, f (Re): as a function of the Reynolds number.*

The variation in the drag coefficient of bean grains as a function of water content and Reynolds number is shown in Figure 2B. As this property is inversely proportional to the terminal velocity, an expected linear drag coefficient increase was verified by reducing the product's water content. The same behavior was observed as a function of the Reynolds number. For the water content range evaluated in this study, the drag coefficient varied between 1.09 and 1.56 (dimensionless). This variation represents an increase of approximately 43% in this property during drying. Several works have highlighted that experimental data on the drag coefficient of grains and seeds are crucial and necessary for designing and operating various types of equipment throughout the agricultural production chain (Bako and Bardey, 2020; Masoumi et al., 2020; Mudarisov et al., 2020). With this data in hand, it is also possible to incorporate the effect of air resistance and the effect of an air current in simulations and modeling to optimize equipment and post-harvest operations (Binelo et al., 2019).

The average values of the mass, projected area, and geometric diameter of the bean grains used to obtain the drag coefficient are shown in Table 1. Both properties suffered a reduction during drying. The grain unit mass reduction, as presented for the 1000-grain weight, is related to the reduction in the water content in the grains during drying. In addition, during drying, the contraction of the viscoelastic matrix of the grains tends to occupy the

place previously occupied by water, generating, consequently, a reduction of the orthogonal axes (L, W, and T) that affects both the projected area and the geometric diameter of the grains.

Table 1 – Mean values and respective deviations of mass, projected area, and geometric diameter of bean grains as a function of water content.

Water content (decimal, d.b.)	Unit mass average (g)	Projected area average (mm^2)	Geometric diameter average (mm)
0.407	0.322 ± 0.015	63.911 ± 0.428	7.545 ± 0.233
0.384	0.307 ± 0.018	62.933 ± 0.510	7.481 ± 0.270
0.364	0.298 ± 0.020	62.221 ± 0.489	7.442 ± 0.266
0.338	0.298 ± 0.011	61.113 ± 0.512	7.430 ± 0.263
0.274	0.292 ± 0.018	60.365 ± 0.458	7.389 ± 0.244
0.254	0.274 ± 0.012	59.726 ± 0.520	7.372 ± 0.294
0.236	0.274 ± 0.009	59.541 ± 0.495	7.359 ± 0.275
0.219	0.269 ± 0.013	59.387 ± 0.516	7.352 ± 0.289
0.200	0.266 ± 0.017	59.436 ± 0.547	7.348 ± 0.256
0.176	0.256 ± 0.014	59.128 ± 0.453	7.346 ± 0.231

3.3. Thermal properties

The specific heat variation of common bean grains during drying is shown in Figure 3A. The specific heat reduced linearly with the reduction of the water content of the grains. Mean values ranged from 2839.4 to 2461.6 J kg^{-1} K^{-1} for water contents of 0.407 and 0.176 (decimal, d.b.), respectively. Similar results were observed during the drying of canola seeds (Yu et al., 2015), bambara groundnut (Abioye et al., 2016), faba bean, and lentil (Matouk et al., 2018), among others. Perussello et al. (2014) reported that the amount of water in the product directly influences its specific heat. These results were expected since the reduction in water content during drying decreases the contribution of this constituent to the specific heat of the grains.

The thermal conductivity values as a function of the water content of the bean grains are shown in Figure 3B. A non-linear reduction was observed from 0.32 to 0.17 W m^{-1} K^{-1} during drying. Therefore, the results indicate that heat conduction in bean grains is better when wet than dry. The results found in this study are in line with those observed for ajwain

seeds (Singh and Megahwal, 2019) and jack bean seeds (Oriola et al., 2020). According to Sweat (1986), the thermal conductivity of porous foods strongly depends on their porosity. In addition, the author reported the thermal conductivity result for 25 agricultural products, with values varying between 0.1 and 0.8 W m^{-1} K^{-1}, a range that includes the results presented in this study. As Ikegwu (2021) reported, thermal conductivity is extremely important, as it controls the heat flux in food during processing, being highly dependent on water content, temperature, porosity, and phase distribution of the components.

The effect of water content on the thermal diffusivity of bean grains is shown in Figure 3C. Thermal diffusivity varied between 8.8×10^{-8} and 1.5×10^{-7} m^2 s^{-1} for water contents of 0.176 and 0.407 (decimal, d.b.), respectively. The reduction of thermal diffusivity during drying was also reported for mung beans (Ravikanth et al., 2012), seeds of kerstingiella geocarpa (Ikegwu and Ezeh, 2012), and velvet beans (Adeyanju et al., 2022). Data on thermal diffusivity are critical when transient heat flux significantly affects grains. For example, during storage in metal silos, thermal diffusion elucidates the grain heating rate due to external (environment) effects, mainly in the grain layer close to the wall, where convective air currents are responsible for moisture and heat migration (Pohndorf et al., 2017).

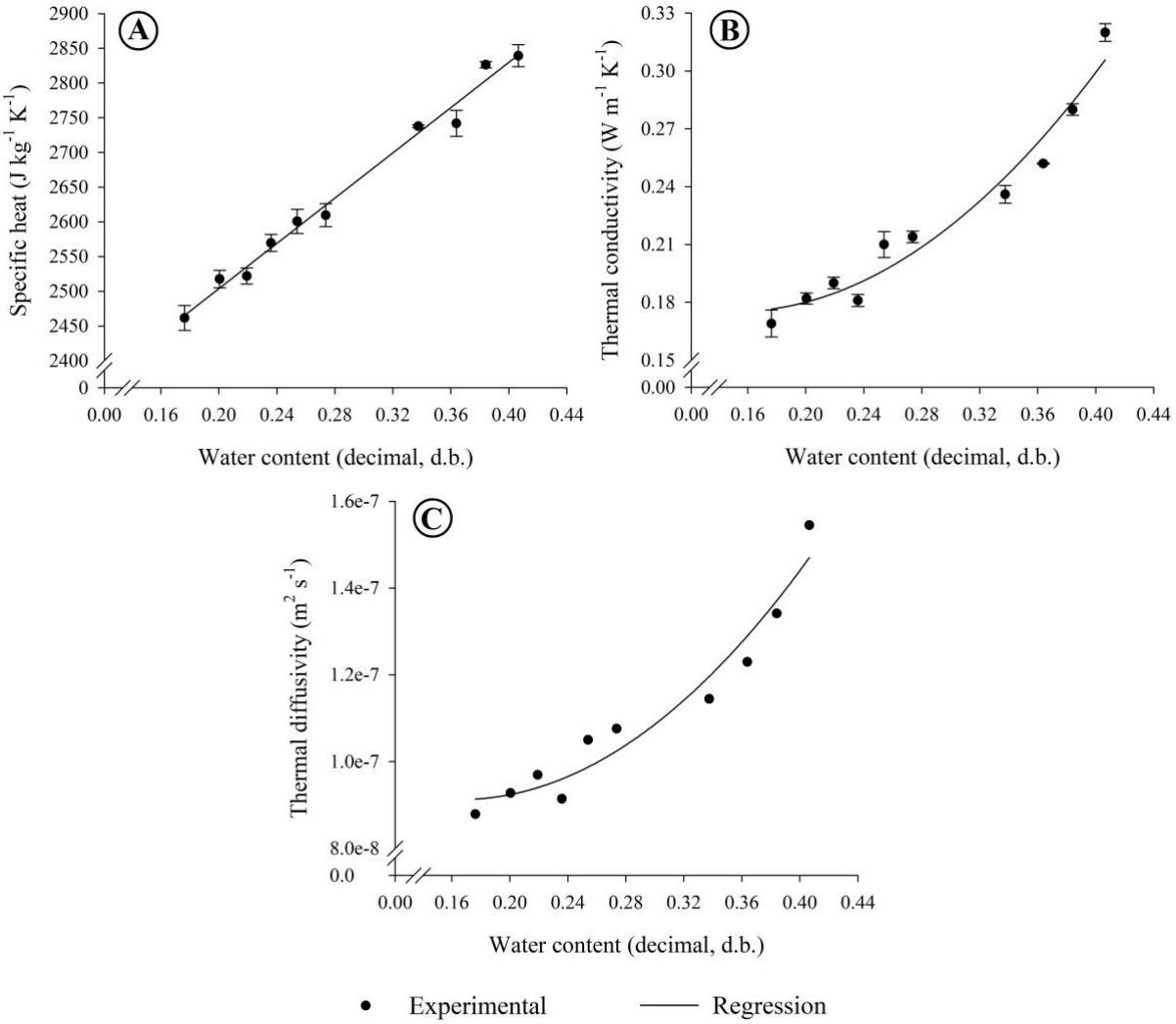

Figure 3. Thermal properties of common bean grains during drying, (A) specific heat, (B) thermal conductivity, and (C) thermal diffusivity. Error bars represent the standard deviation.

Table 2 summarizes the regression models that best represented each property evaluated in this study. Except for thermal conductivity and thermal diffusivity, which better fit the second-degree polynomial model (Equation 12), all other properties were represented by the linear model (Equation 13). All adjustments showed a high coefficient of determination values, satisfactorily representing the evaluated properties.

$$\phi = \beta_0 + \beta_1 U + \beta_2 U^2 \quad (12)$$

$$\phi = \beta_0 + \beta_1 U \quad (13)$$

Where,

ϕ – Evaluated property;

U – water content (decimal d.b.); and

β_0, β_1, β_2 – Regression coefficients.

Table 2 – Coefficients of regression models adjusted for bean grains' physical, aerodynamic, and thermal properties as a function of water content.

Properties	β_0	β_1	β_2	R^2
True density	1149.576	102.974^{++}	-	0.989**
Bulk density	822.236	-215.070^{++}	-	0.974**
Porosity	28.651	23.827^{++}	-	0.981**
1000-grain weight	220.032	209.473^{++}	-	0.998**
Terminal velocity	4.966	8.473^{++}	-	0.992**
Drag coefficient f(U)	1.995	-2.295^{++}	-	0.981**
Drag coefficient f(Re)	3.165	-5.113e-4^{++}	-	0.987**
Specific heat	2178.033	1629.336^{++}	-	0.987**
Thermal conductivity	0.220	-0.594^{+}	1.982^{+}	0.957**
Thermal diffusivity	1.176e-7	-3.186e-7^{+}	9.612e-7^{+}	0.942**

U – water content (decimal, d.b.); Re – Reynolds number (dimensionless); f() – as a function of.

$^{++}$ Significant at 1% probability by thet-test; $^{+}$ Significant at 5% probability by thet-test; ** Significant at 1% probability by the F-test.

3.4. Percentage variation as a function of water content

The percentage variation of each property was calculated to show the results of this study in general terms (Figure 4). The value of 100% was attributed to each property at the highest water content evaluated. Note that this result only expresses the variation of the property compared to the observed initial value. The curves were plotted based on the respective regression curves for each property. Among the physical properties evaluated in this study, the 1000-grain weight showed the highest total variation during drying, approximately 16.2%. Porosity, bulk density, and true density showed a total variation of about 14.7, 7.0, and 2.1%, respectively. For the aerodynamic properties, the drag coefficient presented the highest percentage variation (43.1%) with the reduction of the water content from 0.407 to 0.176 (decimal, d.b.), followed by the terminal velocity with a variation of

22.3%. Thermal conductivity showed the most significant variation (47.2%) among thermal properties, followed by thermal diffusivity (43.1%) and specific heat (13.3%). Some helpful information can be observed by evaluating the results presented in Figure 4. First, it is noted that the classification or separation of bean grains using aerodynamic methods can be more efficient than using densimetric methods since the aerodynamic properties showed more significant variation during drying. Thermal properties indicate that drier grains are more heat transfer-resistant than wet grains. Although this behavior is known, the magnitude of this variation can be extremely important to understand how temperature and airflow parameters should be used to optimize drying and aeration processes.

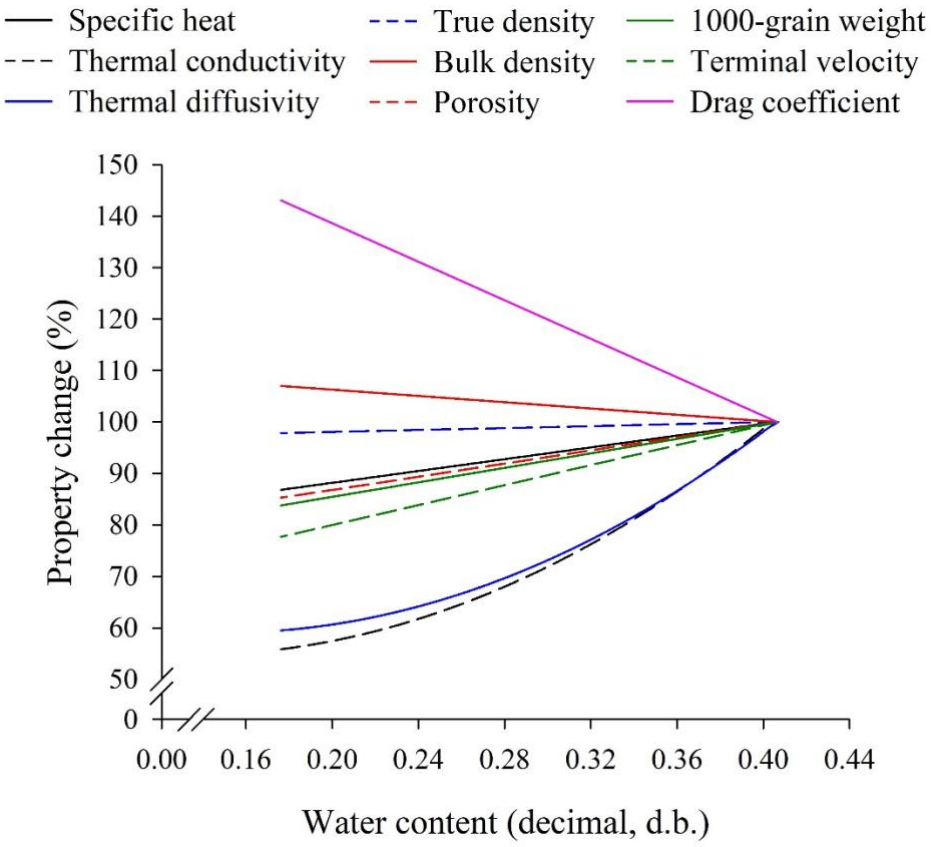

Figure 4. Percentage variation of evaluated properties as a function of the water content of common bean grains.

4. CONCLUSION

This study sought to determine and model the variation of common bean grains' physical, aerodynamic, and thermal properties during drying. For the evaluated water content, the following conclusions can be made.

- Among the analyzed physical properties, only the bulk density increased during drying; all other properties decreased with the reduction in the water content of the grains. The 1000-grain weight showed the most significant variation during drying (16.2%), with values ranging between 306.3 and 256.7 g for water contents between 0.407 and 0.176 (decimal, d.b.), respectively. The porosity of the grain mass reduced from 38.9 to 33.1% during drying. The bulk density increased about 7% with the reduction in water content, with values varying between 729.6 and 780.8 kg m^{-3}. True density showed the lowest percentage variation during drying, only 2.1%, with values ranging between 1193.1 and 1167.4 kg m^{-3} for water contents of 0.407 and 0.176 (decimal, d.b.), respectively.
- The drag coefficient showed the most significant variation among the evaluated aerodynamic properties, an increase of about 43.1%. The terminal velocity of bean grains varied between 8.4 and 6.5 m s^{-1} (-22.3%) for water contents ranging between 0.407 and 0.176 (decimal, d.b.), respectively.
- For the evaluated thermal properties, thermal conductivity, and diffusivity showed the greatest variations during drying. Thermal conductivity showed a reduction of 47.2% during drying, with values varying between 0.32 and 0.17 W m^{-1} K^{-1}. Thermal diffusivity ranged between 8.8×10^{-8} and 1.5×10^{-7} m^2 s^{-1} for water contents of 0.176 and 0.407 (decimal, d.b.), respectively. Finally, the specific heat was reduced by approximately 13.3% during drying, with values between 2839.4 and 2461.6 J kg^{-1} K^{-1}.

5. REFERENCES

Abioye, A.O., Adekunle, A.A., Agbasi-Ebere, V. Some moisture-dependent physical and thermal properties of bambara groundnut. **Journal of Environmental Science, Toxicology and Food Technology**, v.10, p.65-74, 2016.

Adeyanju, J.A., Abioye, A.O., Adekunle, A.A., Ajala, A.S., Oloyede, A.A., Afolayan, E.T. Assessment of Physical and Thermal Properties of Velvet Bean (*Mucuna pruriens*) as Potentials for Development of Processing Machines. **Journal of Engineering and Technology**, v.7, p.122-125, 2022.

Ajermoun, N., Aghris, S., Ettadili, F., Alaoui, O.T., Laghrib, F., Farahi, A., Lahrich, S., Bakasse, M., Saqrane, S., El Mhammedi, M.A. Phytotoxic effect of the insecticide imidacloprid in *Phaseolus vulgaris* L. plant and evaluation of its bioaccumulation and translocation by electrochemical methods. **Environmental Research**, v.214, 113794, 2022.

Altuntas, E., Yildiz, M. Effect of moisture content on some physical and mechanical properties of faba bean (*Vicia faba* L.) grains. **Journal of Food Engineering**, v.78, p.174-183, 2007.

Araujo, M.E.V., Barbosa, E.G., Oliveira, A.C.L., Milagres, R.S., Pinto, F.A.C., Corrêa, P.C. Physical properties of yellow passion fruit seeds (*Passiflora edulis*) during the drying process. **Scientia Horticuturae**, v.261, 109032, 2020.

Araujo, M.E.V., Corrêa, P.C., Barbosa, E.G., Martins, M.A. Variation of the physical and aerodynamic properties of coffee cherries during drying: Determination and modeling. Journal of **Food Process Engineering**, v.44, e13801, 2021.

ASTM D 792. **Standard test methods for density and specific gravity (relative density) of plastics by displacement.** ASTM International (ASTM). 1991.

Aviara, N.A., Power, P.P., Abbas, T. Moisture-dependent physical properties of *Moringa oleifera* seed relevant in bulk handling and mechanical processing. **Industrial Crops and Products**, v.42, p.96-104, 2013.

Azadbakht, M., Khoshtaghaza, M.H., Ghobadian, B., Minaei, S. Thermal properties of soybean pod as a function of moisture content and temperature. **American Journal of Food Science and Technology**, v.1, p.9-13, 2013.

Bako, T., Bardey, I.A. Engineering properties of acha (*Digitaria exilis*) grains in relation to the design of grain processing machines. **Agricultural Engineering International**, v.22, p.159-170, 2020.

Bhushan, B., Raigar, R.K. Influence of moisture content on engineering properties of two varieties of rice bean. **Journal of Food Process Engineering**, v.43, e13507, 2020.

Binelo, M.O., Lima, R.F., Khatchatourian, O.A., Stránský, J. Modelling of the drag force of agricultural seeds applied to the discrete element method. **Biosystems Engineering**, v.178, p.168-175, 2019.

Bitra, V.S.P., Banu, S., Ramkrishna, P., Narender, G., Womac, A.R. Moisture dependent thermal properties of peanut pods, kernels, and shells. **Biosystems Engineering**, v.106, p.503-512, 2010.

BRASIL. Ministério da Agricultura, Pecuária e Abastecimento. **Regras para análise de sementes**. Secretaria de Defesa Agropecuária. Brasília: MAPA/ACS, 399p. 2009.

Cetin, M. Physical properties of barbunia bean (*Phaseolus vulgaris* L. cv. 'Barbunia') seed. **Journal of Food Engineering**, v.80, p.353-538, 2007.

Corrêa, P.C., Baptestini, F.M., Zeymer, J.S., Araujo, M.E.V., Freitas, R.C.P., Leite, R.A. Dehydration of infrared ginger slices: Heat and mass Transfer coefficient and modeling. **Ciência e Agrotecnologia**, v.43, e025318, 2019.

Gely, M.C., Pagano, A.M. Effect of moisture content on engineering properties of sorghum grains. **Agricultural Engineering International**, v.19, p.200-209, 2017.

Gharibzahedi, S.M.T., Ghasemlou, M., Razavi, S.H., Jafarii, S.M., Faraji, K. Moisture-dependent physical properties and biochemical composition of red lentil seeds. **International Agrophysics**, v.25, p.343–347, 2011.

Huertas, R., Allwood, J.W., Hancok, R.D., Stewart, D. Iron and zinc bioavailability in common bean (*Phaseolus vulgaris*) is dependent on chemical composition and cooking method. **Food Chemistry**, v.387, 132900, 2022.

Ikegwu, O.J. Effect of moisture and temperature on thermal conductivity of pigeon pea seeds. **Agricultural Engineering International: CIGR Journal**, v.23, p.217-224, 2021.

Ikegwu, O.J., Ezeh, C.Q. Thermal properties of kerstingiella geocarpa seeds as influenced by moisture content. **Nigerian Food Journal**, v.30, p.100-105, 2012.

Isik, E., Unal, H. Some engineering properties of white kidney beans (*Phaseolus vulgaris* L.). **African Journal of Biotechnology**, v.10, p.19126-19136, 2011.

Izli, N. Effect of moisture on the physical properties of three varieties of kenaf seeds. **Journal of Food Science and Technology**, v.52, p.3254-3263, 2015.

Kareem, I., Owolorafe, O.k., Ajavi, O.A. Moisture-Dependent Physical Properties of Kola Nut (*Cola nitida*) Seed. **Food and Bioprocess Technology**, v.6, p.2938-2942, 2013.

Khodabakhshian, R., Emadi, B., Abbaspour-Fard, M.H., Golzarian, M.R. Aerodynamic separation and cleaning of pomegranate arils from rind and white segments (*Locular septa*). **Journal of the Saudi Society of Agricultural Sciences**, v.17, p.61-68, 2018.

Masoumi, M., Mahmoudi, A., Alizaeh, M.R., Abdollhpour, S. Effect of awn on aerodynamic properties of paddy grains (*Oryza Sativa* L.). **Agricultural Engineering International**, v.22, p.208-216, 2020.

Matouk, A.M., Abd El-Latif, S.M., Tharwat, A. Aerodynamics and mechanical properties of some oil-producing crops. **Journal of Agricultural Science**, v.33, p.4195-4211, 2008.

Matouk, A.M., El-Kholy, M.M., Tharwat, A., Shamala, S.F. Thermal properties of some legume seeds. **Journal of Soil Sciences and Agricultural Engineering**, v.9, p.261-267, 2018.

Mohsenin, N.N. **Physical properties of plant and animal materials**. New York: Gordon and Breach Publishers, 1986. 841p.

Mohsenin, N.N. **Thermal properties of foods and agricultural materials**. New York: Gordon and Breach Science Publishers Inc., 1980. 407p.

Momanyi, M.R., Nduko, J.M., Omwamba, M. Effect of hermetic Purdue Improved Crop Storage (PICS) bag on chemical and anti-nutritional properties of common Bean (*Phaseolus vulgaris* L.) varieties during storage. **Current Research in Food Science**, v.5, p.107-116, 2022.

Moreira, S. M., Chaves, M., Oliveira, L. Comparação da eficiência de líquidos na determinação da massa específica aparente de grãos agrícolas. **Revista Brasileira de Armazenamento**, v.9, p.22–24, 1985.

Mudarisov, S., Badretdinov, I., Rakhimov, Z., Lukmanov, R., Nurullin, E. Numerical simulation of two-phase "Air-Seed" flow in the distribution system of the grain seeder. **Computer and Electronics in Agriculture**, v.168, 105151, 2020.

Munder, S., Argyropoulos, D., Muller, J. Class-based physical properties of air-classified sunflower seeds and kernels. **Biosystems Engineering**, v.164, p.124–134, 2017.

Ndukwu, M.C., Ohia, A., Anozie, O. Influence of Moisture Content and Compression Axis on Mechanical, Physical, and Phytochemicals Properties of Akuamma (*Picralima nitida*) Fruits and Seeds. **Journal of the Institution of Engineers (India): Series A**, v.100, p.417-426, 2019.

Onwe, D.N., Umani, K.C., Olosunde, W.A., Ossom, I.S. Comparative analysis of moisture-dependent physical and mechanical properties of two varieties of African star apple (*Chrysophyllum albidum*) seeds relevant in engineering design. **Scientific African**, v.8, e00303, 2020.

Oriola, K.O., Hussein, J.B., Oke, M.O., Abimbola, A. Description and evaluation of physical and moisture-dependent thermal properties of jack bean seeds (*Canavalia ensiformis*). **Journal of Food Processing and Preservation**, v.45, e15166, 2020.

Pabis, S., Jayas, D.S., Cenkowski, S. **Grain drying: theory and practice**. New York: John Wiley Sons, Inc., 1998. 303p.

Paixão, A.A., Corrêa, P.C., Baptestini, F.M., Zeymer, J.S., Bustos-Vanegas, J.D. Physical properties of beans of the brsmg majestoso cultivar during drying. **Bioscience Journal**, v.36, p.1911-1918, 2020.

Perussello, C.A., Mariani, V.C., Amarante, A.C.C. Thermophysical Properties of Okara During Drying. **International Journal of Food Properties**, v.17, p.891-907, 2014.

Pohndorf, R.S., Rocham J.C., Lindemann, I., Peres, W.B., Oliveira, M., Elias, M.C. Physical properties and effective thermal diffusivity of soybean grains as a function of moisture content and broken kernels. **Journal of Food Process Engineering**, v.41, e12626, 2017.

Ramaswamy, H., Raghavan, V., Chakraverty, A., Mujundar, A. **Handbook of Postharvest Technology**. CRC Press, 2003.

Ravikanth, L., Jayas, D.S., Alagusundaram, K., Chelladurai, V. Measurement of Thermal Properties of Mung Bean (*Vigna radiata*). **Transacrions of the ASABE**, v.55, p.2245-2250, 2012.

Rawal, V. Navarro, D.K., eds. 2019. **The Global Economy of Pulses**. Rome, FAO. 2019.

Shahbazi, D. Evaluation and modeling of aerodynamic properties of mung bean seeds. **International Agrophysics**, v.29, p.121-126, 2015.

Shahbazi, F., Valizadeh, S., Dowlatshah, A. Aerodynamic properties of Makhobeli, triticale and wheat seeds. **International Agrophysics**, v.28, p.389–394, 2014.

Sharanagat, V.S., Goswami, T.K. Effect of moisture content on physiomechanical properties of coriander seeds (*Coriandrum sativum*). **Agricultural Engineering International**, v.16, p.166-172, 2014.

Shi, L., Song, J., Guo, C., Wang, B., Guan, Z., Yang, P., Chen, X., Zhang, Q., King, G.J., Wang, J., Liu, K. A CACTA-like transposable element in the upstream region of BnaA9.CYP78A9 acts as an enhancer to increase silique length and seed weight in rapeseed. **The Plant Journal**, v.98, p.524-539, 2019.

Singh, H., Meghwal, M. Physical and thermal properties of various ajwain (*Trachyspermum ammi* L.) seed varieties as a function of moisture content. **Journal of Food Process Engineering**, v.43, e13310, 2019.

Sologubik, C.A., Campanone, L.A., Pagano, A.M., Gely, M.C. Effect of moisture content on some physical properties of barley. **Industrial Crops and Products**, v.43, p.762–767, 2013.

Song, N.D., Peng, W., Zhan, J., Shi, J., Wang, X., Liu, G., Wang, H. Maternal control of seed weight in rapeseed (*Brassica napus* L.): the causal link between the size of pod (mother, source) and seed (offspring, sink). **Plant Biotechnology Journal**, v.17, p.736-749, 2018.

Soylu, S., Çarman, K., Çitil, E. Fuzzy Knowledge-Based Model for Prediction of the Terminal Velocities of the Chickpea and Dry Bean Seeds. **Selcuk Journal of Agricultural and Food Sciences**, v.34, p.99-106, 2020.

Sweat, V.E. **Engineering Properties of Foods**, New York: Marcel Dekker, 1986.

Vashishth, R., Semwal, A.D., Pal Murugan, M., Raj, T.G., Sharma, G.K. Engineering properties of horse gram (*Macrotyloma uniflorum*) varieties as a function of moisture content and structure of grain. **Journal of Food Science and Technology**, v.57, p.1477-1485, 2020.

Vishwakarma, R.K., Shivhare, U.S., Nanda, S.K. Physical properties of guar seeds. **Food and Bioprocess Technology**, v.5, p.1364-1371, 2012.

Wei, T., Luo, M., Zhang, H., Jia, W., Zeng, Y., Jiang, Y. Curvularia verruculosa as new causal pathogen of common bean leaf spot disease in China. **Crop Protection**, v.162, 106091, 2022.

Yu, D.U.,Shrestha, B.L., Baik, O.D. Thermal conductivity, specific heat, thermal diffusivity, and emissivity of stored canola seeds with their temperature and moisture content. **Journal of Food Engineering**, v.165, p.156-165, 2015.

CHAPTER 3

DRYING KINETICS, CFD MODELING AND THERMODYNAMIC PROPERTIES OF COMMON BEAN GRAINS (*PHASEOLUS VULGARIS* L.)

Abstract: Understanding bean kinetics and thermodynamic properties of the drying process is essential for designing and optimizing equipment and drying control. Therefore, this study aimed to evaluate and model the drying kinetics of common beans, experimental and numerically, by Computational Fluid Dynamics (CFD) technique and the thermodynamic properties at different temperatures. The bean grains were dried in a cylindrical tray dryer at different temperatures (40, 50, 60, 70, and 80 ± 2 °C). Several mathematical models describing the drying of agricultural products were fitted to experimental data. The effective diffusion coefficient was obtained considering the equivalent radius of the grains as constant and variable (as a function of water content). The activation energy was obtained, and the thermodynamic properties, enthalpy, entropy, and Gibbs free energy of activation were determined. A thin layer model and a single grain model were implemented in CFD to predict the drying behavior. The Henderson and Pabis modified model satisfactorily represented the drying of bean grains. Drying time varied between 585 and 150 minutes for temperatures of 40 and 80 °C, respectively. The diffusion coefficients varied between 1.1388×10^{-10} and 2.5694×10^{-10} m^2 s^{-1}, considering the initial equivalent radius of the grains, and between 1.1090×10^{-10} and 2.5035×10^{-10} m^2 s^{-1} considering the equivalent radius as variable, for temperatures from 40 to 80 °C, respectively. The activation energy was approximately 19.4 kJ mol^{-1}. The enthalpy varied between 16.77 and 16.43 kJ mol^{-1}, the entropy changed between -374.63 and -375.63 J mol^{-1} K^{-1}, and the Gibbs free energy increased from 134.1 to 149.1 kJ mol^{-1} for temperatures of 40 and 80 °C, respectively.

Keywords: Activation energy. Diffusion coefficient. Mathematical modeling Moisture diffusivity.

1. INTRODUCTION

The common bean (*Phaseolus vulgaris* L.) is undoubtedly one of the most essential legumes for human consumption worldwide (El-Saadony, 2021). In 2020, world production of dried beans was approximately 27.5 million tons and about 34.8 million hectares of cultivated land, according to data published by the Food and Agriculture Organization (FAO, 2022). The common bean has a high nutritional value, a good ratio between carbohydrates and proteins, and a high diversity of amino acids. Its composition also includes minerals, phenolic compounds, unsaturated fatty acids, and a good amount of dietary fiber and oligosaccharides (Sandoval-Peraza et al., 2021). In addition to its important nutritional properties, this crop has a low production cost and is considered a critical food in many countries, especially in developing countries. Besides, beans are well suited for long-term storage if drying is carried out correctly and the initial water content of the product is reduced to adequate levels (Resende et al., 2022).

Drying is one of the oldest methods used for preserving agricultural products and one of the most important unit operations in the food processing industry. The main drying objective is to reduce water activity and prolong the product's shelf life (Pandiselvam et al., 2023). Reducing the product's water content reduces microbial growth and enzymatic activity, preventing deterioration. In addition, drying contributes to reducing the weight and volume of the product, facilitating, and reducing the cost of storage and transportation (Mousakhani-Ganjeh et al., 2021; Pravallika et al., 2023). During drying, there is simultaneous interaction of different thermophysical, chemical, and enzymatic processes in the product. The level of interaction of these processes depends on the hygroscopic and biological properties of the raw material (Granella et al., 2022). When conducted improperly, drying can lead to undesirable results, mainly related to the deterioration of product quality. Thus, efficient drying techniques are not only based on reducing energy consumption and dehydration period but also on preserving the stability of the product and its quality components (Xu et al., 2022).

Drying is a complex process involving simultaneous heat and mass transfer, which are affected by internal and external product resistances (Adnouni et al., 2023). During the drying of agricultural products, the inner moisture transfer mechanism is mainly composed of capillary forces in the period of constant drying rate and diffusion during the decreasing drying rate (Yu et al., 2020). As for the external resistances, these are mainly dependent on

the temperature, flow rate, and relative humidity of the drying medium (Hatami et al., 2020). Capillary movement and diffusion of water vapor in the product are directly related to the drying conditions used (Granella et al., 2022). Detailed knowledge of the kinetic behavior of drying the product, the parameters involved, and the thermodynamic properties of this process are essential for designing, optimizing, and controlling drying (Bissaro et al., 2022).

Drying kinetics is the basis for understanding and describing drying mechanisms, controlling, and optimizing process parameters, predicting drying data, modeling heat and mass transfer, effective moisture diffusivity, and activation energy (Mishra et al., 2021). This technique helps to understand how the product's water removal progress occurs and determine the most suitable conditions for drying. Furthermore, in practical terms, it can be time-consuming and costly to optimize this process at full scale through trial and error (Delfiya et al., 2021; Najib et al., 2022). Mathematical models provide a better fit for the experimental data. They have been used to explain the product's behavior during drying and to extrapolate the results to other operational conditions, allowing the design and optimization of dryers. Among them are the thin-layer models developed based on Newton's law of cooling (Lewis, Page, and Modified Page), Fick's second law of diffusion (Logarithmic, Henderson and Pabis, exponential models of 2 and 3 terms and exponential models modified), among others (Kumar et al., 2022).

Throughout the drying process, it is interesting not only to evaluate the drying kinetics through the curves of water content reduction as a function of time but also to study the thermodynamic properties of the process. These properties (enthalpy, entropy, and Gibbs free energy) play a crucial role in describing the phenomena that occur at the intramolecular level in biological materials (Karataş and Arslan, 2022). Enthalpy changes measure the energy change that occurs when water molecules interact with product constituents during sorption processes (Silva et al., 2016). Entropy is related to the degree of disorder; that is, it is associated with the spatial arrangement of the water-product ratio. Gibbs free energy, in turn, is a parameter used to assess the spontaneity of water desorption (Corrêa et al., 2017). The study of these properties is an essential source of information for designing drying equipment, calculating the energy required in this process, studying the properties of adsorbed water, evaluating the microstructure of food, and studying the physical phenomena that occur on the surface of the product (Öztekin et al., 2022).

Numerical modeling of the drying process is an effective alternative to experimental approaches to develop new procedures or optimize existing processes with relatively low costs and has attracted the attention of several researchers (Azmir et al., 2020). Among

several numerical models, computational fluid dynamics (CFD) is a highly versatile tool that can be used to study different processes (Prommuak et al., 2020). The CFD method solves the governing transport equations, which include coupled non-linear differential equations to describe the conservation laws, by discretizing them into a set of algebraic equations. However, in-depth knowledge of heat and mass transfer fundamentals is essential for this approach. According to Jubaer et al. (2019), this method has been used with the same frequency as the traditional didactic methods of performing experiments and mathematical modeling to solve problems involving fluid flow and heat and mass transfer in the industrial and academic areas.

Driven by the continued development of computers, the adoption of numerical approaches has become increasingly common to investigate the characteristics of heat, mass, and momentum transfer in various complex processes. The CFD technique offers the advantage of saving cost and time during experimentation while simultaneously overcoming the limitations of analytical solutions (Jubaer et al., 2019). In addition, computer simulation can act as virtual sensors of humidity, speed, and temperature allowing internal parameters in inaccessible places to be possible. Furthermore, it is sensitive to small changes, and there are no limitations in testing different and unusual drying conditions (Malekjani and Jafari, 2018).

Although the drying process is an essential operation in post-harvest processing, and updated data are critical for the design and optimization of equipment and procedures, the literature on numerical modeling, drying kinetics, and determination of thermodynamic properties of common bean grains is limited, and most data needs to be updated. Given the above, this work aimed to evaluate and model the drying kinetics of common bean grains and thermodynamic properties at different temperatures. Furthermore, two CFD numerical models of the drying process were considered and validated. The results of this study will be beneficial to the bean industry, providing data to design and optimize equipment and the drying process.

2. MATERIAL AND METHODS

2.1. Obtaining the raw material

This study was carried out at the Laboratory of Physical Properties and Quality Assessment of Agricultural Products at the National Center for Storage Training (CENTREINAR), located at the Federal University of Viçosa (UFV), Viçosa - Minas Gerais,

Brazil. Common bean grains of the BRS–Estilo variety were used in this study. The samples used in this study were collected wet, with an initial water content of 0.41 (decimal, d.b.), in the experimental area belonging to the Department of Agronomy of the Federal University of Viçosa (20°45'00" S, 42°56'15" W; 643 m a.s.l.). The harvested pods were subjected to the manual threshing process to reduce the mechanical damage to the wet grains. The threshed grains were submitted to an initial sorting and selected for color uniformity (eliminating green grains that did not reach physiological maturity) and average size (eliminating sluggish and malformed grains). The threshed grains were immediately stored in the biochemical oxygen demand (BOD) chamber at 4 ± 2 °C until the beginning of the experiments.

2.2. Drying kinetics

In this study, common bean grains were dried in a GrainMan 6623 cylindrical tray dryer. Four removable trays were placed on top of the dryer's four fixed trays, making it easier to weigh the product during drying. To perform the drying kinetics, 200 grams of grains were placed on each of the four removable trays. The grains were dried at temperatures of 40, 50, 60, 70, and 80 ± 2 °C in an air flow with a velocity of 1 m s^{-1} in each tray. During drying, the product's mass reduction was monitored every 5 minutes using a digital scale (Marte® AS2020) with a precision of 0.01 g.

The samples' initial and final water content were determined by the standard oven method at 105 ± 2 °C for 24 hours in four replications, according to the standard method described in Brasil (2009), and the results were expressed on a dry basis (d.b.). A Marte® AY220 analytical balance with a precision of 0.0001g was used to measure the weight of the samples during the determination of the water content. Table 1 presents the mathematical models commonly used to describe the drying kinetics of agricultural products (Corrêa et al., 2019; Salehi and Satorabi, 2021). These models were adjusted to dry bean grain data for each temperature. The modeling was performed to moisture content around 0.1364 (decimal, d.b.) according to the Resolution RDC No. 272 of September 22 of ANVISA National Health Surveillance Agency (Brasil, 2005).

Table 1 – Mathematical models traditionally used to describe agricultural products' thin-layer drying process.

Model designation	Model	Eq.
Newton	$M_R = \exp(-kt)$	(1)
Page	$M_R = \exp(-kt^n)$	(2)
Henderson and Pabis	$M_R = a\exp(-kt)$	(3)
Logarithm	$M_R = a\exp(-kt) + b$	(4)
Midilli	$M_R = a\exp(-kt^n) + bt$	(5)
Two-terms	$M_R = a\exp(-k_0 t) + b\exp(-k_1 t)$	(6)
Verna	$M_R = a\exp(-k_0 t) + (1-a)\exp(-k_1 t)$	(7)
Diffusion approximation	$M_R = a\exp(-kt) + (1-a)\exp(-kbt)$	(8)
Two-term exponential	$M_R = a\exp(-kt) + (1-a)\exp(-kat)$	(9)
Henderson and Pabis modified	$M_R = a\exp(-kt) + b\,exp(-gt) + c\,exp(-ht)$	(10)

Where,

M_R – Moisture ratio, decimal;

t – Drying time, min;

k, k_0, k_1 – Drying constants, min^{-1};

a, b, c, g, h, n – Model coefficients.

The moisture ratio of the bean grains for the different drying temperatures was determined according to Equation 11. The grains were not dried until the equilibrium moisture content, so data obtained in the literature for bean grains were used. The equilibrium water content was obtained according to Equation 12 (Resende et al., 2006). The relative humidity of the drying air was determined by psychrometry. First, the ambient temperature was obtained using K-type thermocouples connected to an ICP CON LR-7518 data acquisition module. The data were then transmitted to an ICP CON LR-7520 serial converter module connected to the computer. The relative humidity of the ambient air was obtained by the average of the direct reading of 3 analog hygrometers. Data were read every 5 minutes throughout the drying process.

$$M_R = \frac{M_T - M_E}{M_0 - M_E} \tag{11}$$

$$M_E = \left[\frac{\exp(6.1927 - 0.0348T)}{-\ln(RH)}\right]^{1/2.0973} \tag{12}$$

Where,

M_R – Moisture ratio, decimal;

M_T – Moisture content on time, decimal, d.b.;

M_0 – Initial moisture content, decimal, d.b;

M_E – Equilibrium moisture content, decimal, d.b;

T – Drying air temperature, °C; and

RH – Relative humidity of the drying air, decimal;

To define the best model to represent the drying of common bean grains, nonlinear regression analyzes were performed using the statistical software STATISTICA 8.0®. The model was chosen based on a series of statistical parameters, such as the coefficient of determination (R^2), the magnitude of the mean relative error (RME), the standard deviation of the estimate (SE), the behavior of the distribution of residuals and the significance of the regression coefficients, adopting the levels of 1 and 5% probability. The mean relative error and standard deviation of the estimate were calculated according to Equations 13 and 14, respectively.

$$RME = \frac{100}{n}\sum_{i=1}^{n}\frac{\left|Y_i - \hat{Y}_i\right|}{Yi} \tag{13}$$

$$SE = \sqrt{\frac{\sum_{i=1}^{n}\left(Y_i - \hat{Y}_i\right)^2}{DFR}} \tag{14}$$

Where,

Y_i – Observed value;

$\hat{Y}_i$ – Estimated value;

n – Number of observed data; and

DFR – Degrees of freedom of the residue.

The effective diffusion coefficient of common bean grains was obtained by adjusting the mathematical model of liquid diffusion, according to Equation 15 (Lisboa et al., 2019). The approximated solution by Fourier series (Equation 15) of Fick's second law assumes the condition of known water content on its surface. According to Doymaz (2008), the effective diffusion coefficient for agricultural products is in the order of 10^{-11} to 10^{-9} m^2 s^{-1}. A finite number of terms (n) of the serie can be used for a specified precision. This study established the number of terms when the diffusion coefficient variation was less than 1×10^{-14} m^2 s^{-1} at all evaluated temperatures.

$$M_R = \frac{6}{\pi^2}\sum_{i=1}^{n}\frac{1}{n^2}\exp\left[-\frac{n^2\pi^2\,D_{ef}\,t_s}{r_e^2}\right] \quad (15)$$

Where,

D_{ef} – Effective diffusion coefficient, m^2 s^{-1};

n – Number of terms in the series;

t_s – Drying time, s; and

r_e – Equivalent radius of the product, m.

The equivalent radius used in the diffusion model is defined as the radius of the sphere whose volume is equal to that of the product. The volume of common bean grains can be calculated according to Equation 16 (Mohsenin, 1986). Thus, it is easy to deduce that the equivalent radius can be calculated according to Equation 17. To determine the equivalent radius, 50 bean grains with initial water content had their characteristic dimensions measured using a digital caliper with a resolution of 0.01 mm (Mitutoyo 500-174B). A parallel experiment was conducted to verify the influence of volumetric grain contraction on the effective diffusion coefficient. Thus, 1 kg of beans was dried in a forced circulation oven at 45 ± 2 °C. During drying, 50 grains were measured for ten different water content levels. Regression analysis showed that the equivalent grain radius could be expressed as a function of water content. Finally, the equation obtained replaced the fixed value of the equivalent radius in Equation 15. The values of the diffusion coefficient, adopting the equivalent radius as fixed and variable, were compared using the Tukey test, assuming the 5% probability level.

$$V = \frac{\pi LWT}{6} \quad (16)$$

$$r_e = \frac{\sqrt[3]{LWT}}{2} \quad (17)$$

Where,

V – Product volume, m^3;

L – Beans length, m;

W – Beans width, m; and

T – Beans thickness, m;

The Arrhenius equation (Equation 18) was used to evaluate the effect of drying air temperature on the effective diffusion coefficient of common bean grains. It can be seen from the composition of the equation that the ratio of ln (D_{ef}) as a function of the inverse of temperature (T_{abs}^{-1}) results in a straight line. The angular coefficient of this straight line makes it possible to estimate the activation energy value for the evaluated experiment. During the drying processes, the lower the activation energy, the greater the diffusivity of water in the product. The activation energy is a barrier that must be overcome to trigger the diffusion process in the product (Kashaninejad et al., 2007).

$$D_{ef} = D_0 \exp\left(-\frac{E_a}{R\,T_{abs}}\right) \quad (18)$$

Where,

D_0 – Maximum effective diffusion coefficient (at infinite temperature), $m^2\,s^{-1}$;

E_a – Activation energy, J mol^{-1};

R – Gas constant, 8,314 J mol^{-1} K^{-1}; and

T_{abs} – Absolute drying air temperature, K.

Different thermodynamic parameters of the drying of bean grains were obtained from the activation energy values. Among these, enthalpy, entropy, and Gibbs free energy were calculated according to Equations 19, 20, and 21, respectively (Jideani and Mpotokwana, 2009).

$$\Delta H^* = E_a - R\,T_{abs} \quad (19)$$

$$\Delta S^* = R\left[\ln A - \ln\left(\frac{k_b}{h_p}\right) - \ln T_{abs}\right] \quad (20)$$

$$\Delta G^* = \Delta H^* - T_{abs}\Delta S^* \quad (21)$$

Where,

ΔH^* – Enthalpy, J mol^{-1};

ΔS^* – Entropy, J mol^{-1} K^{-1};

ΔG^* – Gibbs free energy, J mol^{-1};

A – The ordinate intersection in the activation energy regression analysis;

k_b – Boltzmann constant, 1.38×10^{-23} J K^{-1}; and

h_p – Planck constant, 6.626×10^{-34} J s^{-1}.

2.3. CFD numerical modeling of common bean grain drying process

The drying process of bean grains in CFD was modeled in two different ways. Firstly, a layer of grains was modeled as a porous medium with known properties. In a second way, an alternative single-grain approach was used. The considerations for modeling both cases will be discussed below.

2.3.1. Numerical model for thin layer drying (porous medium)

The present model modeled a thin layer of grains as a porous medium. It was considered that the grains were in temperature equilibrium with the intergranular drying air, since the drying curve of these products is mainly governed by the decreasing drying rate (Thorpe et al., 2008).

2.3.1.1. Governing equations

The equations of continuity and conservation of momentum of the drying air were solved according to Equations 22 and 23 respectively (Ranjbaran et al., 2014). The boundary

conditions for Equation 23 include the no-slip condition on the walls, prescribed air mass flow rate at the inlet, and prescribed air pressure at the outlet.

$$\frac{\partial \rho_a}{\partial t} + \nabla \cdot (\rho_a \vec{u}) = 0 \tag{22}$$

$$\frac{\partial (\rho_a \vec{u})}{\partial t} + \nabla \cdot (\rho_a \vec{u}\, \vec{u}) = -\nabla P + \nabla \cdot \bar{\bar{\tau}} + \rho_a \vec{g} + S_m \tag{23}$$

Where,

t – Time, s;

ρ_a – Air density, kg m^{-3};

$\vec{u}$ – Velocity vector, m s^{-1};

P – Pressure, Pa;

$\vec{g}$ – Gravitational acceleration vector, m s^{-2};

S_m – Momentum source term, Pa m^{-1};

$\bar{\bar{\tau}}$ – Reynolds stress tensor, Pa.

Heat transfer within the porous zone was modeled using the energy balance equation (Equation 24) (Ramachandran et al., 2018). Boundary conditions for this equation include adiabatic grain bed walls and prescribed inlet drying air temperature. The effective thermal conductivity (k_{eff}) was obtained according to Equation 25. The enthalpies of air and solids were defined according to Equations 26 and 27, respectively.

$$\frac{\partial}{\partial t}(\rho_a \varepsilon I_a + \rho_s (1-\varepsilon) I_s) + \nabla \cdot (\rho_a \vec{u}\, I_a) = k_{eff} \nabla^2 T + S_h \tag{24}$$

$$k_{eff} = \varepsilon k_a + (1-\varepsilon) k_s \tag{25}$$

$$I_a = (C_{pa} + w C_{pv}) T \tag{26}$$

$$I_s = C_{ps} T \tag{27}$$

Where,

ε – Porosity, $m^3\ m^{-3}$;

I_a – Air enthalpy, $J\ kg^{-1}$;

ρ_s – Solid density, $kg\ m^{-3}$;

I_s – Solid enthalpy, $J\ kg^{-1}$;

k_a – Thermal conductivity of air, $W\ m^{-1}\ K^{-1}$;

k_s – Thermal conductivity of the product, $W\ m^{-1}\ K^{-1}$;

k_{eff} – Effective thermal conductivity, $W\ m^{-1}\ K^{-1}$;

S_h – Energy source term, $W\ m^{-3}$;

C_{pa} – Specific heat of air, $J\ kg^{-1}\ K^{-1}$;

C_{pv} – Specific heat of vapor, $J\ kg^{-1}\ K^{-1}$;

C_{ps} – Specific heat of solid, $J\ kg^{-1}\ K^{-1}$;

T – Temperature, K.

The drying air humidity was defined as a user-defined scalar (UDS) to simulate the moisture distribution within the porous medium. Thus, an additional equation was solved to predict moisture transport in the air (Equation 28) (Ranjbaran et al., 2014). The boundary conditions for this equation include zero moisture flow into the walls and prescribed absolute air humidity at the inlet.

$$\frac{\partial(\rho_a w)}{\partial t} + \nabla\cdot(\rho_a \vec{u} w) = \nabla\cdot(\rho_a D_{eff} \nabla \mathrm{w}) + S_w \tag{28}$$

Where,

w – Absolute air humidity, d.b., $kg\ kg^{-1}$.

D_{eff} – Effective diffusion coefficient of the product, $m^2\ s^{-1}$;

S_w – Humidity source term, $kg\ m^{-3}\ s^{-1}$.

2.3.1.2. Source terms

The resistance of the porous medium to the drying airflow in the vertical direction can be expressed by Equation 29 (Kumar and Saha, 2021). This source term describes the resistance to airflow due to the porous medium. Resistance to airflow can be divided into

viscous (Equation 30) and inertial (Equation 31) resistances. These terms refer to the vertical resistances in the grain bed. Thus, a pressure drop in the horizontal direction of 70% of the pressure drop in the vertical direction was used, as presented by Ranjbaran et al. (2014).

$$S_m = \frac{dP}{dy} = -\left(\frac{\mu}{\alpha} v + C_2 \frac{1}{2} \rho_a v^2\right) \quad (29)$$

$$\alpha = \frac{{d_p}^2 \varepsilon^3}{150 (1-\varepsilon)^2} \quad (30)$$

$$C_2 = \frac{1.75 (1-\varepsilon)}{d_p \varepsilon^3} \quad (31)$$

Where,

μ – Air viscosity, Pa s;

α – Permeability, m^2;

C_2 – Inertial resistance factor, m^{-1};

d_p – Average grain diameter, m.

The moisture source term due to the evaporation of water from grains can be described according to Equation 32 (Ranjbaran et al., 2014).

$$S_w = -(1-\varepsilon)\rho_s \frac{\partial M}{\partial t} \quad (32)$$

To predict the drying rate of the product in each computational cell, the best fit model to the experimental data for moisture ratio was used. Equation 12 was used to predict the equilibrium water content of common bean grains.

The energy source term due to evaporative cooling can be obtained according to Equation 33. The latent heat of vaporization of free water can be obtained according to Equation 34 for the temperature range used in this study (Ranjbaran and Zare, 2012).

$$S_h = (1-\varepsilon)\rho_s \frac{\partial M}{\partial t} h_{fg} \quad (33)$$

$$h_{fg} = 2503000 - 2386\,(T - 273.15)\ for\ 273.15 < T(K) < 533.15 \quad (34)$$

2.3.1.3. Equations for grain properties

The properties of bean grains dependent on the water content used were obtained from previous chapters of this study, according to equations 35-38.

$$C_{ps} = 2178.033 + 1629.336\,M \quad (35)$$

$$K_s = 0.220 - 0.594\,M + 1.982\,M^2 \quad (36)$$

$$\varepsilon = 28.651 + 23.827\,M \quad (37)$$

$$\rho_s = 822.236 - 215.070\,M \quad (38)$$

2.3.1.4. Equations for drying air properties

The thermodynamic properties of the drying air were estimated according to the relationships shown in Equations 39-43 (Ranjbaran et al., 2014).

$$\rho_a = \frac{101.325}{0.278\,T} \quad (39)$$

$$C_{pa} = 1009.26 - 4.0403 \times 10^{-3}(T - 273.15) + 6.1759 \times 10^{-4}(T - 273.15)^2 - 4.097 \times 10^{-7}(T - 273.15)^3 \quad (40)$$

$$\mu = 1.691 \times 10^{-5} + 4.984 \times 10^{-8}(T - 273.15) - 3.187 \times 10^{-11}(T - 273.15)^2 + 1.319 \times 10^{-14}(T - 273.15)^3 \quad (41)$$

$$P_{vs} = 0.1 \exp\left(27.0214 - \frac{6887}{T} - 5.31 \ln\left(\frac{T}{273.16}\right)\right) \quad (42)$$

$$RH = \frac{101.3w}{0.62189\ P_{vs} + wP_{vs}} \quad (43)$$

Where,

P_{vs} – Saturation vapor pressure, kPa;

RH – Relative humidity, decimal.

2.3.1.5. Physical model and simulation procedure

The physical model used in this case consisted of a grain layer with a height of 5 cm. The diameter of the grain layer was 20 cm, a value corresponding to the diameter of the dryer tray used in the experimental formulation. A plenum chamber was added just below the porous bed, with a height of 5 cm. The physical model was generated using the Design Modeler pre-processing software, and the computational domain was divided into finite volumes using meshes with hexahedral elements. Mesh independence tests were performed by successively refining the mesh until the temperature and velocity variables at a given point (in the center of the grain layer) varied less than 0.1 °C and 10^{-2} m s^{-1}, respectively. The final mesh for this case had 13.62×10^4 elements and 19.85×10^4 nodes. Table 2 shows a summary of the element and node numbers, as well as the temperatures and velocities verified during the mesh independence test. Figure 1 presents the physical model and the final mesh applied for the final simulations.

Table 2 – Mesh independence test evaluating temperature and velocity for modeling thin layer drying.

Test 1		***Test 2***	
Elements	3.01×10^4	Elements	8.60×10^4
Nodes	4.56×10^4	Nodes	12.33×10^4
Temperature (ºC)	59.7	Temperature (ºC)	59.8
Velocity (m s^{-1})	1.08	Velocity (m s^{-1})	1.10
Test 3 (Mesh used)		***Test 4***	
Elements	13.62×10^4	Elements	22.75×10^4
Nodes	19.85×10^4	Nodes	32.97×10^4
Temperature (ºC)	59.9	Temperature (ºC)	59.9
Velocity (m s^{-1})	1.12	Velocity (m s^{-1})	1.12

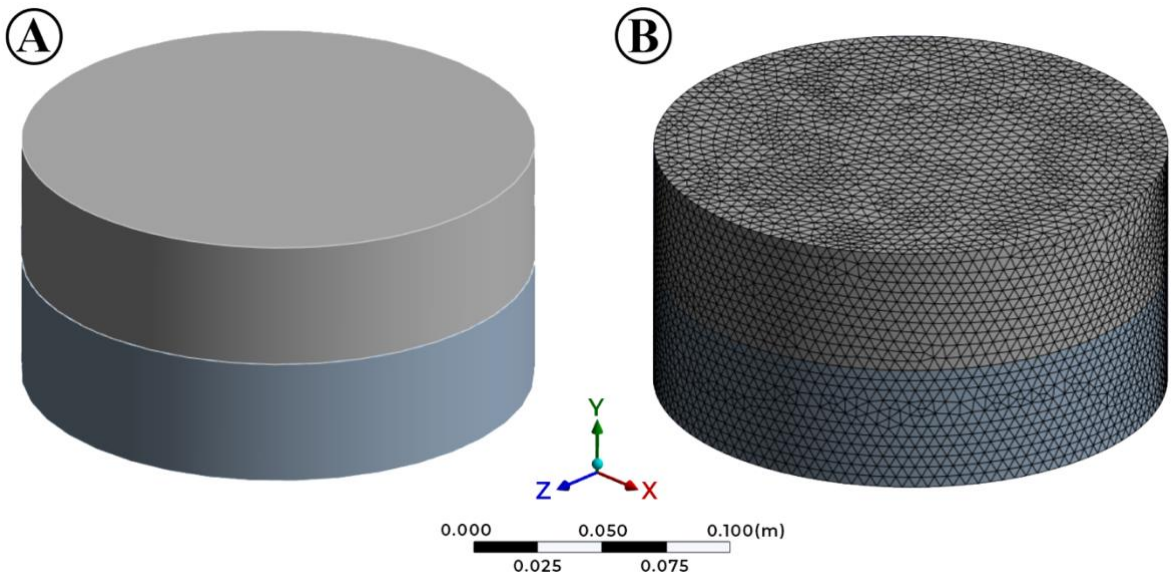

Figure 1. Details of (A) physical model and (B) final mesh used to simulate the thin layer model composed of a 5 cm grain layer at the top and a 5 cm plenum at the bottom.

The set of governing equations was integrated over the control volumes, producing a set of algebraic equations. The technique based on finite control volumes was used for this purpose. The equations were implemented and solved using the commercial software ANSYS FLUENT version 22.2. A User-Defined Function (UDF) written in C language was used for additional calculations and updates (updating the water content of grains; calculation of properties dependent on water content; calculation of heat source and humidity terms). The

thermal equilibrium model was used based on the double cell approach in the porous medium. Therefore, each cell in the computational domain of the porous medium is composed of fluid and solid overlapping. The initial moisture and moisture balance of the drying air were implemented as a User-Defined Scalar (UDS). The airflow in the porous zone was considered laminar. The typical values of under-relaxation factors were 0.4–0.8, according to the need to achieve convergence. The complete simulation settings and boundary conditions are listed in Table 3.

Table 3 – Description of simulation settings for the thin layer model.

Description	Method/value
Operating, boundary, and initial conditions	
Operating pressure (Pa)	101325
Gravitational acceleration (m s^{-2})	9.81
Inlet boundary condition	Velocity-inlet 1 m s^{-1}, Temperature
Outlet boundary condition	Pressure-outlet, zero gage pressure
Wall boundary condition	Wall, adiabatic
Solution	
Solver	Pressure based
Discretization method	Second-order upwind
Pressure discretization	Second-order
Time step (s)	0.01
Unsteady formulation	Second-order implicit
Maximum number of iterations per time step	20
Convergence criteria	10^{-4}
Under-relaxation factors	0.4 – 0.8
Pressure-velocity coupling	SIMPLE

2.3.2. Numerical model for the single grain

In the present model, a single grain was considered during drying in an upward airflow. For this case, a multiphase model of thermal equilibrium between the drying air and the bean grain was considered. Among the available multiphase models, the Volume of Fluid (VOF) model was used. The VOF model can model two or more immiscible fluids by solving a single set of momentum equations and tracking the volume fraction of each of the fluids

across domains. For this approach, the grain is modeled as a porous medium with a porosity of 0.005. The properties of bean grains characterize the solid part of the porous medium. The fluid domain is then composed of 3 phases, water-liquid, vapor, and air. The VOF model then solves the equations between the mass exchange within the phases, and the exchange on the grain surface, representing the drying process. The advantage of the VOF model is that in each control volume, the volume fractions of all phases add up to unity. Fields for all variables and properties are shared across phases and represent the volumetric average of values. Thus, the variables and properties in any given cell are either purely representative of one of the phases or representatives of a mixture of the phases, depending on the volume fraction values. Therefore, in this case, solving the additional psychrometric equations for the drying air is unnecessary, as the air properties are updated as a mixture between the phases after each exchange.

2.3.2.1. Governing equations

The interface(s) between the phases is tracked by solving a continuity equation for the volume fraction of one (or more) of the phases. For the phase, the continuity equation can then be written according to Equation 44 (Ferreira et al., 2015).

$$\frac{1}{\rho_q}\left[\frac{\partial}{\partial t}\left(\alpha_q \rho_q\right) + \nabla.\left(\alpha_q \rho_q \vec{u}_q\right) = \sum_{p=1}^{n}\left(\dot{m}_{pq} - \dot{m}_{qp}\right)\right] \tag{44}$$

Where,

$\dot{m}_{pq}$ – Mass transfer from phase p to phase q, kg s^{-1};

$\dot{m}_{qp}$ – Mass transfer from phase q to phase p, kg s^{-1};

α_q – Phase volume fraction, dimensionless; and

ρ_q – Mixture phase density, kg m^{-3}.

A single momentum equation is solved for the entire computational domain, and the resulting velocity field is shared between phases. The momentum equation (Equation 45) is therefore dependent on the volume fractions of all phases through the ρ and μ properties (Sun

et al., 2012). Furthermore, the surface tension force $\overrightarrow{F}_{cs}$ is modeled as a volumetric force using the continuous surface force model of Brackbill et al. (1992) according to Equation 46.

$$\frac{\partial(\rho\,\vec{u})}{\partial t} + \nabla\cdot(\rho\,\vec{u}\,\vec{u}) = -\nabla \mathrm{P} + \nabla\cdot[\mu(\nabla\,\vec{u} + \nabla\,\vec{u}^{T})] + \rho\,\overrightarrow{g} + \overrightarrow{F}_{cs} \tag{45}$$

$$\overrightarrow{F}_{cs} = \sigma\,\frac{\rho k \nabla \alpha_v}{0.5\,(\rho_l + \rho_v)} \tag{46}$$

Where,

$\overrightarrow{F}_{cs}$ – Surface tension force, N m^{-3};

σ – Surface tension coefficient, N m^{-1};

k – Interface curvature, m^{-1};

α_v – Vapor volume fraction, dimensionless;

ρ_l – Liquid phase density, kg m^{-3}; and

ρ_v – Vapor phase density, kg m^{-3}.

The energy equation is also shared between the phases and can be expressed according to Equation 47. The VOF model treats energy (E) and temperature (T) as mass-averaged variables (Equação 48) (Szijártó et al., 2017).

$$\frac{\partial}{\partial t}(\rho E) + \nabla\cdot\left(\vec{u}\,(\rho E + p)\right) = \nabla\cdot\left(k_{eff}\nabla T\right) \tag{47}$$

$$E = \frac{\sum_{q=1}^{n}\alpha_q\rho_q E_q}{\sum_{q=1}^{n}\alpha_q\rho_q} \tag{48}$$

The mass transfer mechanism between the phases was modeled using the Lee model. This is a physically based mechanistic model widely used in VOF models. In the Lee model, liquid-vapor mass transfer (evaporation and condensation) is governed by vapor transport, as per Equation 49.

$$\frac{\partial}{\partial t}(\alpha_v\rho_v) + \nabla.\,(\alpha_v\rho_v\vec{u}_v) = \dot{m}_{lv} - \dot{m}_{vl} \tag{49}$$

Where,

$\dot{m}_{lv}$ – Volumetric rate of mass transfer due to evaporation, kg s^{-1} m^{-3};

$\dot{m}_{vl}$ – Volumetric rate of mass transfer due to condensation, kg s^{-1} m^{-3}.

2.3.2.2. Physical model and simulation procedure

The physical model used in this case consisted of a single bean grain, approximately 10 mm long, and a cylindrical drying tray with a diameter of 30 mm and a height of 150 mm. For a more accurate representation, the bean grain geometry was built in the Fusion 360 Software (Autodesk) based on the images obtained from the grains. The grain geometry was imported into the Design Modeler pre-processing software, and the cylindrical drying chamber was added. As the bean grain was the object of greatest interest in this model, the mesh independence tests were performed considering the average temperature of the volume composed of the grain, until the variation was less than 0.1 °C. The mesh was generated with hexahedral elements and a 2-layer refinement was added to the bean grain domain. The final mesh for this case had 15.09×10^4 elements and 21.76×10^4 nodes. Table 4 summarizes element and node numbers, and temperatures verified during the mesh independence test. Figure 2 presents the physical model and the final mesh applied for the final simulations.

Table 4 – Mesh independence test evaluating temperature for modeling single grain drying.

Test 1		***Test 2***	
Elements	4.23×10^4	Elements	9.60×10^4
Nodes	6.32×10^4	Nodes	14.22×10^4
Temperature (ºC)	69.7	Temperature (ºC)	69.9
Test 3 (Mesh used)		***Test 4***	
Elements	15.09×10^4	Elements	20.34×10^4
Nodes	21.76×10^4	Nodes	29.48×10^4
Temperature (ºC)	70.0	Temperature (ºC)	70.0

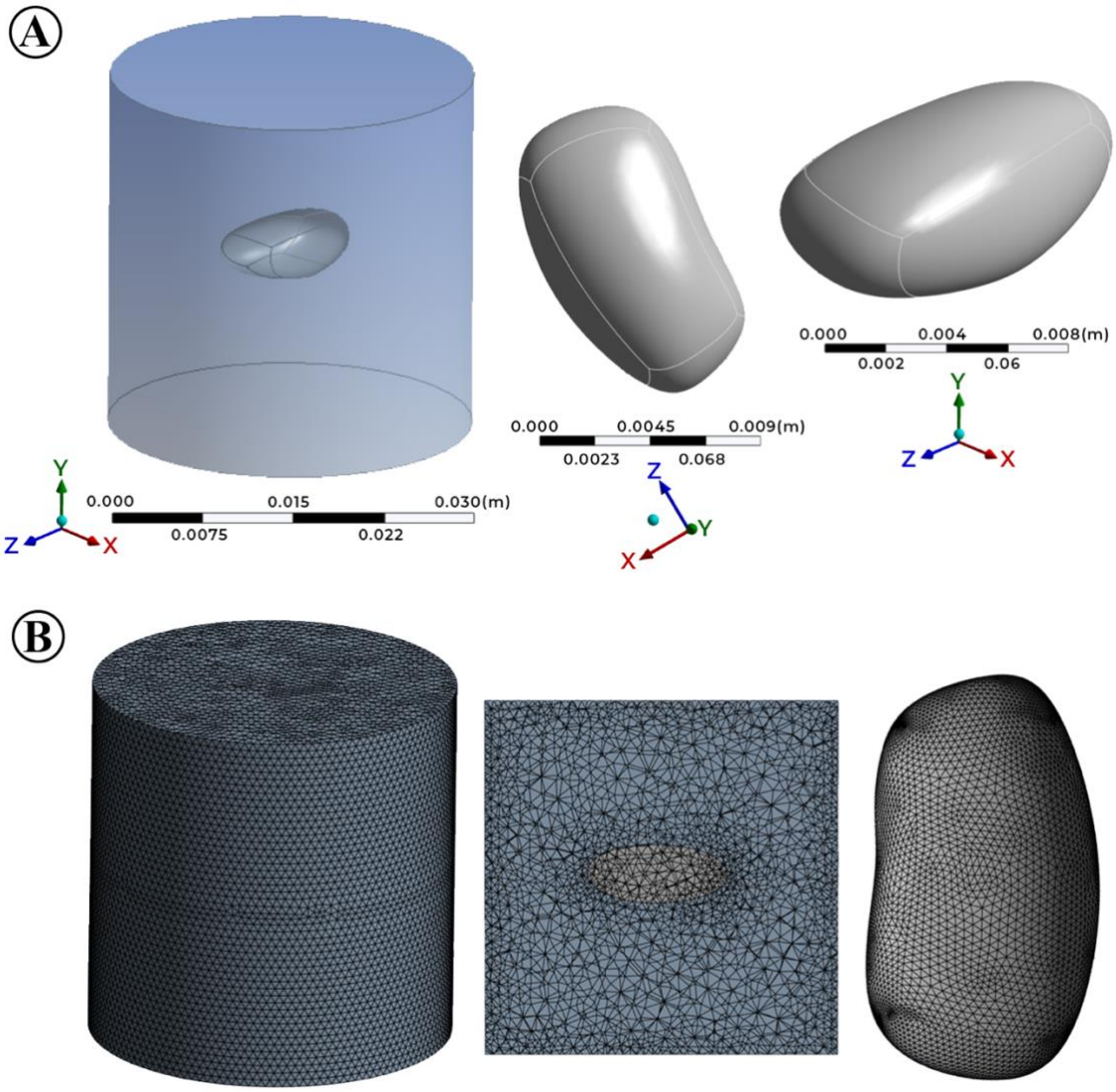

Figure 2. Details of (A) physical model and (B) final mesh used to simulate the single grain model.

The single grain model was also solved in commercial software ANSYS FLUENT version 22.2. The thermal equilibrium model was used based on the double cell approach in the porous medium. The initial grain moisture was treated as the fraction of the water-liquid phase within the common bean grain domain. The initial value is specified directly in the initialization conditions of the solution. A similar procedure is used to specify the absolute humidity of the drying air. The airflow was assigned as turbulent for this case, and the k-omega SST model was used. The values of relaxation factors and under-relaxation factors were adjusted as needed to achieve convergence. The drying process in this model is given by the transfer of mass from the water-liquid phase to the vapor phase. The flow resistances in the porous medium for the water and air phases controlled the mass transfer between the

phases. The adjustment process was carried out until reaching a result adequate to the experimental data for one of the drying temperatures. The complete simulation settings and boundary conditions are listed in Table 5.

Table 5 – Description of simulation settings for the single grain model.

Description	Method/value
Model	
Multiphase modeling	Volume of Fluid (VOF)
Volume fraction parameters	Implicit
Body force formulation	Implicit body force
Number of Eulerian phases	3
Operating, boundary, and initial conditions	
Operating pressure (Pa)	101325
Gravitational acceleration (m s^{-2})	9.81
Inlet boundary condition	Velocity-inlet 1 m s^{-1}, Temperature
Outlet boundary condition	Pressure-outlet, zero gage pressure
Wall boundary condition	Wall, adiabatic
Solution	
Solver	Pressure based
Pressure discretization	PRESTO!
Momentum discretization	First-order upwind
Volume fraction discretization	Modified HRIC
Turbulent Kinetic Energy discretization	First-order upwind
Specific Dissipation Rate discretization	First-order upwind
Energy discretization	Second-order upwind
Time step type	Adaptative – Multiphase-Specific
Initial time step (s)	0.00001
Unsteady formulation	First-order implicit
Maximum number of iterations per time step	20
Convergence criteria	10^{-4}
Under-relaxation factors	0.4 – 1.0
Explicit relaxation factors	0.7 – 0.9
Pressure-velocity coupling	Coupled

2.3.3. Validation procedure

The simulation results were validated using experimental data on the drying kinetics of common bean grains. Validations of CFD simulations were performed by calculating The Mean Relative Deviation (MRD) and Percent Relative Error (PRE), calculated according to Equations 50 and 51, respectively (Ranjbaran et al., 2014).

$$MRD = 100 \times \sqrt{\frac{1}{n}\sum_{j=1}^{n}\left(\frac{\varphi_{exp,j} - \varphi_{pre,j}}{\varphi_{exp,j}}\right)^2} \quad (50)$$

$$PRE = \frac{\varphi_{exp,j} - \varphi_{pre,j}}{\varphi_{exp,j}} \quad (51)$$

Where,

exp – Experimental;

pre – Predicted by simulation;

n – Number of points taken;

φ – Variable considered.

3. RESULTS AND DISCUSSION

3.1. Drying kinetics and thermodynamic properties

The drying curves of common bean grains express the loss of water from the grains over time, as seen in Figure 3. As expected, the drying time decreases as the temperature of the drying air increases. Increasing the temperature of the drying air increases the amount of heat transferred to the grains. Consequently, the speed of migration of the water inside the grains to its surface increases, and the water evaporates more quickly. Drying times varied between 585 and 150 minutes for temperatures of 40 and 80 °C, respectively.

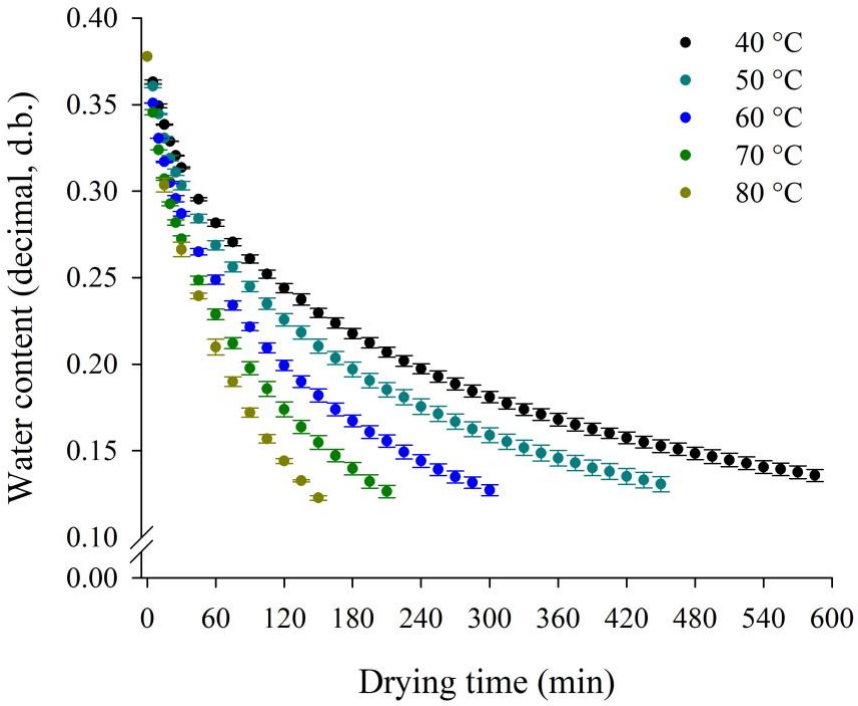

Figure 3. Experimental water content versus drying time of common bean grains at different temperatures. Error bars represent the standard deviation.

It is observed that the bean grains did not present a period of constant drying rate. Brooker et al. (1992) point out that the period of continuous drying rate occurs between water contents of 2.33 and 3.00 (decimal, d.b.), values much higher than those observed in this study. Mass transfer processes occur more quickly during the period of constant drying rate since a large amount of free water in the product is available. In this drying period, the water evaporates as free water. This is because the vapor pressure of free water in the product equals the vapor pressure of pure water at product temperature.

On the other hand, during the decreasing drying rate period, the product's surface is no longer saturated with water, and drying is regulated by the diffusion of moisture from the product's interior to its surface (Waheed and Komolafe, 2019). As Brooker et al. (1992) reported, the internal resistance to water transport in the product is greater than the external resistance in this period. Therefore, during the decreasing drying rate, there is a gradual reduction in the ability to remove water from the product that is more tightly bound to the cells. Consequently, this period requires greater energy for the diffusion of water from the product's interior to its surface (Siqueira et al., 2020).

Table 6 presents the statistical parameters of the drying modeling of common bean grains. It is observed that except for the Newton model, all other models showed a coefficient

of determination greater than 0.95 for all evaluated temperatures. Although the coefficient of determination is still frequently used in the context of the performance or validity of a given model, Spiess and Neumeyer (2010) point out that this coefficient may need to be revised for nonlinear regression. Therefore, parameters such as the mean relative error and the standard error of the estimate are essential to ensure the choice of an adequate model (Avhad and Marchetti, 2016). All evaluated models presented low values for the standard error of the estimate, and, except the Newton model, all also presented good values of the mean relative error. However, it is observed that the Page, Midilli, and Henderson and Pabis modified models presented the lowest values of these parameters for most drying temperatures. Only the Henderson and Pabis modified model showed random residual distribution for all temperatures. According to Corrêa et al. (2014), a model is considered inadequate if the distribution of residuals is biased. Therefore, the Henderson and Pabis modified model was selected as the best option to represent the drying of common bean grains.

Table 6 – Relative mean error (RME), the standard deviation of the estimate (SE), coefficient of determination (R^2), and residue distribution (RD) values for the mathematical models used in modeling the drying of common bean grains.

Model	40 °C				50 °C				60 °C			
	SE	RME (%)	R^2	RD	SE	RME (%)	R^2	RD	SE	RME (%)	R^2	RD
Newton	0.0680	15.3240	0.9153	B	0.0701	13.9077	0.9052	B	0.0702	12.3844	0.9015	B
Page	0.0051	0.4652	0.9995	R	0.0062	0.6859	0.9993	R	0.0033	0.2964	0.9998	R
Henderson and Pabis	0.0417	8.5342	0.9689	B	0.0432	7.7593	0.9651	B	0.0407	6.3634	0.9682	B
Logarithm	0.0215	3.8177	0.9919	B	0.0209	3.3062	0.9921	B	0.0216	3.0332	0.9914	B
Midilli	0.0044	0.4050	0.9997	R	0.0048	0.4361	0.9996	R	0.0033	0.3228	0.9998	R
Two-terms	0.0067	1.5099	0.9992	R	0.0071	1.3741	0.9991	R	0.0071	1.1909	0.9991	R
Verna	0.0071	1.6713	0.9991	R	0.0074	1.4920	0.9990	R	0.0075	1.2974	0.9990	R
Diffusion approximation	0.0071	1.6714	0.9991	R	0.0074	1.4920	0.9990	R	0.0075	1.2974	0.9990	R
Two-term exponential	0.0414	8.9686	0.9692	B	0.0437	8.4026	0.9642	B	0.0438	7.4310	0.9632	B
Henderson and Pabis modified	0.0008	0.1401	1.0000	R	0.0015	0.1914	1.0000	R	0.0013	0.1901	1.0000	R

Model	70 °C				80 °C			
	SE	RME (%)	R^2	RD	SE	RME (%)	R^2	RD
Newton	0.0678	11.1825	0.9068	B	0.0421	6.9259	0.9634	B
Page	0.0037	0.3391	0.9997	B	0.0046	0.4505	0.9996	B
Henderson and Pabis	0.0402	5.7194	0.9690	B	0.0326	4.7735	0.9802	B
Logarithm	0.0221	3.0425	0.9912	B	0.0164	2.0107	0.9955	R
Midilli	0.0038	0.3694	0.9998	B	0.0075	1.0703	0.9992	B
Two-terms	0.0053	0.8395	0.9995	R	0.0075	1.0702	0.9992	R
Verna	0.0054	0.8791	0.9995	R	0.0070	1.0663	0.9992	R
Diffusion approximation	0.0054	0.8791	0.9995	R	0.0070	1.0663	0.9992	R
Two-term exponential	0.0405	6.4343	0.9686	B	0.0171	2.4706	0.9946	B
Henderson and Pabis modified	0.0011	0.1504	1.0000	R	0.0039	0.3120	0.9998	R

Where, R: random; B: biased.

The moisture ratio curves estimated by the Henderson and Pabis modified model are presented in Figure 4. The estimated curves prove the excellent fit of the model to the observed experimental data. Several authors point out that the Henderson and Pabis modified model satisfactorily represents the drying of several biological materials, such as olive-wast cake (Vega-Gálvez et al., 2010), dika kernels (Aregbesola et al., 2015), garlic slices (Younis et al., 2018), purple basil leaves (Altay et al., 2019), pear slices (Araujo et al., 2021), pequi slices (Pinheiro et al., 2021), among others. The coefficients of the modified Henderson and Pabis model adjusted to the experimental data are presented in Table 7.

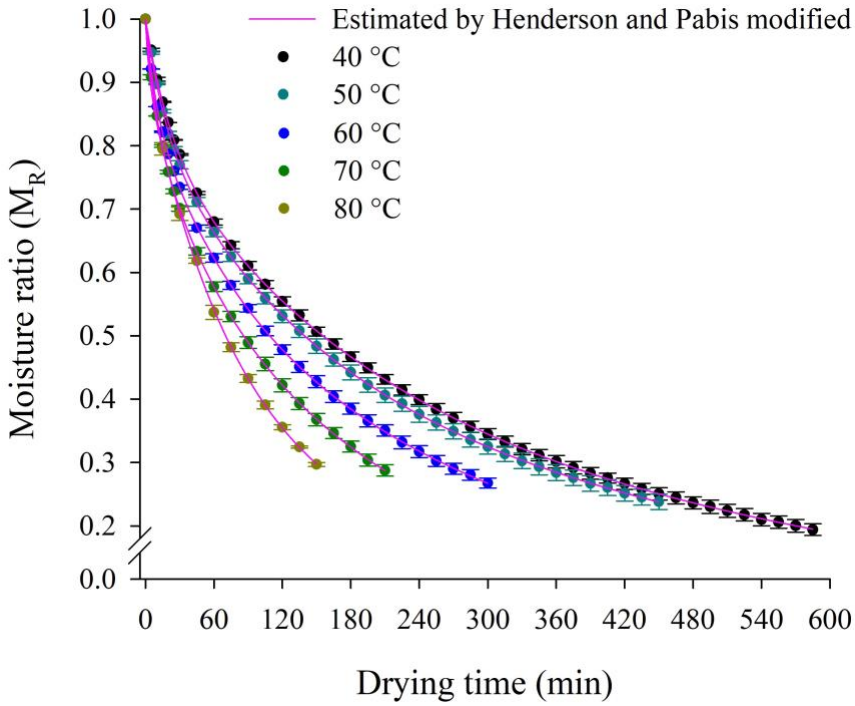

Figure 4. Moisture ratio versus drying time for common bean grains at different temperatures, observed and estimated by the Henderson and Pabis modified model. Error bars represent the standard deviation.

Table 7 – Coefficients of Henderson and Pabis modified model adjusted to experimental data from common bean grain drying at different temperatures.

Temperature	Model coefficients					
(°C)	a	k	b	g	c	h
40	0.4424	0.0015	0.1805	0.0456	0.3776	0.0059
50	0.4675	0.0016	0.1638	0.0574	0.3708	0.0077
60	0.5589	0.0025	0.1336	0.1013	0.3073	0.0128
70	0.5932	0.0036	0.1392	0.1085	0.2673	0.0165
80	0.4195	0.0043	0.0868	0.7746	0.4937	0.0149

The variation in the equivalent radius of common bean grains during drying is shown in Figure 5. The equivalent radius showed a nonlinear reduction during drying, satisfactorily represented by a quadratic regression. The resulting regression equation was then used to obtain the effective diffusion coefficient shown in Equation 15.

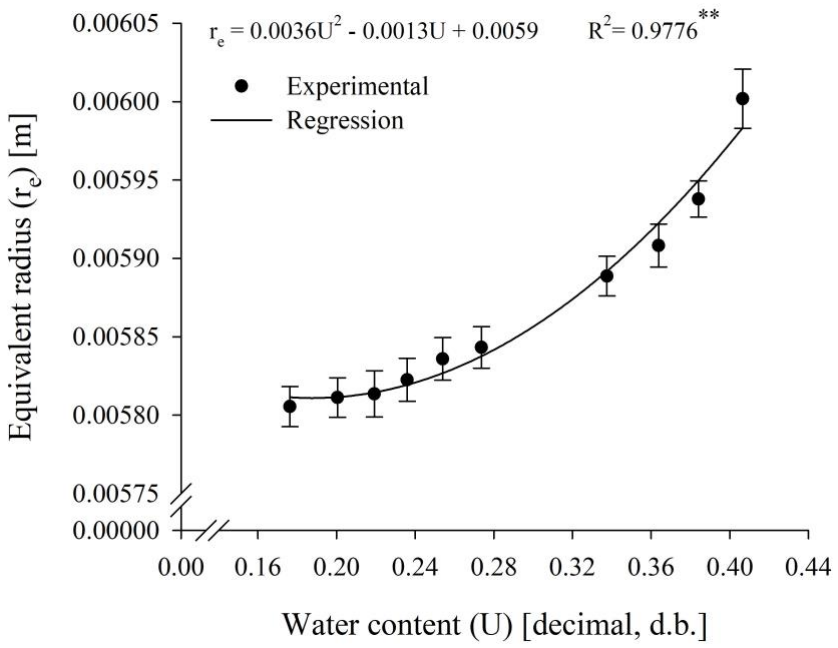

Figure 5. Variation of the equivalent radius (r_e) of common bean grains as a function of water content. Error bars represent the standard deviation. ** Significant at 1% probability by F test.

Table 8 presents effective diffusion coefficients of common bean grains for different temperatures considering the equivalent radius as constant (value for initial water content = 0.005866 m) and variable. In this study, the Fick model was adjusted until the number of

terms in the series was equal to 5, guaranteeing a variation of less than 1×10^{-14} m^2 s^{-1} for all evaluated temperatures. For all drying temperatures, the diffusion coefficient for the common bean grains, considering the volumetric contraction of the grains (variable equivalent radius), was statistically lower than the values obtained from the constant equivalent radius (obtained at the beginning of drying). A similar result was previously reported by Corrêa et al. (2006) for red bean grains. In the present study, bean grains showed a slight variation during drying, enough to statistically differ the diffusion coefficient values. This result indicates that ignoring this phenomenon can lead to erroneous results in products with more volumetric contraction during drying, such as fruits or grains with high water content. According to Brooker et al. (1992), several models used to represent the water movement in agricultural products neglect the importance of the volumetric contraction of the product.

Table 8 – Effective diffusion coefficient (D_{eff}) of common bean grains at 40, 50, 60, 70, and 80 °C for constant and variable equivalent radius during drying.

Temperature	Constant equivalent radius		Variable equivalent radius	
(°C)	D_{eff} x 10^{-10} (m^2 s^{-1})	R^2	D_{eff} x 10^{-10} (m^2 s^{-1})	R^2
40	1.139 b	0.9853	1.109 a	0.9859
50	1.242 b	0.9827	1.210 a	0.9833
60	1.595 b	0.9810	1.554 a	0.9816
70	2.023 b	0.9746	1.972 a	0.9754
80	2.569 b	0.9568	2.504 a	0.9574

Means followed by the same letter on the line do not differ from each other at the 5% level of probability by the Tukey test.

The effective diffusion coefficients for the common bean grains varied between 1.139×10^{-10} and 2.569×10^{-10} m^2 s^{-1}, considering the initial equivalent radius of the grains, and between 1.109×10^{-10} and 2.504×10^{-10} m^2 s^{-1} considering the equivalent radius as a function of the water content of the product, for the temperature range of 40 to 80 °C. The values found are close to those presented by Almeida et al. (2009) for adzuki bean grains. In the study, the authors found that the effective diffusion coefficient of adzuki bean grains varied between 0.51×10^{-10} and 2.23×10^{-10} m^2 s^{-1} for a temperature range of 30 to 70 °C. According to Doymaz et al. (2006), the diffusion coefficient of agricultural products varies in the order of 10^{-11} to 10^{-9} m^2 s^{-1}. It is observed that increasing the drying temperature results in an increase in the effective diffusion coefficient. The increasing temperature's diffusivity dependence suggests

that the water molecules' vibration level favors moisture vapor diffusivity during product drying (Cavalcanti-Mata et al., 2020).

As the results of the diffusion coefficient were close for both scenarios evaluated in this study, the following results are presented only considering the variable equivalent radius. The values of ln (D_{ef}) as a function of the inverse temperature are shown in Figure 6. The line representing the dependence of the diffusion coefficient on temperature is satisfactorily described by an Arrhenius-type equation (Corrêa et al., 2019; Luthra and Sadaka, 2021). The slope of the Arrhenius curve gives the E_a/R ratio, while its intersection with the ordinate axis indicates the value of D_0.

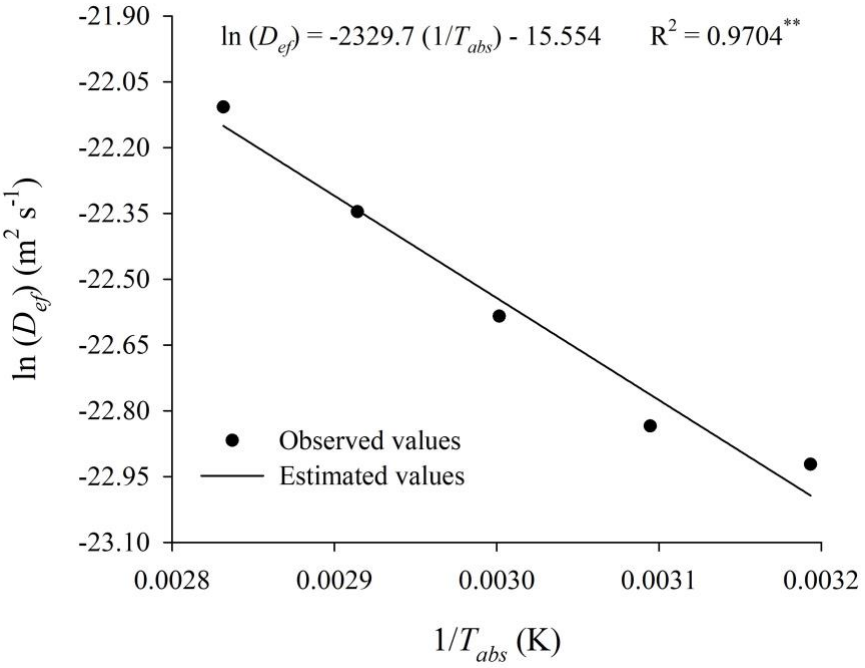

Figure 6. Arrhenius representation for the effective diffusion coefficient of common bean grains at temperatures of 40, 50, 60, 70, and 80 °C. ** Significant at 1% probability by F test.

Equation 52 presents the coefficients of the adjusted equation for the effective diffusion coefficient of common bean grains, obtained according to Equation 18. It is observed that the activation energy for liquid diffusion of common bean grains was approximately 19.4 kJ mol^{-1}. Similar results are found for several agricultural products, such as 9.4-17.5 kJ mol^{-1} for maize grains (Asemu et al., 2019), 13.6 kJ mol^{-1} for chickpeas (Cavalcanti-Mata et al., 2020), among others. According to Zogzas et al. (1996), activation energy values for agricultural products are commonly found in 12.7 to 110.0 kJ mol^{-1}. The

activation energy value can be defined as the minimum energy required to trigger the diffusion process in the product (Kashaninejad et al., 2007).

$$D_{ef} = 1.76 \times 10^{-7} \exp\left(-\frac{19{,}369.13}{8.314\, T_{abs}}\right) \quad (52)$$

Table 9 shows the results of thermodynamic properties (enthalpy, entropy, and Gibbs free energy) of bean grains as a function of drying air temperature. It is observed that the enthalpy presented results inversely proportional to the temperature increase. Enthalpy values varied between 16.77 and 16.43 kJ mol-1 for temperatures of 40 and 80 °C, respectively. Positive enthalpy values indicate an endothermic transformation with heat absorption. This behavior is associated with the increase in the partial pressure of water vapor in the bean grains caused by the increase in temperature. As a result, there is an increase in the moisture diffusivity rate of the grains from their interior to their surface, allowing the desorption process to occur (Araújo et al., 2017). Correa et al. (2017) highlighted that lower enthalpy values mean less energy is required for the process to occur. Therefore, less energy is needed for drying bean grains at higher temperatures.

Table 9 – Thermodynamic properties as a function of drying temperature of common bean grains.

Temperature (°C)	Temperature (K)	Enthalpy (J mol^{-1})	Entropy (J mol^{-1} K^{-1})	Gibbs free energy (J mol^{-1})
40	313.15	16765.60	-374.63	134081.14
50	323.15	16682.46	-374.89	137828.76
60	333.15	16599.32	-375.15	141578.95
70	343.15	16516.18	-375.39	145331.64
80	353.15	16433.04	-375.63	149086.75

Like the results presented for enthalpy, entropy also showed inversely proportional values with the increase in drying temperature. Entropy values varied between -374.63 and -375.63 J mol^{-1} K^{-1} for temperatures of 40 and 80 °C, respectively. This behavior indicates an increase in the order of the system that is entropically unfavorable. With increasing drying temperature, there is an excitation of water molecules in the product, which decreases molecular heterogeneity, and therefore the order of the water-product system is also high

(Guimarães et al., 2018). In the context of drying, entropy is associated with the forces of attraction or repulsion of water molecules to the components of the material (Goneli et al., 2010). The negative values for entropy are related to the structural change in the adsorbent and the existing chemical adsorption (Martins et al., 2015).

Gibbs free energy increased from 134.1 to 149.1 kJ mol^{-1} by increasing the drying air temperature from 40 to 80 °C. This property indicates the amount of work done by the system during drying. Positive values of Gibbs free energy suggest that the process is endergonic and requires the addition of external energy to occur (Moura et al., 2021). Therefore, the results were expected since the desorption process is non-spontaneous and requires the addition of external energy (drying air) to remove water from the grains.

The results of this study will be very useful for the bean industry. Knowledge about drying kinetics and thermodynamic properties is essential for equipment design and optimization and for controlling the drying process. In addition, the results can be used to obtain the amount of energy required to remove water from the product, allowing to evaluate and make drying more efficient from an energy point of view.

3.2. CFD Numerical Modeling

The results of numerical CFD modeling of common bean drying are presented in this section. Figure 7 shows the results of the modeling referring to the water content of the grains during drying. It is observed that both proposed models adequately represented the drying process of bean grains. The maximum values of MRD and PRE did not exceed 1.51 and 2.19% for the thin layer model and 1.47 and 3.91% for the single grain model, respectively. The thin layer model (Figure 7A) showed behavior similar to that observed experimentally during the entire drying process. This result is linked to the fact that the experimental drying curve itself is inserted in the numerical model from the UDF. However, it is worth mentioning that this modeling requires that the drying curve be updated in the UDF for each drying temperature. For the single-grain model (Figure 7B), a certain deviation of the modeling in relation to the experimental data is observed at the beginning of drying. After a few minutes, the model satisfactorily represents drying for all evaluated temperatures. This result can be attributed to the difficulty of obtaining convergence within each timestep during the beginning of the simulations in this case. The advantage of this model is that the resistance values that govern drying were obtained only for one of the drying temperatures (60 ºC) and did not need to be updated at each temperature. Note, however, that the prediction was

adequate for all temperatures. Therefore, this model presents greater versatility for evaluating different drying conditions.

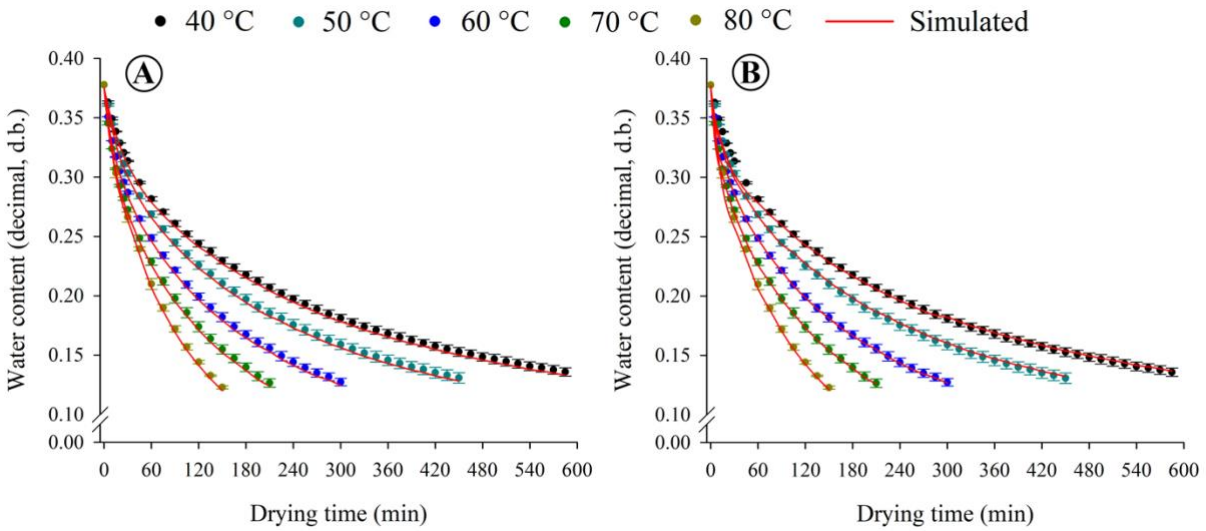

Figure 7. Experimental and simulated water content for (A) the thin layer model and (B) the single grain model. Error bars represent the standard deviation.

Although the single-grain model considered the grain a porous medium, it is noteworthy that there are no velocity profiles within the grain (Figure 8). This formulation is necessary for the multiphase models to be applied properly.

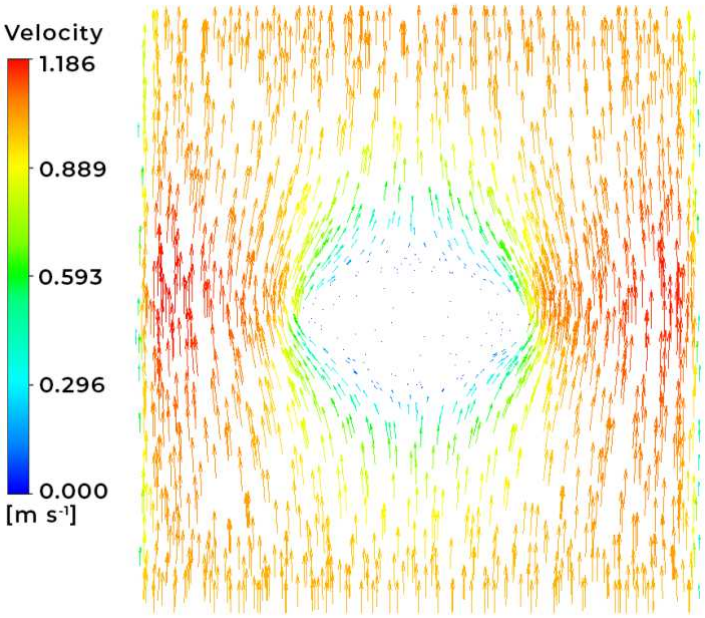

Figure 8. Example of velocity vectors around the bean for the single grain model.

Figure 9 presents the average grain layer temperatures for the thin layer model (Figure 9A) and the average volumetric grain temperatures for the single grain model (Figure 9B). It is observed that although the assumption that the grains are in equilibrium with the intergranular air temperature is valid, a temperature gradient is observed in the first instants of drying. This happens because it was considered that the grains were at a temperature of 25 ºC before the start of drying. It is also observed that with the increase in the drying temperature, the faster the grains reach the temperature of the drying air. Although the validation of these temperatures is not possible in this study due to a lack of data, the observed behavior is in line with those reported by other authors during the modeling of the drying process (ElGamal et al., 2013; Mahmoudi and Peters, 2014; Ranjbaran et al. 2014). For the single grain model, the average temperature of the grain reaches the drying air temperature faster. This result may be related to the mass and total thickness of the product considered in the different models.

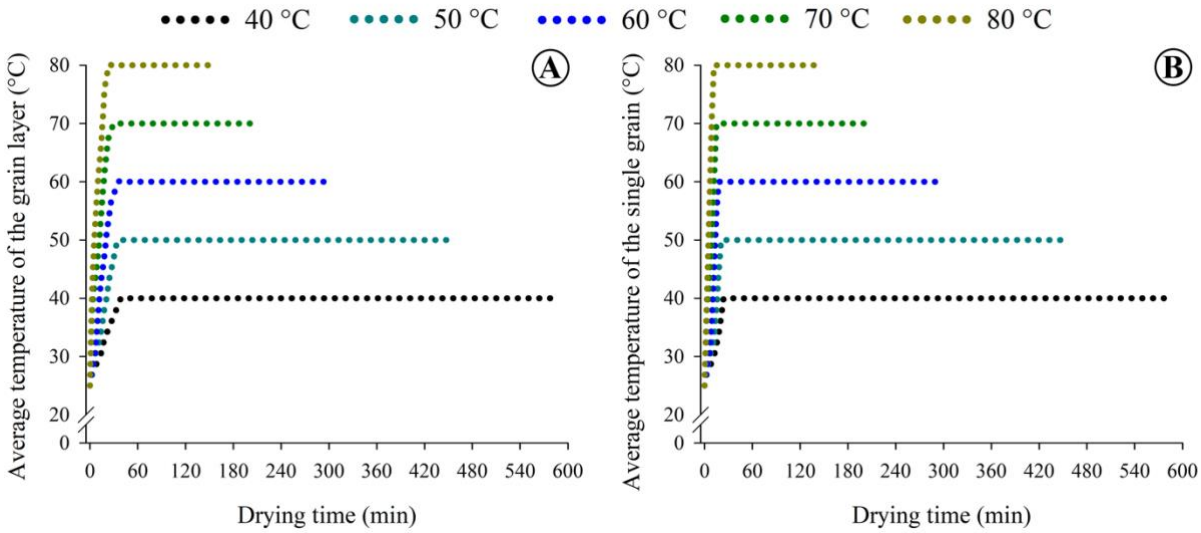

Figure 9. Simulated average temperatures for (A) the thin layer model and (B) the single grain model.

Although the thermal equilibrium model was considered in this study, the single-grain model allows a detailed local temperature assessment. In Figure 10 it can be observed how the local effects can be evaluated. For this case, the temperature variation is almost zero due to the assumption of equilibrium. However, an improvement of this model with the implementation of a non-thermal equilibrium model in the future will open a new range of local evaluations in grains during drying.

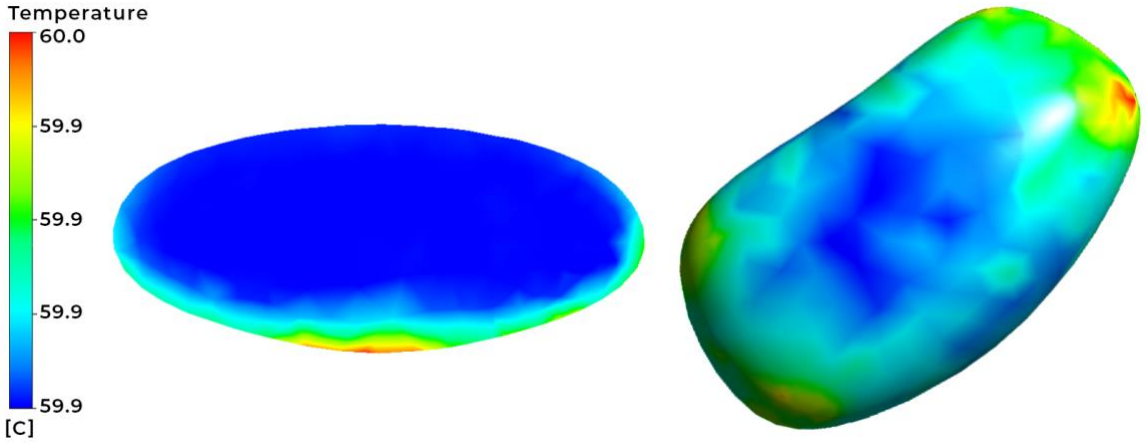

Figure 10. Example of local temperature profiles in the axial plane and on the bean surface for a single-grain model.

4. CONCLUSION

The characteristics of thin-layer drying kinetics and thermodynamic properties of common bean grains were investigated at five different temperatures in a tray dryer. The diffusion coefficient was determined considering and not considering the volumetric contraction of the grains. Two numerical CFD models were evaluated to predict the drying of common bean grains. Evaluating the results of these analyses, the following conclusions can be drawn.

- Models from the literature were adjusted to experimental data on drying common bean grains at different temperatures. The modified Henderson and Pabis model satisfactorily represented the drying of bean grains for all evaluated temperatures. Drying time varied between 585 and 150 minutes for temperatures of 40 and 80 °C, respectively.
- The diffusion coefficient of bean grains considering the equivalent radius as a variable differed statistically from the values considering the constant equivalent radius (obtained for the initial water content). The values varied between 1.1388×10^{-10} and 2.5694×10^{-10} m^2 s^{-1}, considering the initial equivalent radius of the grains, and between 1.1090×10^{-10} and 2.5035×10^{-10} m^2 s^{-1} considering the equivalent radius as a function of the water content of the product, for the temperature range of 40 to 80 °C, respectively.
- The activation energy for liquid diffusion of common bean grains was approximately 19.4 kJ mol^{-1}. Enthalpy and entropy showed a small reduction with increasing drying temperature from 40 to 80 ºC. This reflects the importance of the grains' internal resistance to the drying process. The Gibbs free energy increased from 134.1 to 149.1 kJ mol^{-1} for the temperatures of 40 and 80 °C, respectively, indicating an increase in the energy available to the process to carry out drying.
- The numerical models in CFD adequately represented the drying of bean grains. The maximum values of MRD and PRE did not exceed 1.51 and 2.19% for the thin layer model and 1.47 and 3.91% for the single grain model, respectively.

5. REFERENCES

Adnouni, M., Jiang, L., Zhang, X.L., Zhang, L.Z., Pathare, P.B., Roskilly, A.P. Computational modelling for decarbonised drying of agricultural products: Sustainable processes, energy efficiency, and quality improvement. **Journal of Food Engineering**, v.338, 111247, 2023.

Almeida, D.P., Resende, O., Costa, L.M., Mendes, U.C., Sales, J.F. Cinética de secagem do feijão adzuki (*Vigna angularis*). **Global Science and Technology**, v.2, p.72-83, 2009.

Altay, K., Hayaloglu, A.A., Dirim, S.N. Determination of the drying kinetics and energy efficiency of purple basil (*Ocimum basilicum* L.) leaves using different drying methods. **Heat and Mass Transfer**, v.55, p.2173-2184, 2019.

Araujo, M.E.V., Barbosa, E.G., Lopes, R.P., Corrêa, P.C., Barbosa, E.G. Infrared drying of pear slices: Drying kinetics, energy, and exergy analysis. **Journal of Food Process Engineering**, v.44, e13915, 2021.

Araújo, W.D., Goneli, A.L.D., Corrêa, P.C., Hartmann Filho, C.P., Martins, E.A.S. Modelagem matemática da secagem dos frutos de amendoim em camada delgada. **Revista Ciência Agronômica**, v.48, p.448 – 457, 2017.

Aregbesola, O.A., Ogunsina, B.S., Sofolahan, A.E., Chime, N.N. Mathematical modeling of thin layer drying characteristics of dika (*Irvingia gabonensis*) nuts and kernels. **Nigerian Food Journal**, v.33, p.83-89, 2015.

Asemu, A.M., Habtu, N.G., Delele, M.A., Subramanyam, B., Alavi, S. Drying characteristics of maize grain in solar bubble dryer. **Journal of Food Process Engineering**, v.43, e13312, 2019.

Avhad, M.R., Marchetti, J.M. Mathematical modelling of the drying kinetics of Hass avocado seeds. **Industrial Crops and Products**, v.91, p.76-87, 2016.

Azmir, J., Hou, Q., Yu, A. CFD-DEM study of the effects of food grain properties on drying and shrinkage in a fluidised bed. **Powder Technology**, v.360, p.33-42, 2020.

Bissaro, C.A., de Souza Matias, G., Defendi, R.O., de Matos Jorge, L.M. Modeling the drying kinetics of soybeans under intermittent operation in thin layer. **Food and Bioproducts Processing**, v.136, p.226-235, 2022.

Brackbill, J.U., Kothe, D.B., Zemach, C. A continuum method for modeling surface tension. **Journal of Computational Physics**, v.100, p.335-354, 1992.

BRASIL. Agência Nacional de Vigilância Sanitária. Resolução da Diretoria Colegiada - RDC n. 272, de 22 de setembro de 2005. **Regulamento Técnico para produtos de vegetais, produtos de frutas e cogumelos comestíveis**, Diário Oficial da União, Brasília, DF, Brasil, 2005. p.1-6.

BRASIL. Ministério da Agricultura, Pecuária e Abastecimento. **Regras para análise de sementes**. Secretaria de Defesa Agropecuária. Brasília: MAPA/ACS, 2009. 399p.

Brooker, D.B., Bakker-Arkema, F.W., Hall, C.W. **Drying and storage of grains and oilseeds**. The AVI Publishing Company, Westport, Connecticut, USA, 1992.

Cavalcanti-Mata, M.E.R.M., Duarte, M.E.M., Lira, V.V., Oliveira, R.F., Costa, N.L., Oliveira, H.M.L. A new approach to the traditional drying models for the thin-layer drying kinetics of chickpeas. **Journal of Food Process Engineering**, v.43, e13569, 2020.

Corrêa, P.C., Baptestini, F.M., Zeymer, J.S., Araujo, M.E.V., Freitas, R.C., Leite, R.A. Dehydration of infrared ginger slices: Heat and mass Transfer coefficient and modeling. **Ciência e Agrotecnologia**, v.43, e025318, 2019.

Corrêa, P.C., Botelho, F.M., Botelho, S.C.C., Goneli, A.L.D. Isotermas de sorção de água de frutos de *Coffea canefora*. **Revista Brasileira de Engenharia Agrícola e Ambiental**, v.18, p.1047-1052, 2014.

Corrêa, P.C., Oliveira, G.H.H., Oliveira, A.P.L.R., Botelho, F.M., Goneli, A.L.D. Thermodynamic properties of drying process and water absorption of rice grains. **CYTA: Journal of Food**, v.15, p.204– 210, 2017.

Corrêa, P.C., Resende, O., Goneli, A.L.D., Botelho, F.M., Nogueira, B.L. Determinação do coeficiente de difusão liquida dos grãos de feijão. **Revista Brasileira de Produtos Agroindustriais**, v.8, p.117-126, 2006.

Costa, J.M.G., Silva, E.K., Hijo, A.A.C.T, Azevedo, V.M., Borges, S.V. Physical and Thermal Stability of Spray-Dried Swiss Cheese Bioaroma Powder. **Drying Technology**, v.33, p.346-354, 2015.

Delfiya, D.S.A., Prashob, K., Murali, S., Alfiya, P.V., Samuel, M.P., Pandiselvam, R. Drying kinetics of food materials in infrared radiation drying: A review. **Journal of Food Process Engineering**, v.45, p.1-19, 2021.

Doymaz, I. Convective drying kinetics of strawberry. **Chemical Engineering and Processing**, v.47, p.914-919, 2008.

Doymaz, I., Tugrul, N., Pala, M. Drying characteristics of dill and parsley leaves. **Journal of Food Engineering**, 77, 559-565, 2006.

El-Saadony, M.T., Desoky, E.M., Saad, A.M., Eid, R.S.M., Selem, E., Elrys, A.S. Biological silicon nanoparticles improve *Phaseolus vulgaris* L. yield and minimize its contaminant contents on a heavy metals-contaminated saline soil. **Journal of Environmental Sciences**, v.106, p.1-14, 2021.

ElGamal, R., Ronsse, F., Pieters, J. **Modeling deep-bed grain drying using Comsol Multiphysics**. In COMSOL Conference 2013.

FAO, 2022. Food and Agriculture Organization. **Crops and livestock products**. Available in: https://www.fao.org/faostat/en/#data/QCL, accessed on 12 Dec. 2022.

Ferreira, R.B., Falcãp, D.S., Oliveira, V.B., Pinto, A.M.F.R. Numerical simulations of two-phase flow in proton exchange membrane fuel cells using the volume of fluid method – A review. **Journal of Power Sources**, v.277, p.329-342, 2015.

Goneli, A.L.D., Corrêa, P.C., Oliveira, G.H.H., Gomes, C.F., Botelho, F.M. Water sorption isotherms and thermodynamic properties of pearl millet grain. **International Journal of Food Science Technology**, v.45, p.828– 838, 2010.

Granella, S.J., Bechlin, T.R., Christ, D. Moisture diffusion by the fractional-time model in convective drying with ultrasound-ethanol pretreatment of banana slices. **Innovative Food Science Emerging Technologies,** v.76, 102933, 2022.

Guimarães, R.M., Oliveira, D.E.C., Resende, O., Silva, J.S., Rezende, T.A.M., Egea, M.B. Thermodynamic properties and drying kinetics of 'okara'. **Revista Brasileira de Engenharia Agrícola e Ambiental**, v.22, p.418-423, 2018.

Hatami, S., Payganeh, G., Mehrpanahi, A. Energy and exergy analysis of an indirect solar dryer based on a dynamic model. **Journal of Cleaner Production**, v.244, 118809, 2020.

Hunter, A.J. Pressure difference across an aerated seed bulk for some common duct and store cross-sections. **Journal of Agricultural Engineering Research**, v.28, p.437–450, 1983.

Jideani, V.A., Mpotokwana, S.M. Modeling of water absorption of Botswana Bambara varieties using Peleg's equation. **Journal of Food Engineering**, v.92, p.182-188, 2009.

Jubaer, H., Afshar, S., Xiao, J. Chen, X.D., Selomulya, C., Woo, M.W. On the effect of turbulence models on CFD simulations of a counter-current spray drying process. **Chemical Engineering Research and Design**, v.141, p.592-607, 2019.

Karataş, M., Arslan, N. Moisture sorption isotherms and thermodynamic properties of cowpea (*Vigna unguiculate* L. Walp) stored in a chamber under controlled humidity and temperature. Journal of **Food Process Engineering**, v.45, p.1-14, 2022.

Kashaninejad, M., Mortazavi, A., Safekordi, A., Tabil, L.G. Thin-layer drying characteristics and modeling of pistachio nuts. **Journal of Food Engineering**, v.78, p.98-108, 2007.

Kumar, A., Kandasamy, P., Chakraborty. I., Hangshing, L. Analysis of energy consumption, heat and mass transfer, drying kinetics and effective moisture diffusivity during foam-mat drying of mango in a convective hot-air dryer. **Biosystems Engineering**, v.219, p.85-102, 2022.

Kumar, A., Saha, S.K. Performance analysis of a packed bed latent heat thermal energy storage with cylindrical-shaped encapsulation. **International Journal of Energy Research**, v.45, p.13130-13148, 2021.

Lisboa, H.M., Araujo, H., Paiva, G., Oriente, S., Pasquali, M., Duarte, M.E., Cavalcanti Mata, M.E.R.M. Determination of characteristic properties of mulatto beans (*Phaseolus vulgaris* L.) during convective drying. **Journal of Agriculture and Food Research**, v.1, 100003, 2019.

Luthra, K., Sadaka, S.S. Mathematical modeling of rough rice dehydration with dehumidified air in a fluidized bed drying system. **Applied Engineering in Agriculture**, v.37, p.783-791, 2021.

Mahmoudi, A.H., Hoffmann, F., Peters, B. Application of XDEM as a novel approach to predict drying of a packed bed. **International Journal of Thermal Sciences**, v.75, p.65-75, 2014.

Malekjani, N., Jafari, S.M. Simulation of food drying processes by Computational Fluid Dynamics (CFD); recent advances and approaches. **Trends in Food Science & Technology**, v.78, p.206-223, 2018.

Martins, E. A., Lage, E. Z., Goneli, A. L., Hartmann Filho, C. P., Lopes, J. G. Drying kinetics of *Serjania marginata* Casar leaves/Cinetica de secagem de folhas de Timbo (*Serjania marginata* Casar). **Revista Brasileira de Engenharia Agrícola e Ambiental**, v.19, p.238–245, 2015.

Mishra, M., Kandasamy, P., Shukla, R.N., Kumar, A. Convective Hot-air Drying of Green Mango: Influence of Hot Water Blanching and Chemical Pretreatments on Drying Kinetics and Physicochemical Properties of Dried Product. **International Journal of Fruit Science**, v.21, p.732-757, 2021.

Mohsenin, N.N. **Physical properties of plant and animal materials**. New York: Gordon and Breach Publishers, 1986. 841p.

Moura, H.V., Figueirêdo, R.M.F., Queiroz, A.J.M., Silva, E.T.V., Esmero, J.A.D., Lisbôa, J.F. Mathematical modeling and thermodynamic properties of the drying kinetics of trapiá residues. **Journal of Food Process Engineering**, v.44, e13768, 2021.

Mousakhani-Ganjeh, A., Amiri, A., Nasrollahzadeh, F., Wiktor, A., Nilghaz, A., Pratap-Singh, A., Mousavi Khaneghah, A. Electro-based technologies in food drying - A comprehensive review. **LWT-Food Science and Technology**, v.145, 111315, 2021.

Najib, T., Heydari, M.M., Meda, V. Combination of germination and innovative microwave-assisted infrared drying of lentils: effect of physicochemical properties of different varieties on water uptake, germination, and drying kinetics. **Applied Food Research**, v.2, 100040, 2022.

Öztekin, Y.B., Aktaş, M., Dolgún, E.C., Bilim, H.C., Sacilik, K. Drying kinetics and thermodynamic properties of *Uzun pistachios* dried by convective drying. **Journal of Food Processing and Preservation**. v.46, p.1-13, 2022.

Pandiselvam, R., Aydar, A.Y., Kutlu, N., Aslam, R., Sahni, P., Mitharwal, S., Gavahian, M., Kumar, M., Raposo, A., Yoo, S., Han, H., Kothakota, A. Individual and interactive effect of ultrasound pre-treatment on drying kinetics and biochemical qualities of food: A critical review. **Ultrasonics Sonochemistry**, v.92, 106261, 2023.

Pinheiro, S.A.R., Corrêa, P.C., Silva, J.G., Zeymer, J.S., Araujo, M.E.V. Dehydration of pequi slices (*Caryocar brasiliense* Camb.) by infrared: Modeling and effective diffusion coefficient. **Journal of Food Process Engineering**, v.44, e13886, 2021.

Pravallika, K., Chakraborty, S., Singhal, R.S. Supercritical drying of food products: An insightful review. **Journal of Food Engineering**, v.343, 111375, 2023.

Prommuak, C., Tharangkool, N., Pasavant, P., Ponpesh, P., Jarunglumlert, T. Computational fluid dynamic design of spent coffee ground cabinet dryer using recycled heat from air compressor. **Chemical Engineering Research and Design**, v.153, p.75-84, 2020.

Ramachandran, R.P., Akbarzadeh, M., Paliwal, J., Cenkowski, S. Computational Fluid Dynamics in Drying Process Modelling—a Technical Review. **Food and Bioprocess Technology**, v.11, p.271-292, 2018.

Ranjbaran, M., Emadi, B., Zare, D. CFD Simulation of Deep-Bed Paddy Drying Process and Performance. **Drying Technology**, v.32, p.919-934, 2014.

Ranjbaran, M., Zare, D. CFD modeling of microwave-assisted fluidized bed drying of moist particles using two-fluid model. **Drying Technology**, v.30, p.362–376, 2012.

Resende, J.S., dos Santos, T.B., Souza, S.G.H.D. Small heat shock protein (Hsp20) gene family in *Phaseolus vulgaris* L.: Genome-wide identification, evolutionary and expression analysis. **Plant Gene**, v.31, 100370, 2022.

Resende, O., Corrêa, P.C., Goneli, A.L.D., Ribeiro, D.M. Isotermas e calor isostérico de sorção do feijão. **Ciência e Tecnologia de Alimentos**, v.26, p.626-631, 2006.

Salehi, F., Satorabi, M. Influence of Infrared Drying on Drying Kinetics of Apple Slices Coated with Basil Seed and Xanthan Gums. **International Journal of Fruit Science**, v.21, p.519-527, 2021.

Sandoval-Peraza, M., Chel-Guerrero, L., Betancur-Ancona, D. Some physicochemical and functional properties of the rich fibrous fraction of hardened beans (*Phaseolus vulgaris* L.) and its addition in the formulation of beverages. **International Journal of Gastronomy and Food Science**, v.26, 100440, 2021.

Silva, H.W., Rodovalho, R.S., Velasco, M.F., Silva, C.F., Vale, L.S.R. Kinetics and thermodynamic properties related to the drying of 'Cabacinha' pepper fruits. **Revista Brasileira de Engenharia Agrícola e Ambiental**, v.20, p.174-180, 2016.

Siqueira, V.C., Leite, R.A., Mabasso, G.A., Martins, E.A.S., Quequeto, W.D., Isquierdo, E.P. Drying kinetics and effective diffusion of buckwheat grains. **Ciência e Agrotecnologia**, v.44, e011320, 2020.

Spiess, A., Neumeyer, N. An evaluation of R2 as an inadequate measure for nonlinear models in pharmacological and biochemical research: a Monte Carlo approach. **BMC Pharmacology Toxicology**, v.6, p.1-11, 2010.

Sun, D.L., Xu, J.L., Wang, L. Development of a vapor–liquid phase change model for volume-of-fluid method in FLUENT. **International Communications in Heat and Mass Transfer**, v.39, p.1101-1106, 2012.

Szijártó, R., Badillo, A., Niceno, B., Prasser, H.M. Condensation models for the water–steam interface and the volume of fluid method. **International Journal of Multiphase Flow**, v.93, p.63-70, 2017.

Thorpe, G.R. The application of computational fluid dynamics codes to simulate heat and moisture transfer in stored grains. **Journal of Stored Products Research**, v.44, p.21-31, 2008.

Vega-Gálvez, A., Miranda, M., Díaz, L.P., Lopez, L., Rodriguez, K., Scala, K.D. Effective moisture diffusivity determination and mathematical modelling of the drying curves of the olive-waste cake. **Bioresource Technology**, v.101, p.7265-7270, 2010.

Waheed, M.A., Komolafe, C.A. Temperatures dependent drying kinetics of cocoa beans varieties in air-ventilated oven. **Frontiers in Heat and Mass Transfer**, v.12, p.1-7, 2019.

Xu, B., Sylvain Tiliwa, E., Yan, W., Roknul Azam, S.M., Wei, B., Zhou, C., Ma, H., Bhandari, B. Recent development in high quality drying of fruits and vegetables assisted by ultrasound: A review. **Food Research International**, v.152, 110744, 2022.

Younis, M., Abdelkarim, D., El-Abdein, A.Z. Kinetics and mathematical modeling of infrared thin-layer drying of garlic slices. **Saudi Journal of Biological Sciences**, v.25, p.332-338, 2018

Yu, X.L., Zielinska, M., Ju, H.Y., Mujumdar, A.S., Duan, X., Gao, Z.J., Xiao, H.W. Multistage relative humidity control strategy enhances energy and exergy efficiency of convective drying of carrot cubes. **International Journal of Heat and Mass Transfer**, v.149, 119231, 2020.

Zogzas, N.P, Maroulis, Z.B, Marinoskouris, D. Moisture diffusivity data compilation in foodstuffs. **Drying Technology**, 14, 2225-2253, 1996.

GENERAL CONCLUSION

This study experimentally determined geometric, physical, aerodynamic, and thermal properties during drying and the drying kinetics of common bean grains. Furthermore, numerical CFD models were evaluated to predict the drying process of bean grains. The following conclusions can be cited based on the results obtained and for the evaluated water content range.

- Digital image processing was satisfactory for obtaining the dimensions of bean grains, providing reliable data in a faster and more practical way.
- Among the geometric properties evaluated, only the circularity showed no significant difference ($P \leq 0.05$) during the drying process.
- The sphericity and the surface volume ratio of the bean grains increased with the reduction of the water content varying between 64.6-66% (+2.1%) and 0.85-0.87 (+2.2%), respectively. On the other hand, the geometric diameter, projected area, surface area, and volume reduced during drying, with values varying between 7.54–7.31mm (-3.0%), 64.11–59.01 mm^2 (-8.0%), 191.35–180.31 mm^2 (-5.7%), 225.0–208.1 mm^3 (-7.7%), respectively.
- Among the empirical models used, the Araujo-Copace model was selected to describe the volumetric contraction of bean grains during drying. The bean grains presented a volumetric contraction of 7.7%, indicating that the grains suffered a slight variation of the orthogonal axes during drying.
- Among the analyzed physical properties, only the bulk density increased during drying; all other properties decreased with the reduction in the water content of the grains. The 1000-grain weight showed the greatest variation during drying (16.2%), with values ranging between 306.3 and 256.7 g for water contents between 0.407 and 0.176 (decimal, d.b.), respectively. The porosity of the grain mass reduced from 38.9 to 33.1% during drying. The bulk density increased by about 7% with the reduction in water content, with values varying between 729.6 and 780.8 kg m^{-3}. True density showed the lowest percentage variation during drying, only 2.1%, with values ranging between 1193.1 and 1167.4 kg m^{-3} for water contents of 0.407 and 0.176 (decimal, d.b.), respectively.
- The drag coefficient showed the most significant variation among the evaluated aerodynamic properties, an increase of about 43.1%. The terminal velocity of bean

grains varied between 8.4 and 6.5 m s^{-1} (-22.3%) for water contents ranging between 0.407 and 0.176 (decimal, d.b.), respectively.

- For the evaluated thermal properties, thermal conductivity and diffusivity showed the most significant variations during desorption. Thermal conductivity showed a reduction of 47.2% during drying, with values varying between 0.32 and 0.17 W m^{-1} K^{-1}. Thermal diffusivity varied between 8.8×10^{-8} and 1.5×10^{-7} m^2 s^{-1} for water contents of 0.176 and 0.407 (decimal, d.b.), respectively. Finally, the specific heat was reduced by approximately 13.3% during drying, with values between 2839.4 and 2461.6 J kg^{-1} K^{-1}.
- Models from the literature were adjusted to experimental data on drying common bean grains at different temperatures. The modified Henderson and Pabis model satisfactorily represented the drying of bean grains for all evaluated temperatures. Drying time varied between 585 and 150 minutes for temperatures of 40 and 80 °C, respectively.
- The diffusion coefficient of bean grains considering the equivalent radius as a variable differed statistically from the values considering the constant equivalent radius (obtained for the initial water content). The values varied between 1.1388×10^{-10} and 2.5694×10^{-10} m^2 s^{-1}, considering the initial equivalent radius of the grains, and between 1.1090×10^{-10} and 2.5035×10^{-10} m^2 s^{-1} considering the equivalent radius as a function of the water content of the product, for the temperature range of 40 to 80 °C, respectively.
- The activation energy for liquid diffusion of common bean grains was approximately 19.4 kJ mol^{-1}. Enthalpy and entropy showed a small reduction with increasing drying temperature from 40 to 80 ºC. This reflects the importance of the grains' internal resistance to the drying process. The Gibbs free energy increased from 134.1 to 149.1 kJ mol^{-1} for the temperatures of 40 and 80 °C, respectively, indicating an increase in the energy available to the process to carry out drying.
- The numerical models in CFD adequately represented the drying of bean grains. The maximum values of Mean Relative Deviation and Percent Relative Error did not exceed 1.51 and 2.19% for the thin layer model and 1.47 and 3.91% for the single grain model, respectively.